NOTICE

The quality of this microform is heavily dependent upon the quality of the original thesis submitted for microfilming. Every effort has been made to ensure the highest quality of reproduction possible.

If pages are missing, contact the university which granted the degree.

Some pages may have indistinct print especially if the original pages were typed with a poor typewriter ribbon or if the university sent us an inferior photocopy.

Reproduction in full or in part of this microform is governed by the Canadian Copyright Act, R S.C. 1970, c. C-30, and subsequent amendments.

AVIS

La qualité de cette microforme dépend grandement de la qualité de la thèse soumise au microfilmage Nous avons tout fait pour assurer une qualité supérieure de reproduction

S'il manque des pages, veuillez communiquer avec l'université qui a conféré le grade

La qualité d'impression de certaines pages peut laisser à désirer, surtout si les pages originales ont été dactylographiées à l'aide d'un ruban usé ou si l'université nous a fait parvenir une photocopie de qualité inférieure

La reproduction, même partielle, de cette microforme est soumise à la Loi canadienne sur le droit d'auteur, SRC 1970, c. C-30, et ses amendements subséquents

Canada

ISBN 0-315-59170-6

HYGROTHERMAL EFFECT ON THE MECHANICAL PROPERTIES OF POLYPHENYLENE SULFIDE (PPS) COMPOSITES

Jirui Chen

A Thesis

in

the Department

of

Mechanical Engineering

Presented in Partial Fulfillment of the Requirements
for the Degree of Master of Engineering at
Concordia University
Montréal, Québec, Canada

May, 1990

ABSTRACT

Hygrothermal Effect on the Mechanical Properties of Polyphenylene Sulfide (PPS) Composites

Jirui Chen

Hygrothermal effect on the Mode II (in-plane shear loading) interlaminar fracture toughness of a carbon/polyphenylene sulfide (PPS) unidirectional laminate and on the tensile strengths of some glass/PPS composites was investigated. The critical strain energy release rates, G_{IIC}, of the carbon/PPS laminate during crack propagation under Mode II loading for the following temperature/relative humidity conditions were obtained both by linear beam theory and by the area method: 87°C/84%, 87°C/95%, 127°C/84% and 127°C/95%. It was found that the critical strain energy release rate of the carbon/PPS laminate increases with both moisture content and temperature. Large reduction in tensile strengths of the glass/PPS composites was observed when these composites were exposed to 95% relative humidity at 100°C for a period of one to two weeks. While large amount of moisture absorption caused the debonding between the glass fibers and the PPS resin, the fracture of the carbon/PPS laminate was characterized primarily by microcracking at low temperature/low moisture content and by matrix softening and fiber bridging at high temperature/high moisture content.

ACKNOWLEDGEMENTS

The financial support from Natural Sciences and Engineering Research Council of Canada under grant numbers A0413 and A7929, and from the Quebec Ministere de l'Enseignement Superieure is greatly appreciated.

The author wishes to express his sincere gratitude to Dr. S.V. Hoa and Dr. S. Lin, project supervisors, for their guidance, cooperation and encouragement throughout all stages of this research program and the preparation of this thesis.

Special thanks are given to Concordia University for the use of the Composite Materials Lab, Heat Transfer Lab and Thermal Analysis Lab, and to Dr. D. Feldman, lab coordinator, J. Elliot, technicians, D. Banu, M. Brennan and J. Sarruf, for their assistance.

Thanks are also due to the Industrial Materials Research Institute for the use of the research facilities and to J. Dufour for his kind assistance in the molding of the carbon/PPS laminates.

TABLE OF CONTENTS

LIST OF FIGURES

LIST OF TABLES

NOMENCLATURE

a	Crack length (mm)
a_o	Length of the Teflon tape in the interlaminar fracture specimen (≈ 35mm)
a_i	Crack length after crack initiation measured from the delaminated end to the crack tip (mm)
B	Width of the uncracked beam (mm)
C	Compliance (mm/N)
D	Half thickness of specimen (mm)
E	Flexural modulus (MSI) (18 MSI from Table 2.1)
G	Strain energy release rate (J/m^2)
G_C	Critical strain energy release rate (J/m^2)
G_I	Strain energy release rate for crack growth under Mode I loading (J/m^2)
G_{II}	Strain energy release rate for crack growth under Mode II loading (J/m^2)
G_{IC}	Critical strain energy release rate for crack growth under Mode I loading (J/m^2)
G_{IIC}	Critical strain energy release rate for crack growth under Mode II loading (J/m^2)
G_T	Total energy release rate for crack growth (J/m^2) = $G_I + G_{II}$ in the present investigation
I	Moment of inertia (mm^4)
j	Half length of the end block (13mm in this study)
L	Span of interlaminar fracture specimen (mm)
MC	Moisture Content (%)
P	Load (N)

P_c	Critical load at the onset of the crack propagation (N)
u	Flexural deflection as in Appendix B
W_c	Weight fraction crystallinity (%)
δ	Vertical displacement as in Appendix A (mm)
ρ	Density of unoriented PPS film (g/cm^3)
ρ_a	Density of 100% amorphous PPS (1.31 g/cm^3) [21]
ρ_c	Theoretical density of 100% crystalline PPS from unit cell parameters (1.43 g/cm^3) [21]

CHAPTER I

INTRODUCTION

1.1 General

Composites have in the past been utilized mainly for weight savings in secondary structures. Currently, they are being considered for use as primary load bearing structures. To meet the need for improved damage tolerance in composite structures, designers are looking towards tough resin systems to overcome the poor impact and delamination growth resistance of currently used epoxy resins. Elastomer modified epoxies and new thermoplastics are being developed by manufacturers of composite materials. One of the most exciting thermoplastics is polyphenylene sulfide (PPS).

PPS is an engineering thermoplastic consisting of a polymer backbone that contains disubstituted aromatic rings and divalent sulfur atoms. The polymer is produced [1] by the reaction of paradichlorobenzene and sodium sulfide in a polar solvent at an elevated temperature according to the following reaction:

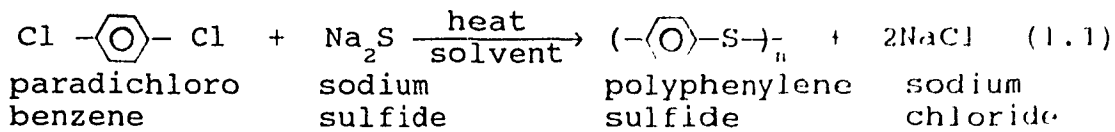

(1.1)

The uncluttered aromatic ring and simple sulfur bonds are remarkably stable. Therefore, PPS exhibits outstanding

high temperature stability, inherent flame resistance, and good chemical resistance. It is essentially insoluble: in fact, no chemical has been found to dissolve it readily below 400°F. Relatively few materials react chemically with PPS even at high temperatures. Its structure also promotes a high degree of crystallinity. Thus, dimensions of molded PPS parts are reproducible and uniform even at high temperatures.

The PPS used as the polymer matrix for high performance composites is a modified polymer [2] in which the polymerization reaction is carried out directly to a high molecular weight. This results in a tough PPS polymer which can be used for injection molding compounds. This polymer has also been used exclusively for long fiber reinforced composites such as random fiber stampable sheets [3], continuous fiber fabric prepregs [4], and unidirectional fiber prepreg tapes. Good descriptions of the processing of the polymer can be found in [5 & 6].

PPS is a semicrystalline polymer with excellent thermal and mechanical properties. It has found widespread use in the electrical, electronic, transportation, appliance and coatings industries in both unreinforced and fiber reinforced forms. Since the PPS polymer matrix does not undergo a chemical curing process during molding, the cycle time for molding is very short. The usual dwell time is 5 minutes.

The full potential of the fiber reinforcement can not be realized due to the random fiber orientation and fiber discontinuity. The recent development of a new, higher molecular weight version of this polymer, followed by its marriage with long fiber reinforcement in composites, has resulted in an even higher performance family of materials. Successful impregnation of continuous high performance fibers has resulted in the production of continuous fiber prepreg tapes containing carbon, aramid and glass reinforcing fibers. These properties make PPS a natural material for certain aerospace and industrial applications.

In summary, PPS composites have:

- High strength
- High stiffness
- Good impact toughness
- High temperature resistance
- Excellent solvent resistance
- Excellent corrosion resistance
- Thermal stability
- Low moisture absorption
- Ease of processing
- Easily controllable, predictable crystallinity
- Faster fabrication rates
- Reduced handling and storage problems
- Improved repairability characteristics
- Capability of fusion bonding
- Short cycle time for molding

- Low smoke generation and flame resistant
- Ability to reuse scraps

1.2 Review of Relevant Literature

Interlaminar cracking, sometimes also called delamination, is one of the most frequently encountered types of damage in advanced composite materials. The presence and growth of interlaminar cracks in composite laminates may lead to severe reliability and safety problems, such as the reduction of structural stiffness, exposure of the interior to adverse environment and disintegration of the material, which may cause the final failure. Thus understanding the basic mechanics of interlaminar cracking is of critical importance in the characterization of flaw criticality and assessment of structural integrity of advanced composite materials and structures.

The ability to resist defect propagation is characterized by a material's fracture toughness. The interlaminar fracture toughness of a composite material is often characterized by the critical strain energy release rate, G_c. A fracture mechanics approach to delamination assumes that fracture occurs when the loading reaches delamination cracking, where the critical energy release rate is equal to or greater than the work required micromechanistically to fracture the material. The stresses

at a delamination crack tip can be decomposed into three components as indicated in Figure 1.1. The critical strain energy release rates are classified as G_{Ic}, G_{IIc} and G_{IIIc} accordingly. Delamination growth in laminated fiber reinforced composite materials consists of three stages, namely, initiation, slow growth and ply separation.

The delamination fracture toughness of a graphite/epoxy composite under various Mode I/Mode II load ratios was investigated experimentally [7]. The critical strain energy release rate was determined by using a double cantilever beam specimen, linear elastic fracture mechanics, linear beam theory, and analysis of an asymmetric loading scheme by superposition of solutions for pure opening and pure bending components. Delamination cracking under Mode II loads traversed entire laminae resulting in considerable fiber breakage and pullout, which accounts for the dramatic increase in initial energy release rate as compared to pure Mode I delamination. The effect of matrix toughness on delamination was studied [8]. It was indicated that the benefits of improved matrix toughness on the composite properties were less under Mode II loading than under Mode I and were reduced further still, or eliminated entirely under Mode II fatigue conditions. Sound experimental evidence has established that the criticality of delaminations in laminated composite structures depends not only on the opening tensile stresses present but rather on the entire out-of-plane tensile/shear (Mode I/Mode II) fracture

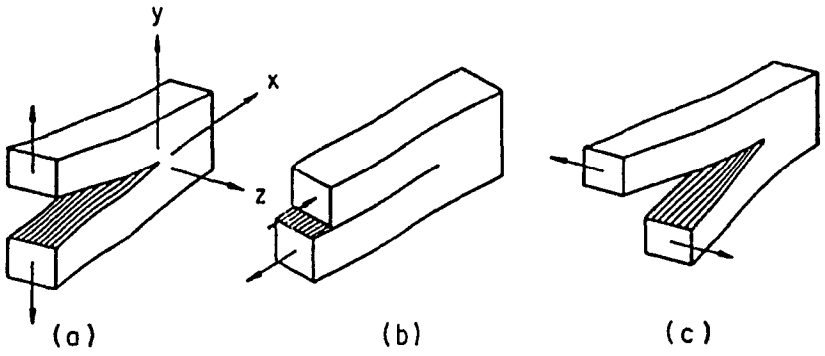

Figure 1.1. Modes of delamination:
(a) Mode I; symmetric loading
(b) Mode II; shear loading
(c) Mode III; antiplane shear loading

a) Double cantilever beam flexure test

b) Edge delamination tensile test (mixed tension/shear)

c) Cracked lap shear test (mixed tension/shear)

d) End-notched flexure test (shear)

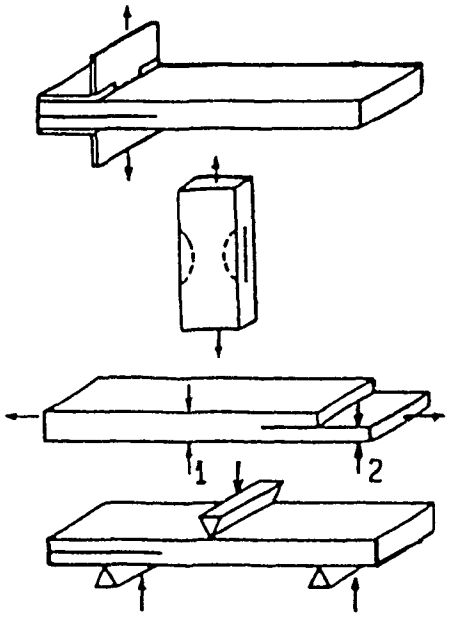

Figure 1.2. Four specimen types used for determination of interlaminar fracture toughness.

envelope. Despite this fact, G_{IIC} is not a parameter that is currently considered when evaluating new matrix-toughened composite materials. The influence of the resin on the mixed-mode fracture was studied [9]. It was shown that high Mode I toughness requires resin dilatation (volume increase). Dilatation is low in unmodified epoxies at room temperature/dry conditions; dilatation is higher in plasticized epoxies, heated epoxies, and in modified epoxies. Modification improves Mode II toughness only slightly compared with Mode I improvements. Mechanisms such as chain extension, crazing, void formation followed by shear band formation, and plasticity can contribute to the volume expansion. Fracture of brittle resins is controlled by the G_{IC} component, whereas fracture of many tough resins is controlled by total strain energy release rate. Loading rate effects on interlaminar fracture toughness were investigated [10 & 11] for graphite/epoxy and graphite/PEEK composites. The results indicated that the toughness of these composites is rate sensitive, and that the interlaminar fracture toughness decreases with increasing loading rate. This decrease was up to 65 percent over the five decades of loading rate employed. A study of moisture content, temperature and ply orientation effects on graphite/epoxy laminates was undertaken by [12]. It was shown that crack extension in Mode I resulted in enhanced fracture energies due primarily to fiber bridging. The maximum or stabilized energy was strongly dependent upon temperature, moisture content and ply orientation in the

delamination plane. Low temperature/dry conditions produced the lowest stabilized fracture toughness whereas the greatest toughness corresponded to hot/wet conditions. Mechanisms of interlaminar fracture in graphite/epoxy systems were investigated [13, 14 & 15]. It was found that interlaminar fracture mechanisms in thermoplastic matrix composites are associated with extensive matrix deformation around the crack tip. A stretching and cavitation process proceeds in the crack tip plastic zone. The extent of matrix deformation depends on the velocity of crack propagation. To increase delamination fracture toughness, both an improved interface and higher resin toughness were found to be required. Increasing Mode II loading, particularly of the more brittle systems, gives a significantly greater resistance to crack propagation as measured by the total energy release rate required to propagate the crack. A comparison of several mechanical tests used to evaluate the toughness of composites was made [16]. Comparisons of composite test data had shown large differences between the various toughness tests, with improvements in one test not necessarily reflected in the others.

Most of these tests are limited to unidirectional laminates where the crack propagates between the plies along the fiber direction. In multidirectional laminates, the crack may have a tendency to branch through the neighboring plies invalidating the coplanar assumption in fracture analysis [17]. Severe edge effects may also occur for

multidirectional laminates.

There are currently four types of tests widely used to measure interlaminar fracture toughness in terms of strain energy release rate G according to [9]. Each specimen type is illustrated in Figure 1.2. Shown first is the double cantilever beam (DCB) specimen, used to determine pure Mode I, pure Mode II or mixed-mode toughness. Second is the edge delamination tension (EDT) test specimen, used to examine a variety of mixed-mode conditions, ranging from $5.7 > G_I/G_{II} > 0.4$, depending on specimen lay-up and geometry. Third is the cracked lap shear (CLS) specimen, which is also used to test a variety of mixed-mode conditions, ranging from $0.6 > G_I/G_{II} > 0.2$, again depending on the specimen geometry. Pure Mode II toughness is found by using the fourth specimen type in the end-notched flexure (EDF) test.

Tensile test is one of the commonly-used methods (even though it might not be the best one) to study the environmental effects on the mechanical properties of a composite material. The resistance of PPS composites in harsh environments has been studied by Vives et al. [18]. In reference [18], PPS composites were subjected to a series of acids, bases, alcohols, aldehydes, ketones, amines, and esters for 24 hours at 93°C. The percent retention of tensile strength was always more than 80% except in the case of 88% formic acid where the percent retention is 75%,

butylamine where the percent retention is 49%, and ethylenediamine where the percent retention is 65%. Even though the thermoplastic material shows good resistance to many chemicals, the resistance of glass-reinforced PPS to the exposure to water is low. At 95°C, a 40% glass reinforced PPS shows a reduction of more than 30% in flexural strength after a five-week exposure period. The same PPS material but unreinforced shows no change in flexural strength with exposure to water.

Most of the work reported to date on delamination fracture of composites has been concerned with the opening mode tensile crack extension in ambient temperature/dry environments. However, predictions based on measurements at a single set of conditions can lead to dangerous overestimate or underestimate of the mechanical properties. To the author's knowledge, no investigations have been made to study the significance of moisture and temperature on the Mode II interlaminar fracture behavior and the tensile strength of the fiber reinforced PPS composites. This fact initiated the following studies.

1.3 Scope of the Present Study

In this thesis, the double cantilever beam (DCB) specimen was used to evaluate Mode II interlaminar fracture toughness of the carbon/PPS laminate under a variety of temperature/relative humidity conditions. The effect of

exposure to 100°C and 95% relative humidity on the tensile strengths of the glass/PPS composites (both short and long fibers) was also examined. Scope of the present study is summarized as follows:

1. Differential scanning calorimetry (DSC) tests of the carbon/PPS prepreg, the glass/PPS composites and the molded carbon/PPS laminate;
2. Moisture absorption behavior of the PPS composites;
3. Load-displacement behavior of the carbon/PPS laminate under different hygrothermal conditions;
4 Stress-strain behavior of the glass/PPS composites at different moisture content levels for 95% relative humidity at 100°C;
5. Mode II critical strain energy release rate of the carbon/PPS laminate at different moisture content levels with the variation of temperature;
6. Tensile strengths of the glass/PPS composites at different moisture contents for 95% at 100°C;
7. Observation by scanning electron microscopy (SEM) of the fracture surfaces and the planar view of the carbon/PPS laminates, and of the failed samples of the glass/PPS composites to study the failure modes of these PPS composites.

CHAPTER II

DESCRIPTION OF THE MATERIALS

2.1 Material Properties

The materials used in the present investigation were supplied from Phillips Petroleum Company. Carbon/PPS prepreg (AC40-66), glass/PPS mat-reinforced stampable sheets (AG11-20 and AG20-40), glass/PPS fabric-reinforced composites (AG31-60 and AG31-40), and glass/PPS injection-molded composites (R-4, R-7, A-100 and A-200) were received.

The nominal properties of the carbon/PPS composite are shown in Table 2.1. Hercules AS-4 carbon fiber rovings containing 12000 filament counts were used to make a prepreg tape 4 inch (100mm) wide and 0.008 inch (0.2mm) thick. The prepreg contains 66% by weight carbon fibers. The diameter of the carbon fiber is 8 μm.

Table 2.1. Nominal properties of the carbon/PPS composite.

Property	ASTM Test	AC40-66 (Unidirectional)
Void Content, Vol.(%)		<1
Tensile Modulus (MSI)	D-3039	19.6
Tensile Strength (KSI)	D-3039	240
Flexural Modulus (MSI)	D-790	18
Flexural Strength (KSI)	D-790	190
Compressive Modulus (MSI)	D-3410 (IITRI)	21
Compressive Strength (MSI)	D-3410 (IITRI)	95
Short Beam Shear (KSI)	D-2344	10

* Source: company literature.

A summary of the characteristics of the as-received glass/PPS composites is shown in Table 2.2.

Table 2.2. Glass/PPS composites tested (as-received).

Composites	E-Glass (%)	Fiber Length	Mineral Filled	Sheet Thickness (mm)
		Injection-molded		
R-4	40	Short	No	3.00
R-7	40	Short	Yes	3.05
A-100	40	Short	No	3.00
A-200	40	Short	No	3.00
		Advanced composites		
AG31-60	60	Long fabric	N/A	0.378
AG31-40	40	Long fabric	N/A	0.378
AG11-20	20	25.4mm chopped	N/A	1.650
AG20-40	40	25.4mm chopped	N/A	1.670

The as-received PPS materials were subjected to differential scanning calorimetry (DSC) tests to determine their glass transition temperature (T_g), melting temperature (T_m) and latent heat of melting. The determination of T_g was carried out according to ASTM D3418 on a Dupont 910 differential scanning calorimeter at a heating rate of 20°C/minute in a nitrogen atmosphere with the temperature ranging from 30 to 330°C for the first run and from 30 to 180°C for the second run.

The first run of AC40-66 prepreg, as shown in Figure 2.1, was performed in order to erase any previous thermal history. Each sample was cooled with liquid nitrogen after the first run. T_g was determined to be 90.8°C by extrapolation as shown in Figure 2.2 in the second run. The

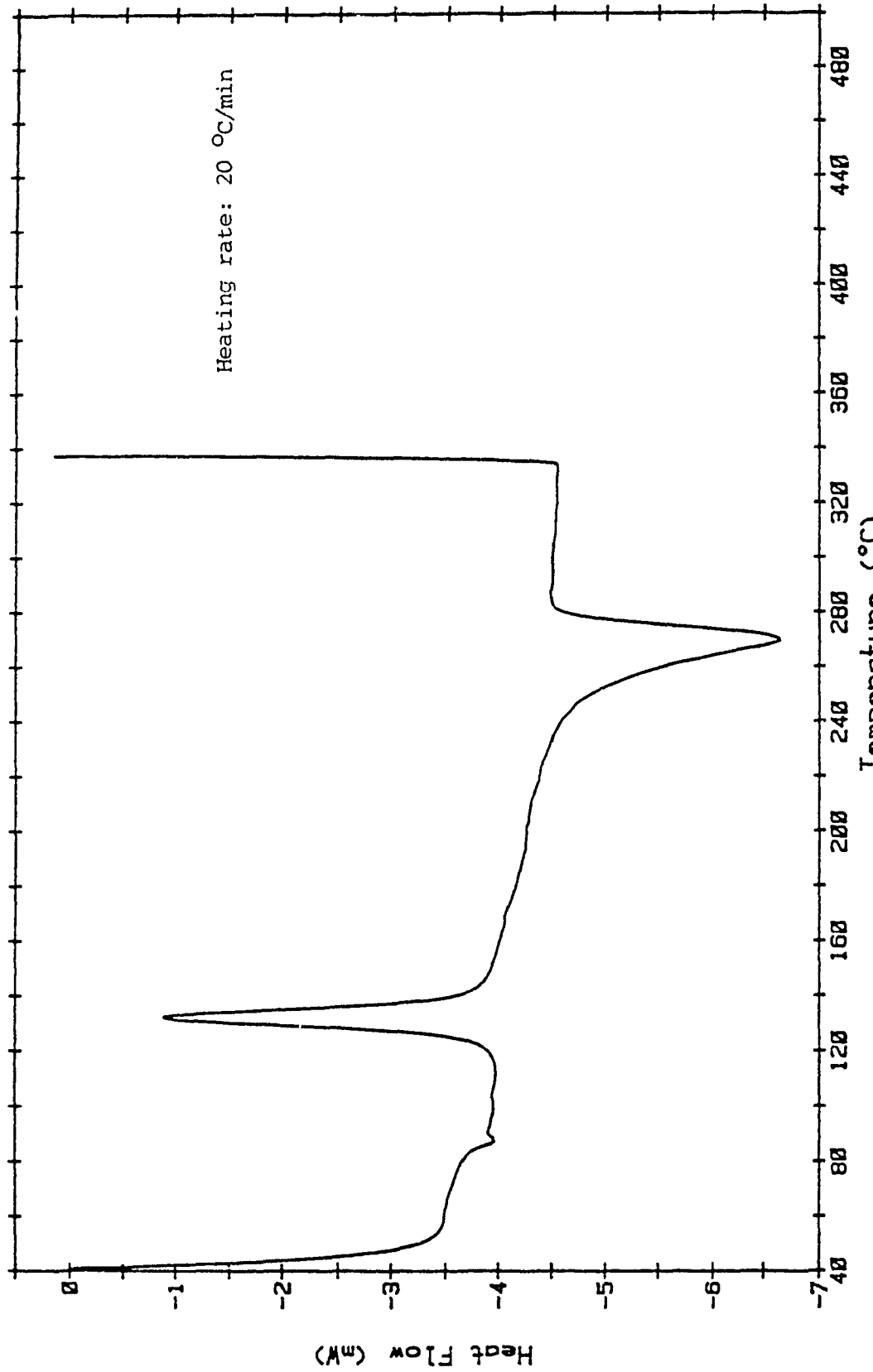

Figure 2.1. DSC test of AC40-66 prepreg - first run (as-received).

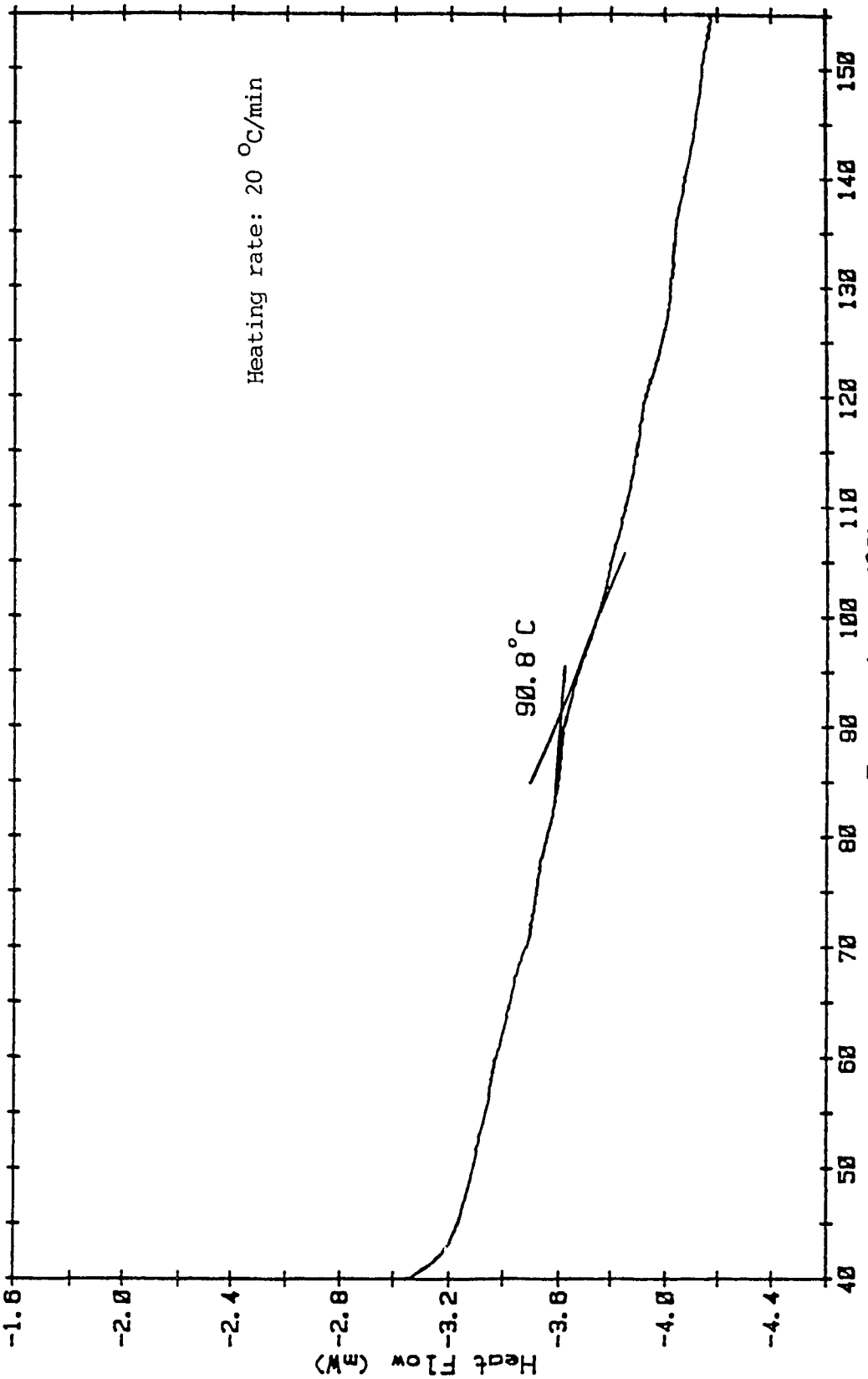

Figure 2.2. DSC test of AC40-66 prepreg - second run (as-received).

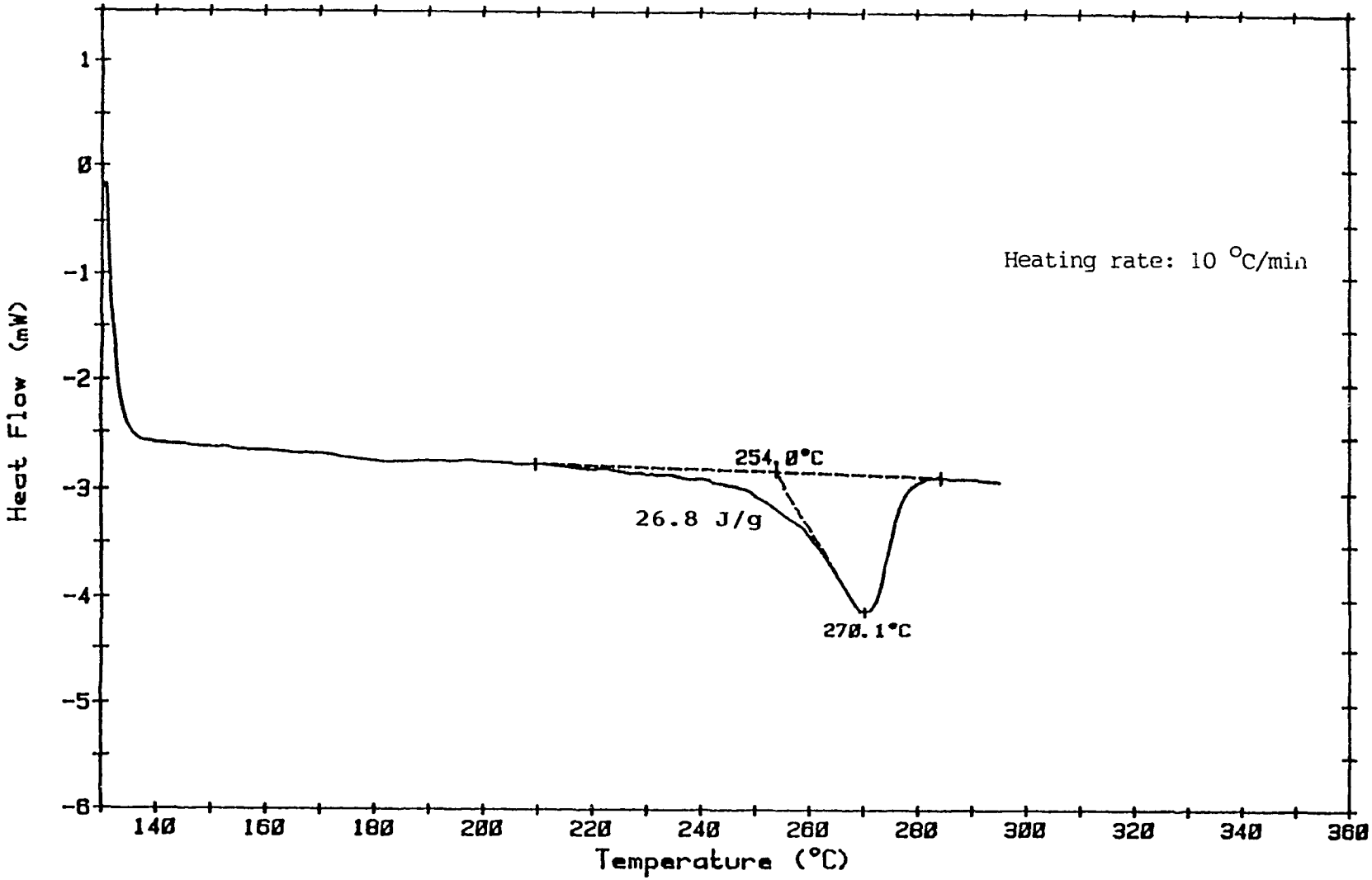

Figure 2.3. Melting temperature and latent heat of melting of AC40-66 prepreg (as-received).

determination of melting temperature and latent heat of melting of AC40-66 prepreg was done according to ASTM D3418 and D3417 at a heating rate of 10°C/minute in a nitrogen atmosphere. The onset of melting temperature on the flow rate-temperature curve was observed by extrapolation to be 254.0°C. The final melting temperature was determined to be 270.1°C and the latent heat of melting was determined to be 26.8 J/g as can be seen from Figure 2.3. The DSC results of the as-received carbon/PPS prepreg are summarized in Table 2.3.

Table 2.3. DSC results of AC40-66 prepreg (as-received).

	Specimen		
	#1	#2	#3
Glass transition temperature (°C)	91.0	90.8	---
Onset melting point (°C)	253.0	254.0	252.9
Final melting point (°C)	269.8	270.1	270.8
Latent heat of melting (J/g)	26.1	26.8	27.7

It must be noted that an exothermic peak was observed to occur in the first run in the range of temperature from 120 to 160°C as shown in Figure 2.1. According to Kays and Hunter [19], this exothermic peak indicates that some further crystallization was taking place and that the material was not as crystallized as possible. As demonstrated in [19], a semicrystalline polymer that has been quenched into the amorphous state will have a large step-change thermal transition at the glass transition temperature (T_g), followed by a crystallization exotherm,

and finally melting. The large transition at T_g followed by the crystallization exotherm at 120°C indicates that the matrix is largely amorphous.

Similar DSC tests were performed on the glass/PPS composites. The first run and second run for the AG31-60 and the AG31-40 samples are shown in Figures 2.4 to 2.7. A summary of the DSC tests of the glass/PPS composites is shown in Table 2.4. Once again, an exothermic peak was observed in the first run for the AG31-60 sample. This lack of crystallinity in the AG31-60 samples caused a large reduction in tensile strength of the samples exposed to hot-moist condition, which will be shown in Chapter IV.

Table 2.4. DSC results of the glass/PPS composites (as-received).

	Specimen			
	AG31-60	AG31-40	AG11-20	AG20-40
Loss in weight (%)	0.18	0.21	0.51	0.35
Glass transition temperature (°C)	90.5	93.0	90.1	91.5
Onset melting point (°C)	259.0	259.9	259.2	259.1
Final melting point (°C)	276.7	276.8	276.4	276.8

The crystallinity of a matrix can be established from the following equation [21]

$$W_c = \frac{\rho_c}{\rho} \frac{(\rho - \rho_a)}{(\rho_c - \rho_a)} = \text{weight fraction crystallinity} \qquad (2.1)$$

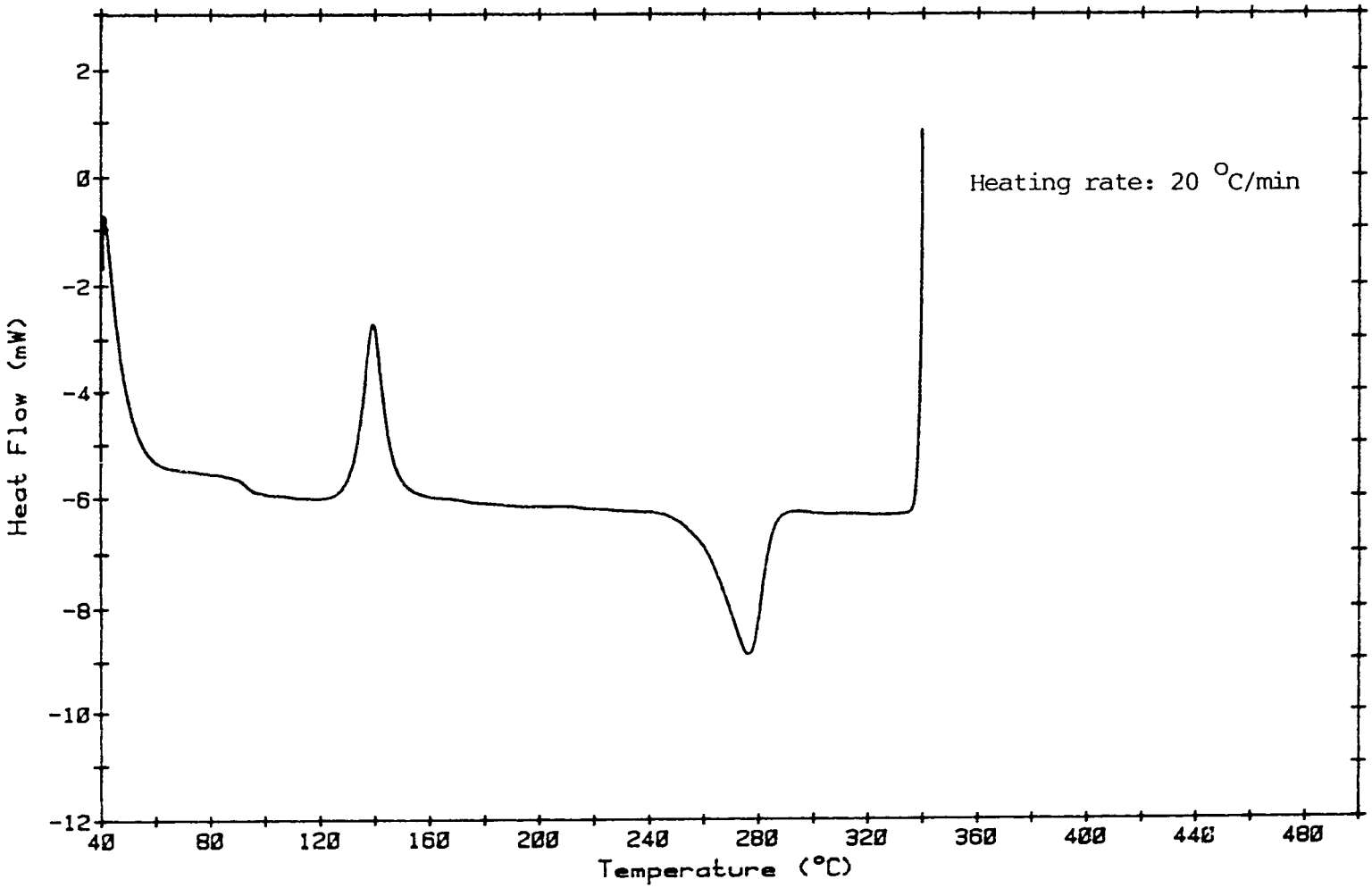

Figure 2.4. DSC curve, the first run for AG31-60 (as-received).

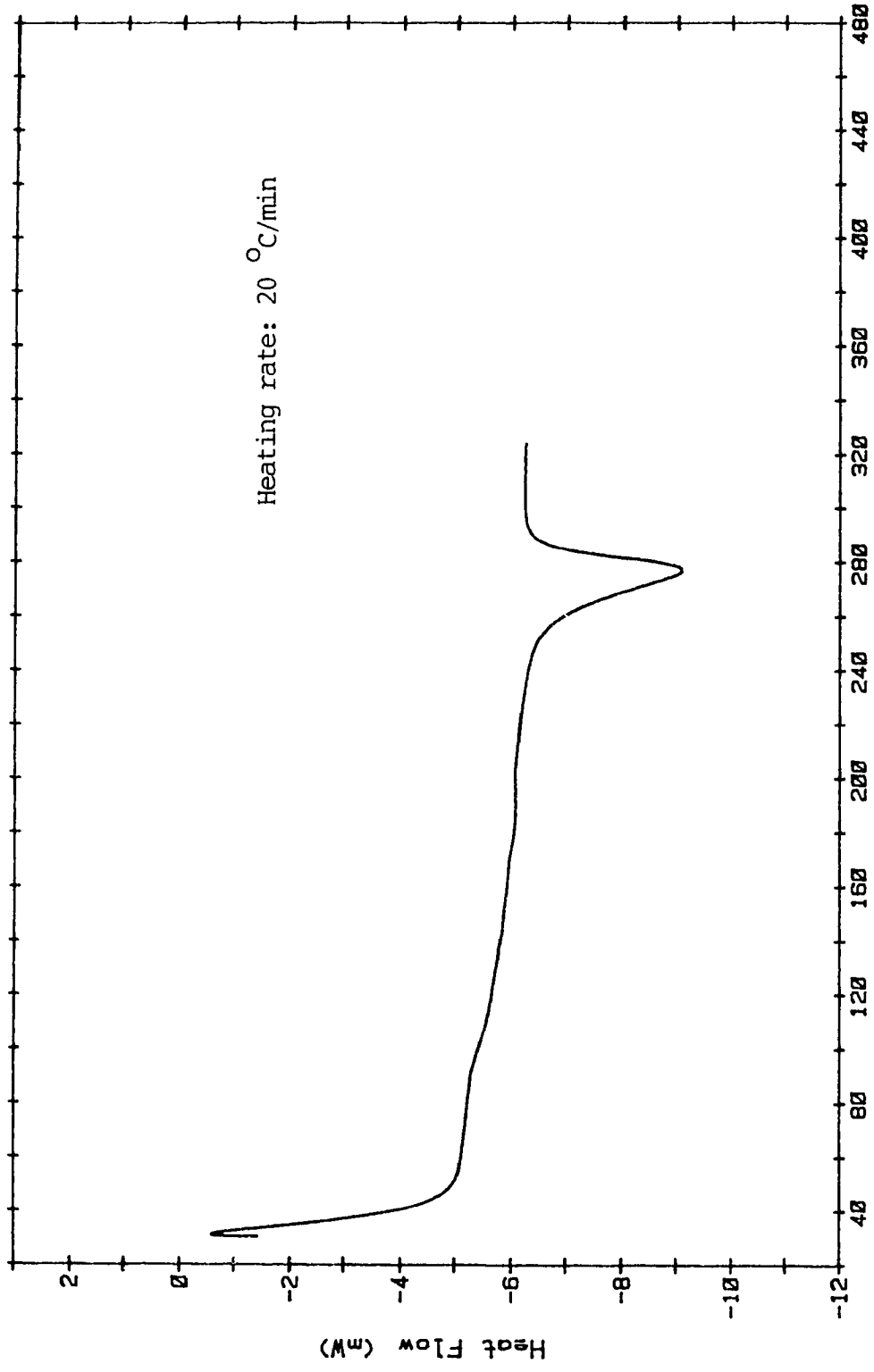

Figure 2.5. DSC curve, the second run for AG31-60 (as-received).

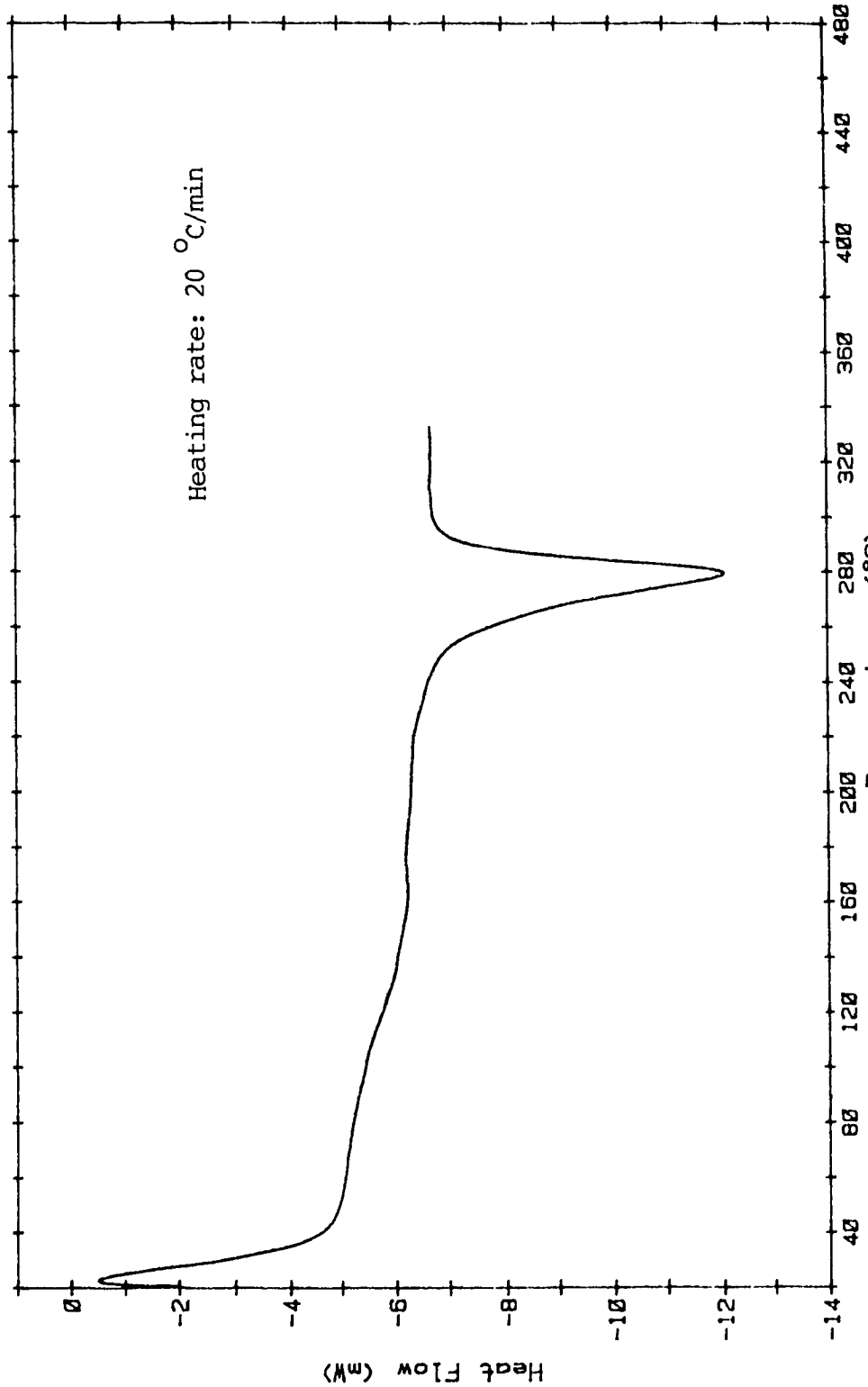

Figure 2.6. DSC curve, the first run for AG31-40 (as-received).

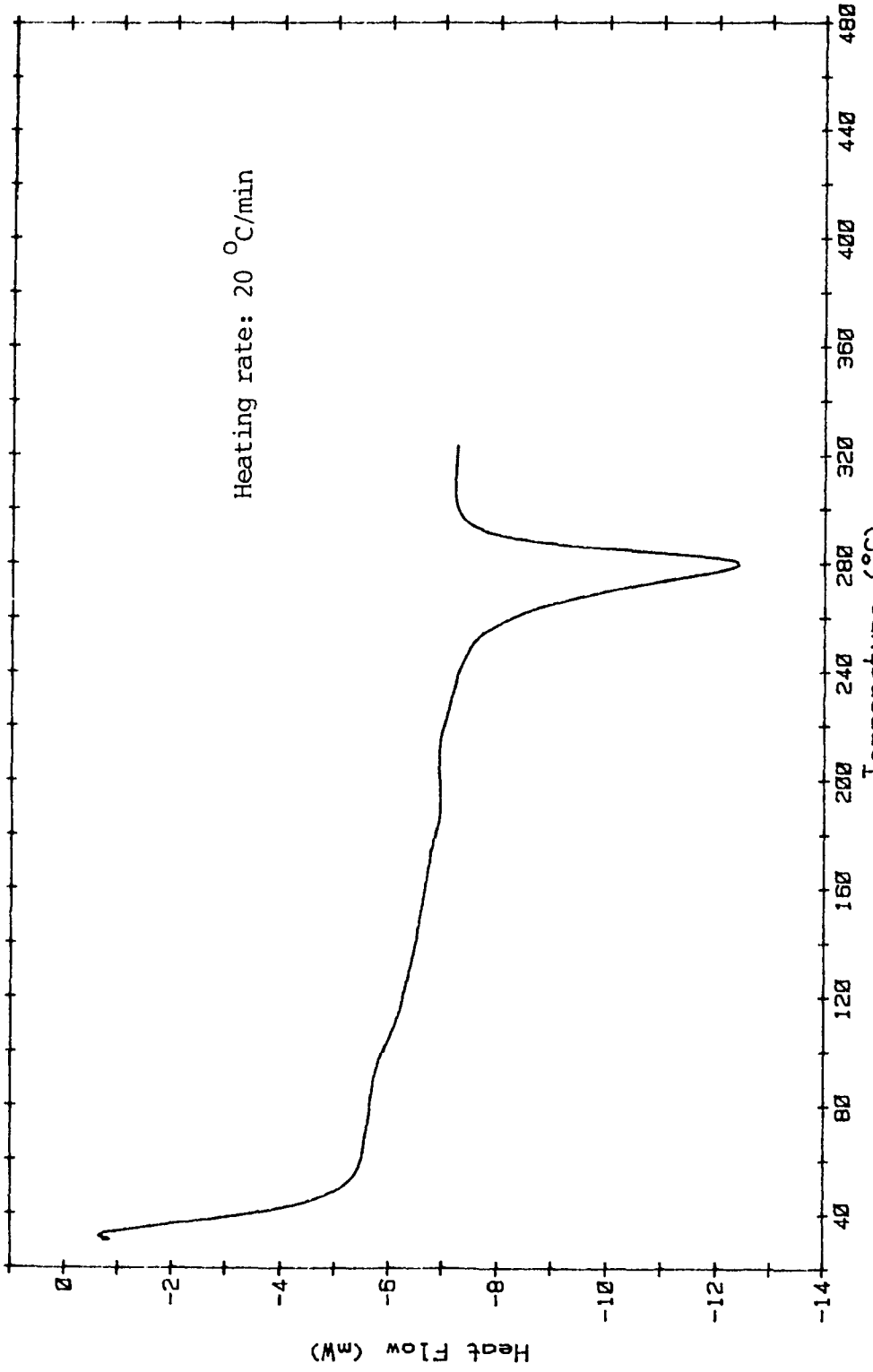

Figure 2.7. DSC curve, the second run for AG31-40 (as-received).

The density of 100% amorphous matrix, ρ_a, and the theoretical density of 100% crystalline matrix, ρ_c, can be obtained from unit cell parameters. Therefore, if the actual density of a matrix, ρ, is known, the crystallinity of the matrix can be obtained by the above equation.

Above their melting temperature (T_m), crystallizable resins are in an amorphous state. Below their glass transition temperature (T_g), crystallization occurs at a very slow rate. Most crystalline polymers will remain nearly completely amorphous when quenched in water from the melt. One way for achieving crystallinity in polymers is to anneal the amorphous film at temperatures between T_g and T_m. According to Mascia [20], as crystallization proceeds the spherulites will eventually touch each other and, as a result, the uncrystallized polymer chains at the boundaries will find it increasingly more difficult to diffuse to the surface of existing crystals or to nucleate into new crystallites. If after crystallization the polymer is heated to temperatures just below the true melting point, some partial melting of the least perfect crystals takes place. The stable crystals, however, will continue to grow into thicker lamellae and a higher level of crystallinity is developed.

Crystallites have a marked influence on material properties. It is not unexpected, therefore, that the melting of the crystallites changes the properties abruptly

and that the temperature at which this occurs sets an upper limit to the working range of most crystalline plastics. The crystallites of plastic materials vary in size and perfection, depending on local variations in molecular structure such as chain branching and on the previous thermal history of the sample. For these reasons, the melting of such crystallites is not a single catastrophic phenomenon occurring over a very narrow temperature range, as is the case for crystals of low molecular weight organic compounds, but a process that takes place progressively with increasing temperature.

In order to gain the maximum crystallinity in the PPS samples, proper molding and annealing of the prepregs are necessary.

2.2 Molding of the Carbon/PPS Prepreg

The extent and type of crystallinity depend primarily on the molding conditions. To assist the molders of carbon/PPS prepreg, a study was designed to determine the optimum molding conditions [21]. The following molding procedure is based on this study.

Composite laminate of 152mm by 150mm was fabricated by the following steps. First, the as-received prepreg (100mm in width) was cut into sizes of 152mm x 100mm and 152mm x 50mm, respectively. Second, the 100mm wide prepreg was

tacked to a 50mm wide prepreg by using a hot soldering iron. It was found [13] that thicker laminates are better suited for testing interlaminar fracture toughness of thermoplastic matrix composites. In the present investigation, 24 plies of prepreg were stacked unidirectionally and the corners tacked to give a prepreg laminate. A teflon tape of 0.0508mm (0.002 inch) thick, 35mm wide and 152mm (6 inch) long, was placed between the central laminae for the purpose of crack initiation. The limit temperature of the teflon tape is 400°C for continuous exposure and 427°C for 30 minutes, respectively. The teflon tape was found to be in intact condition (non-melting) in the molded laminates for the present molding temperature. The stacked prepregs were put into a steel mold of 6 x 6 inch. The mold was then placed between two preheated platens of a platen press at 316°C. Heat was transferred from the two platens to the mold and to the material by conduction.

A thermocouple was put near the internal wall of the mold, and another one was put between the central plies of the laminate to monitor the temperatures of the molding. As indicated in Figure 2.8, the maximum temperature difference of the laminate and the internal wall of the mold was about 3 to 5°C, which shows a fairly good temperature distribution over the material. Contact pressure of 5 psi (0.034 MPa) was applied for 16 minutes until the temperature of the laminate reached 310°C followed by a pressure of 1.0 MPa for additional 3 minutes. During this 3-minute period, the

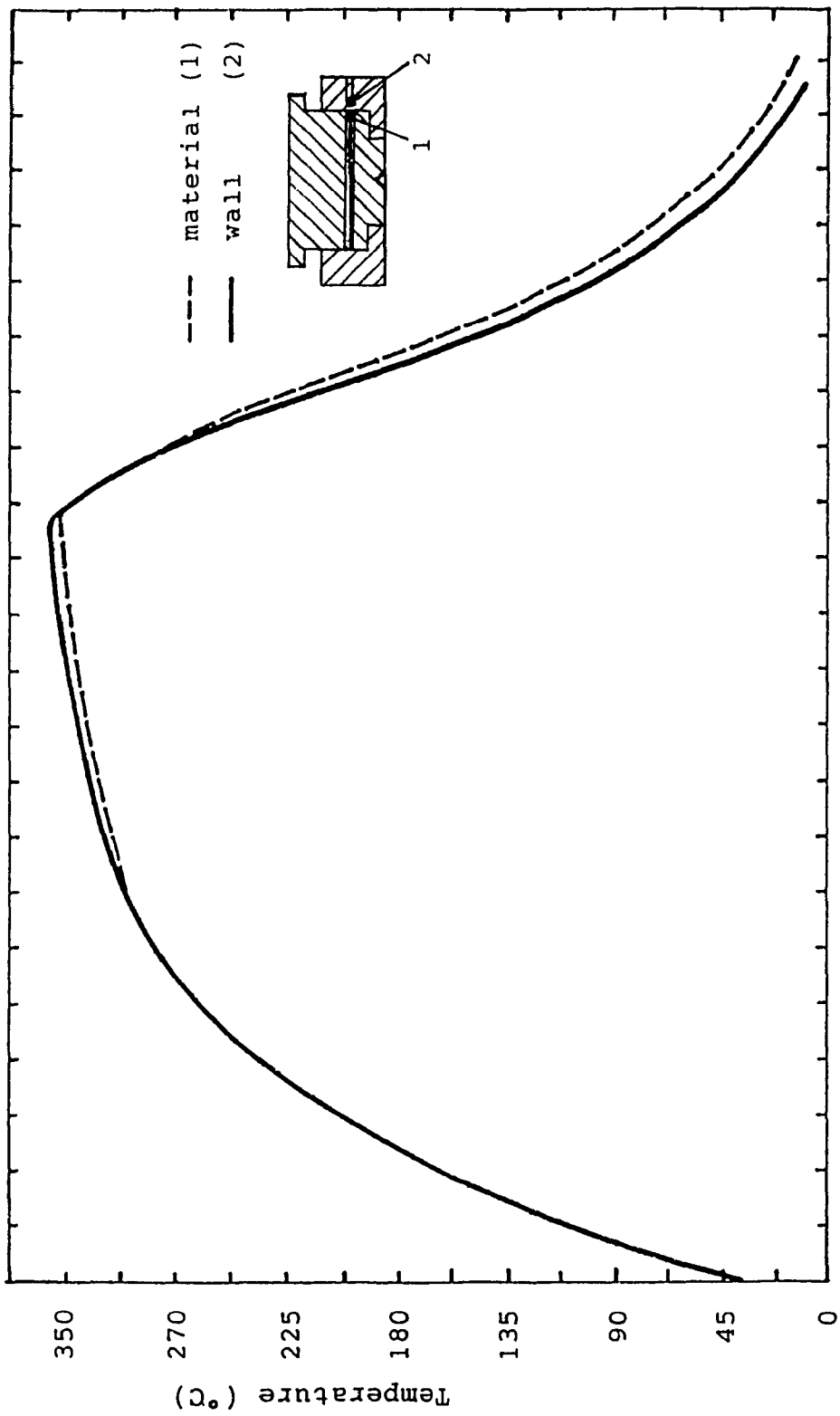

Figure 2.8. Thermal cycle for the molding of AC40-66 laminates.

temperature reached about 316°C. The hot laminate was then cooled under the pressure of 1.0 MPa to 38°C in 18 minutes by cooling the two platens with a mixture of water and air (two-phase flow). The cooling rate can be controlled by adjusting the flow rates of the cooling water and air. It was, however, held constant in the present investigation.

The platen press, made by Wabash Metal Products, Inc., shown in Figure 2.9, has a maximum load of 100 tons and its maximum temperature can be up to 599°C. All the steps in the above molding procedure were pre-programmed and performed automatically by the machine.

The molded laminate was trimmed and cut into specimens of 152mm long, 25mm wide (as B in the Nomenclature), and 3.84mm thick (as 2D). The initial starter crack length is about 35mm (as a_o). Annealing was accomplished by subjecting the laminate to a temperature of 200°C, which is between T_g and T_m as listed in Table 2.3, for a period of 2 hours in the environmental chamber as shown in Figure 2.10. This gives small crystallites for the PPS morphology. The matrix is fully crystallized. The differential scanning calorimetry trace of annealed sample shows only a small change at T_g, T_m and latent heat of melting and the absence of any crystallization exotherm as indicated in Figures 2.11, 2.12 and 2.13. The DSC results of the annealed samples are listed in Table 2.5.

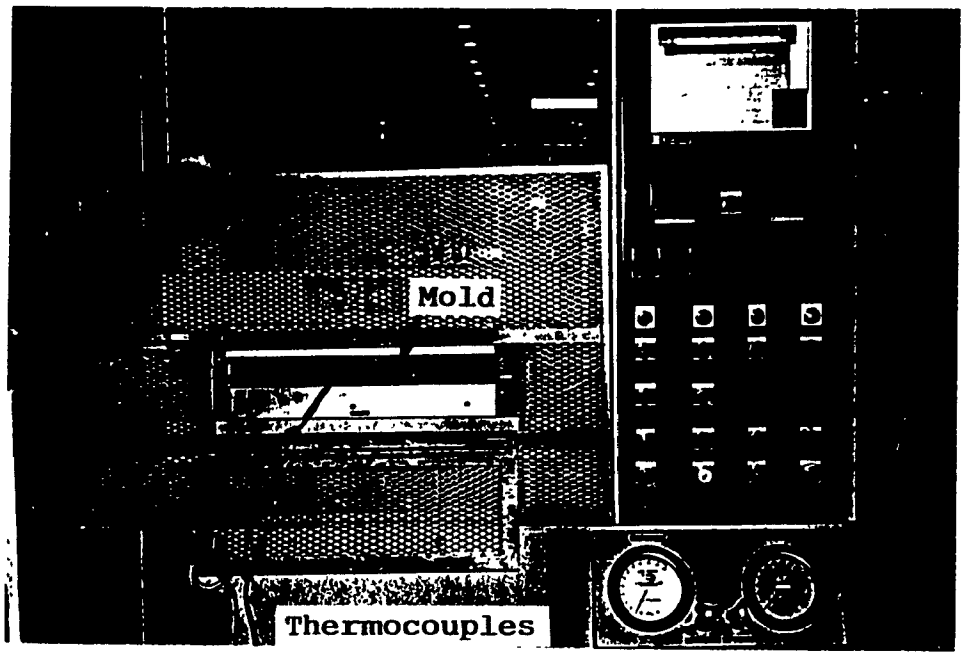

Figure 2.9. Platen press.

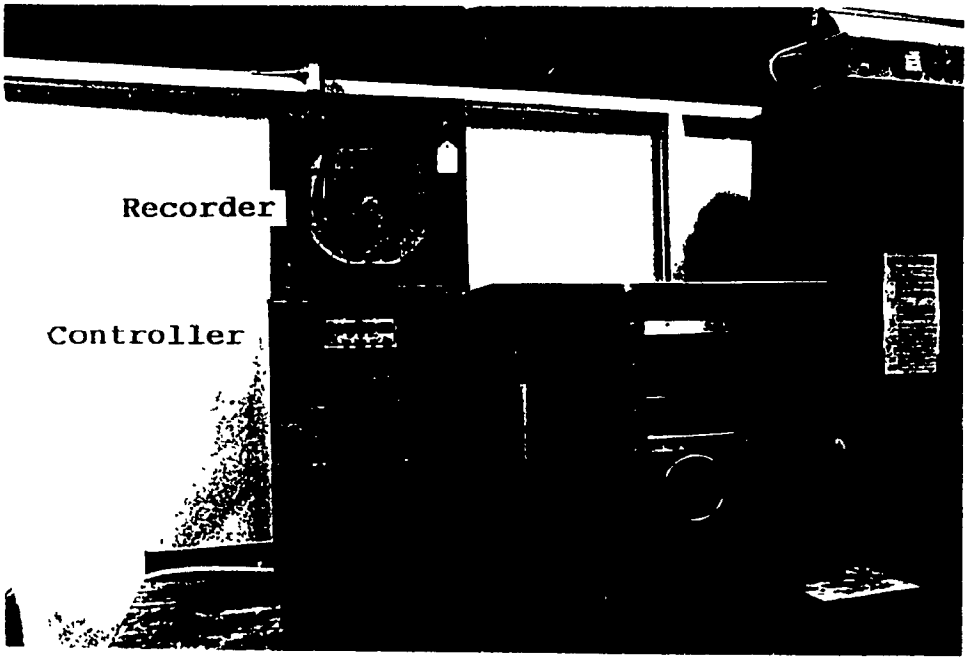

Figure 2.10. Environmental chamber.

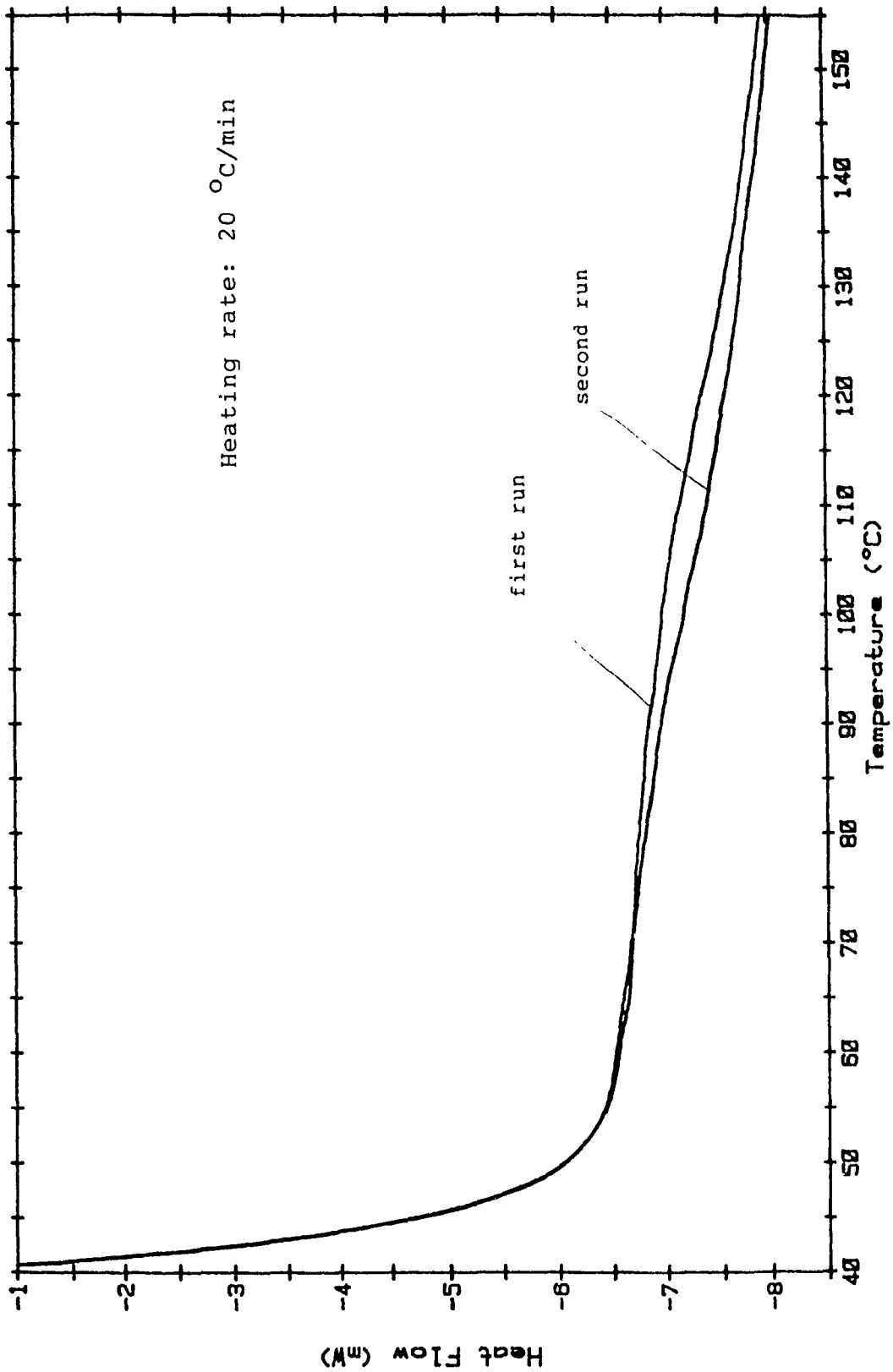

Figure 2.11. DSC test of AC40-66 laminate - first run (annealed).

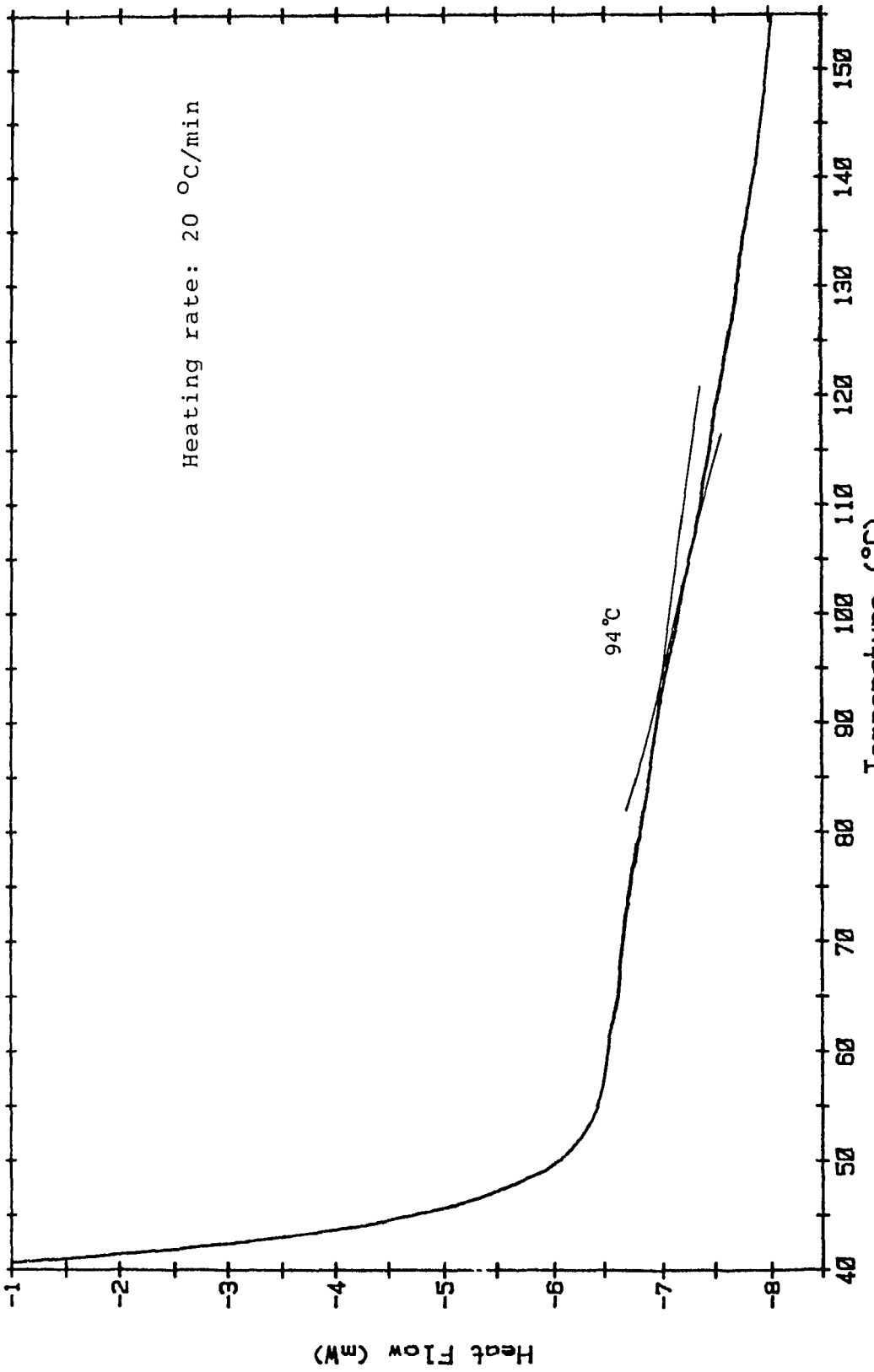

Figure 2.12. DSC test of AC40-66 laminate - second run (annealed).

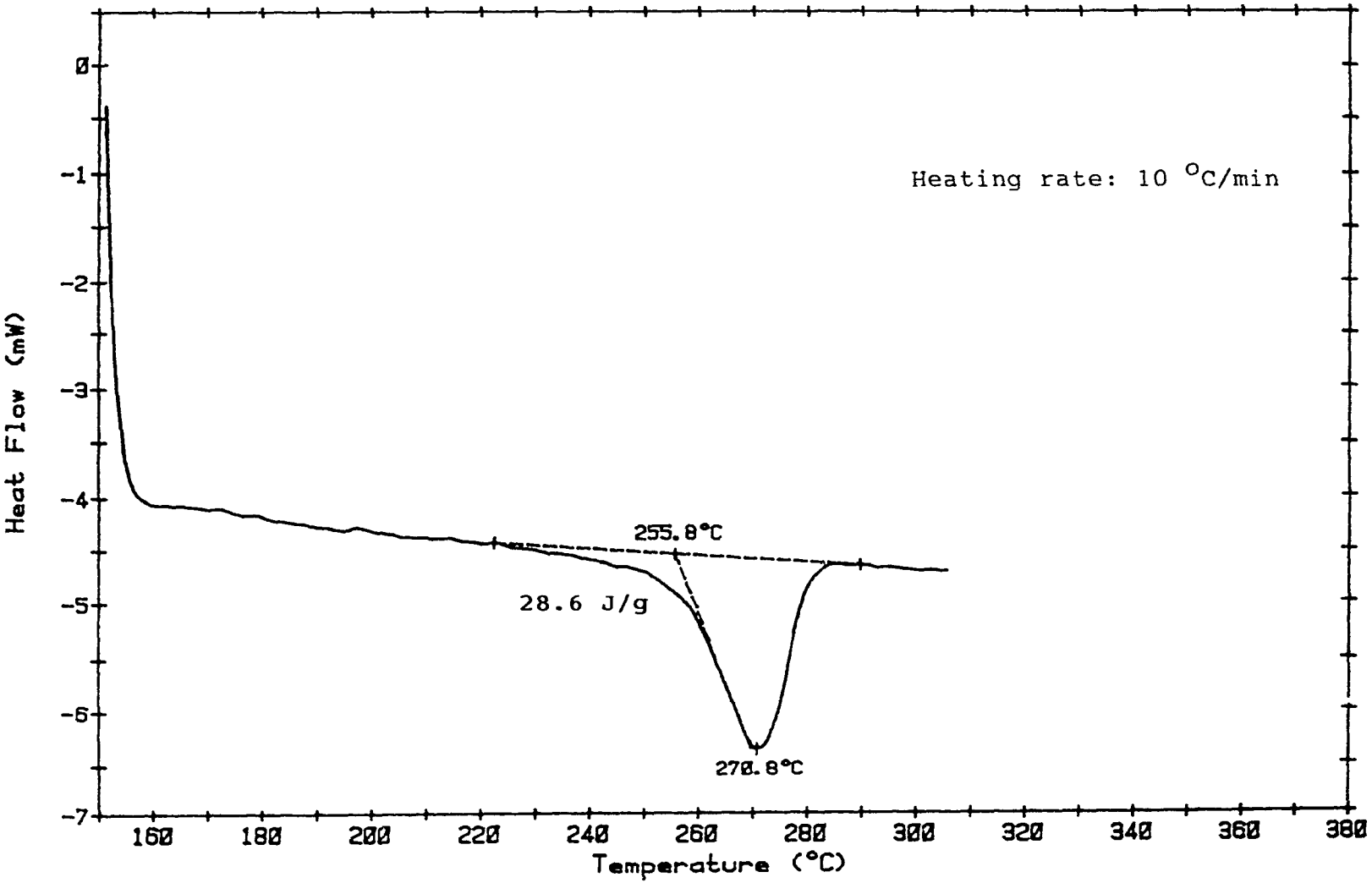

Figure 2.13. Melting temperature and latent heat of melting of AC40-66 laminate (annealed).

Table 2.5. DSC results of AC40-66 laminate (annealed).

	Virgin	87°C	127°C
Glass transition temperature (°C)	94.0	90.5	87.0
Inflexion point (°C)	106.5	102.4	98.2
Onset melting point (°C)	255.8	256.2	253.1
Final melting point (°C)	270.8	270.9	271.3
Latent heat of melting (J/g)	28.6	33.0	47.5

2.3 Molding of the Mat-Reinforced Stampable Sheets

An infrared oven was used to preheat the samples (AG11-20 and AG20-40) and the molding was done on a press where the pressure can be controlled. The as-received sheets were cut into required blanks and put into the infrared oven in which the temperature was monitored and controlled within the range of 320±10°C by a microcomputer-based controller. Heat by radiation was supplied from a single side. The smooth blanks became rough textured on one side in about 9 minutes and then were turned over to be heated from the other side for about 6 minutes. The totally rough textured blanks were taken out of the infrared oven and quickly stacked together and transferred to a nearby press where the blanks were held under a hydraulic pressure of 200 bars as suggested by the company. The molded part was cooled from about 300°C to the room temperature of 24°C in 11 minutes (25°C/minute) to retain its shape.

2.4 Molding of the Fabric-Reinforced Prepregs

The as-received prepregs (AG31-60 and AG31-40) were cut into required sizes and stacked one layer over another first before being put into the infrared oven. Since they were so thin that sufficient heat could easily penetrate several layers (four layers were stacked in this investigation) from one side, there was no need to turn them over. Besides, such turning-over will alter the shape of the molded part. The temperature was controlled within the range of 330±10°C. The prepregs were heated for 12 minutes and then taken out of the heating system and quickly transferred to the press, where they were held under a hydraulic pressure of 200 bars. The molded part was cooled from 300°C to room temperature of 24°C in 10 minutes (27°C/minute) to retain its shape.

CHAPTER III

DATA REDUCTION AND EXPERIMENTAL PROCEDURES

3.1 DATA REDUCTION

A specially designed test fixture for the study of Mode II interlaminar fracture toughness is shown in Figure 3.1. As the crack grows between the central plies of the specimen, energy is released since the cracked section is more compliant than the uncracked.

The small displacement solution for the end notched double cantilever beam (without the end block) may be deduced from the compliance [Appendix A],

$$C = \frac{\delta}{P} = \frac{1}{2EBD^3}\,(3a^3 + L^3) \tag{3.1}$$

The strain energy release rate can be obtained from [Appendix B]

$$G_{II} = \frac{P^2}{2}\,\frac{\partial C}{\partial A} = \frac{P^2}{2B}\,\frac{dC}{da} = \frac{9}{4}\,\frac{P^2a^2}{EB^2D^3} \tag{3.2}$$

The experimental compliance technique was not used here because of the fact that experimental dC/da values are usually found to be subject to large errors due to the small variation in C with a at small a values [12].

The small displacement end block result is

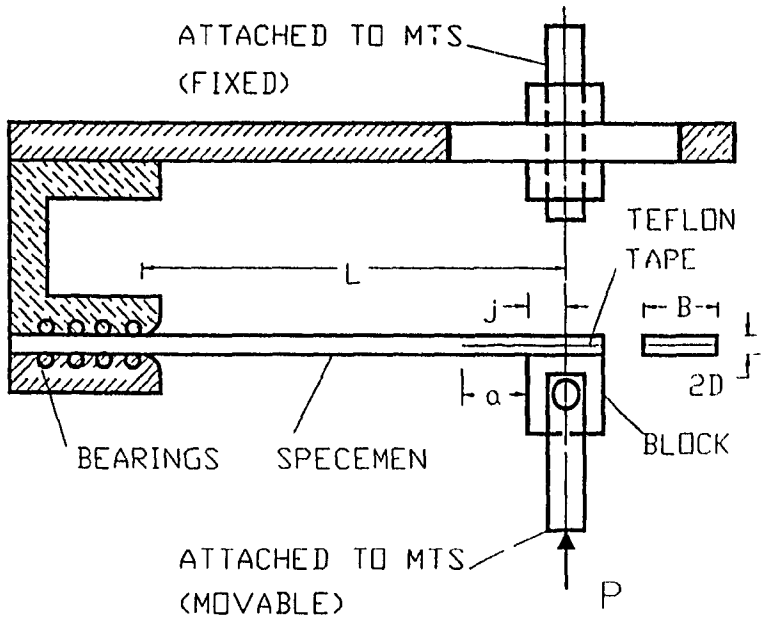

Figure 3.1. Interlaminar fracture test fixture.

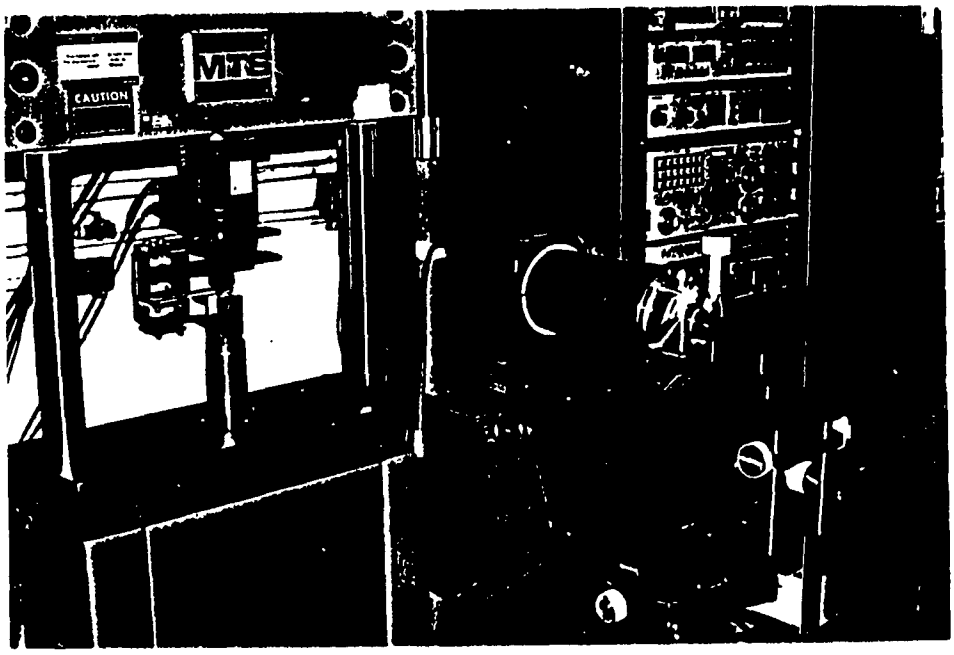

Figure 3.2. Experimental set-up.

$$G_{II} = \frac{9}{4} \frac{P^2(a + j)^2}{EB^2D^3} \tag{3.3}$$

Note that (a + j) in Figure 3.1 is equal to (a) in Appendix A. The critical strain energy release rate, G_{IIC}, can then be obtained from Equation (3.3) by replacing P with P_c, the critical load at the onset of the crack propagation.

The above is the well known linear beam theory. According to [7], nonlinear beam theory gives significantly different predictions from linear beam theory when large deflections and rotations occur. It was found that significant departures from linear predictions occur when

$$\delta/a > 0.4 \tag{3.4}$$

Fortunately, the ratio of the flexural deflection to the crack length, δ/a, was found to be much less than 0.4 for all the Mode II interlaminar fracture tests of the carbon/PPS laminates. Furthermore, the load-displacement curves of these laminates were found to be basically linear except for a few cases. Therefore, the linear beam theory was employed in the present investigation to determine the Mode II critical strain energy release rate, G_{IIC}, of the carbon/PPS laminates. The values of G_{IIC} were also compared to those obtained by the area method to be explained below to validate the application of the linear beam theory in the present investigation.

The area method, whereby the area under a load-displacement record for loading, crack advance from a_1 to a_2, and unloading is determined by integrating and assumed to be equal to the work required to increase the crack area by $B(a_2 - a_1)$. This method assumes that all the work represented by the area bounded by the load, crack advance, unload-displacement curve goes into crack advance. Any far field energy dissipation would erroneously be lumped into the energy absorbed per unit area of crack extension relationship [15].

Another way to correlate the non-linear fracture test data when the flexural deflection is large in both Mode I and Mode II cases is to introduce some correction factor [22].

Tensile tests of the glass/PPS composites were done according to ASTM standard D-3039.

3.2 Stability Analysis of Crack Growth in DCB Specimen Under Mode II Loading

The stability of crack growth may be judged from the sign of dG_{II}/da. Stable crack growth requires dG_{II}/da to be less or equal to zero

$$dG_{II}/da \leq 0 \qquad (3.5)$$

For the present DCB specimen under fixed load condition (load control) dG_{II}/da is obtained from Equation (3.2) as

$$\frac{dG_{II}}{da} = \frac{9P^2a}{2EB^2D^3} \tag{3.6}$$

This quantity is always positive and thus the crack growth is unstable.

For fixed grip condition (displacement control), dG_{II}/da can be obtained after substitution of $P = \delta/C$ into Equation (3.2) and differentiation,

$$\frac{dG_{II}}{da} = \frac{d}{da}\left(\frac{\delta^2}{2BC^2}\frac{dC}{da}\right) = \frac{-\delta^2}{2B}\frac{d^2}{da^2}\left(\frac{1}{C}\right)$$

$$= \frac{\delta^2}{2B}\left[\frac{1}{C^2}\frac{d^2C}{da^2} - \frac{2}{C^3}\left(\frac{dC}{da}\right)^2\right] \tag{3.7}$$

From Equation (3.1),

$$\frac{dC}{da} = \frac{9a^2}{2EBD^3} \tag{3.8}$$

$$\frac{d^2C}{da^2} = \frac{9a}{EBD^3} \tag{3.9}$$

Substitution of Equations (3.8) and (3.9) into Equation (3.7) and rearrangement of Equation (3.7) give

$$\frac{dG_{II}}{da} = \frac{9a\delta^2}{2C^2EB^2D^3}\left(1 - \frac{9a^3}{2CEBD^3}\right)$$

$$= \frac{9a\delta^2}{2C^2EB^2D^3}\left(1 - \frac{9a^3}{3a^3 + L^3}\right) \tag{3.10}$$

For stable crack growth dG_{II}/da has to be less than or

equal to zero. Equation (3.10) gives

$$a/L \geq 1/\sqrt[3]{6} \approx 0.55 \qquad (3.11)$$

In comparison to the case of the End Notched Flexure (ENF) specimen [26] where $a/L \geq 1/\sqrt[3]{3} \approx 0.69$ in order for the crack growth to be stable, the present DCB specimen reaches stable crack growth in a shorter distance.

All the Mode II interlaminar fracture tests were therefore performed under fixed grip condition (displacement control) instead of fixed load condition. This renders the crack growth stable after the crack propagates just more than half of the the span, L.

3.3 Preparation of Interlaminar Fracture Test Specimens

Specimens for interlaminar fracture test were cut from the molded laminates with a water-cooled diamond blade cutoff saw. The edge of the specimen was polished and painted white for better tracking of the crack propagation during the test. The experiment scheme is shown in Table 3.1.

Table 3.1. Interlaminar fracture experiment scheme.

Hygrothermal Condition: (87°C/84%)			
Specimen Numbering			Exposure Time
A111	A112	A113	Dry condition
A121	A122	A123	25 hours
A131	A132	A133	225 hours
A141	A142	A143	312 hour
Hygrothermal Condition: (87°C/95%)			
Specimen Numbering			Exposure Time
A211	A212	A213	116 hours
A221	A222	A223	226 hours
A241	A242	A243	320 hours
Hygrothermal Condition: (127°C/84%)			
Specimen Numbering			Exposure Time
B111	B112	B113	Dry condition
B121	B122	B123	73 hours
B131	B132	B133	230 hours
B141	B142	B143	336 hours
Hygrothermal Condition: (127°C/95%)			
Specimen Numbering			Exposure Time
B221	B222	B223	60 hours
B231	B232	B233	228 hours
B241	B242	B243	336 hours

3.4 Specimen Testing of the Carbon/PPS Laminate

Twelve specimens of the same geometry were put in an environmental chamber for each of the four hygrothermal conditions: 87°C/84%, 87°C/95%, 127°C/84% and 127°C/95%. The behavior of moisture absorption of the laminate was studied by weighing the last three specimens at regular time. Three specimens were taken out of the environmental chamber at certain time interval, weighed and tested on an MTS machine using the test fixture shown in Figure 3.1.

The experimental set-up is shown in Figure 3.2. The

cross head speed of the MTS machine was set at 3mm/minute in displacement control as discussed in Section 3.2. Mode II interlaminar fracture tests were performed by loading the cracked end of the specimen. Some flat bearings were embedded in the test fixture to allow the horizontal translation of the specimen while restricting its vertical displacement. The end block was glued to the specimen by a glue gun.

In order to have the crack initiation, the span, L, of the specimen was set about 37mm to have a larger shear stress at the crack tip. After the crack initiated, the span of the specimen was changed to about 85mm. This way one can observe the crack propagation through most of the specimen. The crack length after crack initiation, a_i, was in the range of 41mm to 51mm. From the analysis in Section 3.2, stable crack growth is expected when the crack propagates about 55% of the span. This occurred usually after the first loading in the present study. Detailed examination will be shown in Section 4.2. The load-displacement curve for each of the specimens was recorded and the crack length was measured with a digital caliper. During the test, a video camera along with a distance microscope was used to record and monitor the initiation and propagation of the crack.

3.5 Specimen Testing of the Glass/PPS Composites

Injection-molded samples as received from Phillips

Petroleum Company were exposed to the hot-moist condition of 100°C and 95% relative humidity for 13 days, and the advanced composites (both as-received and molded) were exposed for 7 days. Samples were taken out of the environmental chamber at certain intervals for the tensile strength tests. During the tests, an extensometer was attached to each specimen and the load-strain curves were recorded. The cross head speed was 5mm/minute.

CHAPTER IV

RESULTS AND DISCUSSIONS

4.1 Moisture Absorption Behavior

4.1.1 The Carbon/PPS Laminate

The average moisture content of the carbon/PPS laminate was obtained by weighing the last three specimens for each of the four hygrothermal conditions. Moisture content versus square root of time is shown in Figure 4.1. It is indicated that moisture content increases with time gradually. The higher the relative humidity is in the environmental chamber, the higher the moisture content of the carbon/PPS laminate will be. For a fixed relative humidity, the higher the temperature is in the environmental chamber, the lower the moisture content will be. All samples exposed to the four hot-moist conditions did not show moisture saturation after about 320 hours. The maximum percent moisture uptake for 87°C/84% is 0.17% after 320 hours. The maximum percent moisture uptake for 127°C/84% is 0.08% after 310 hours. The maximum percent moisture uptake for 87°C/95% is 0.78% after 320 hours. The maximum percent moisture uptake for 127°C/95% is 0.56% after 310 hours. In summary, the laminate absorbs more moisture at low temperature/high relative humidity condition than at high temperature/low relative humidity condition.

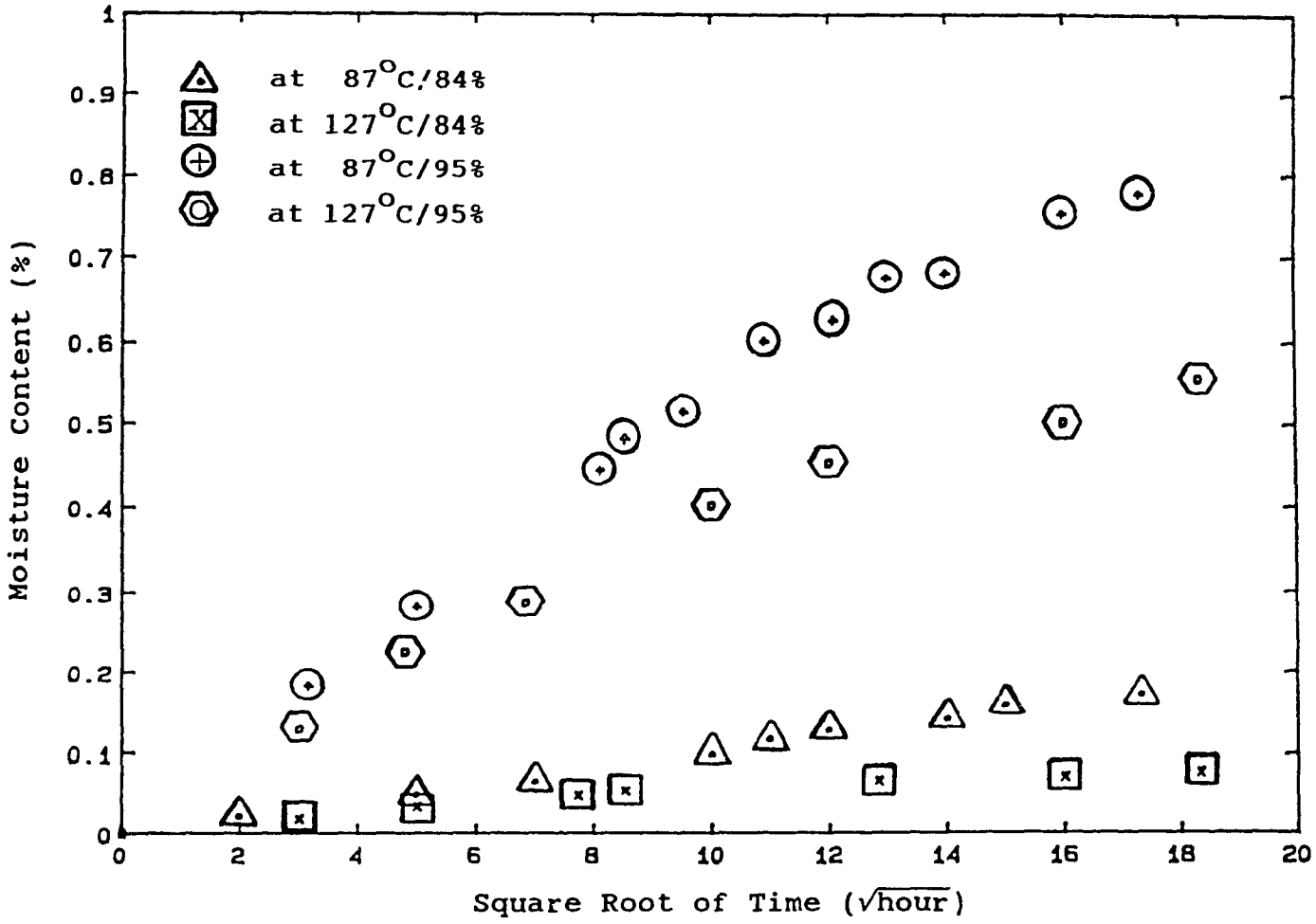

Figure 4.1. Moisture content versus square root of time for AC40-66 laminate.

4.1.2 The Glass/PPS Composites

Percent weight moisture uptakes for the injection-molded (as-received) samples are shown in Figure 4.2. After 13 days, about 0.5% of water was absorbed and all samples did not show saturation of moisture uptake. The largest water uptake was observed in samples R-7, which were mineral filled. Figure 4.3 shows the percent weight uptakes for advanced composite samples. In general, these samples showed much larger percent uptakes than the injection-molded samples. After one week, the stampable chopped fiber mats, AG20-40 (molded), showed the least amount of weight uptake, 4%. The other stampable chopped fiber mats, AG11-20 (molded), showed about 5% weight uptake. The continuous fiber satin weave fabric, AG31-40 (as-received), showed 6% weight uptake after 7 days, while the molded AG31-40 samples showed 10% weight uptake after 7 days. The largest amount of weight uptake (25%) was exhibited in the continuous fiber satin weave fabric, AG31-60 (as-received), whereas the molded AG31-60 samples showed only about 15% weight uptake after 7 days. Compared with the AG31-40, this excessive amount of water uptake in AG31-60 can be due to two factors: the larger amount of glass fibers, and the lower degree of crystallinity in the AG31-60 samples as discussed in Chapter II. It is clear that the characteristics of moisture absorption in these samples were improved after molding the materials, which erased the previous thermal history and annealed the amorphous samples.

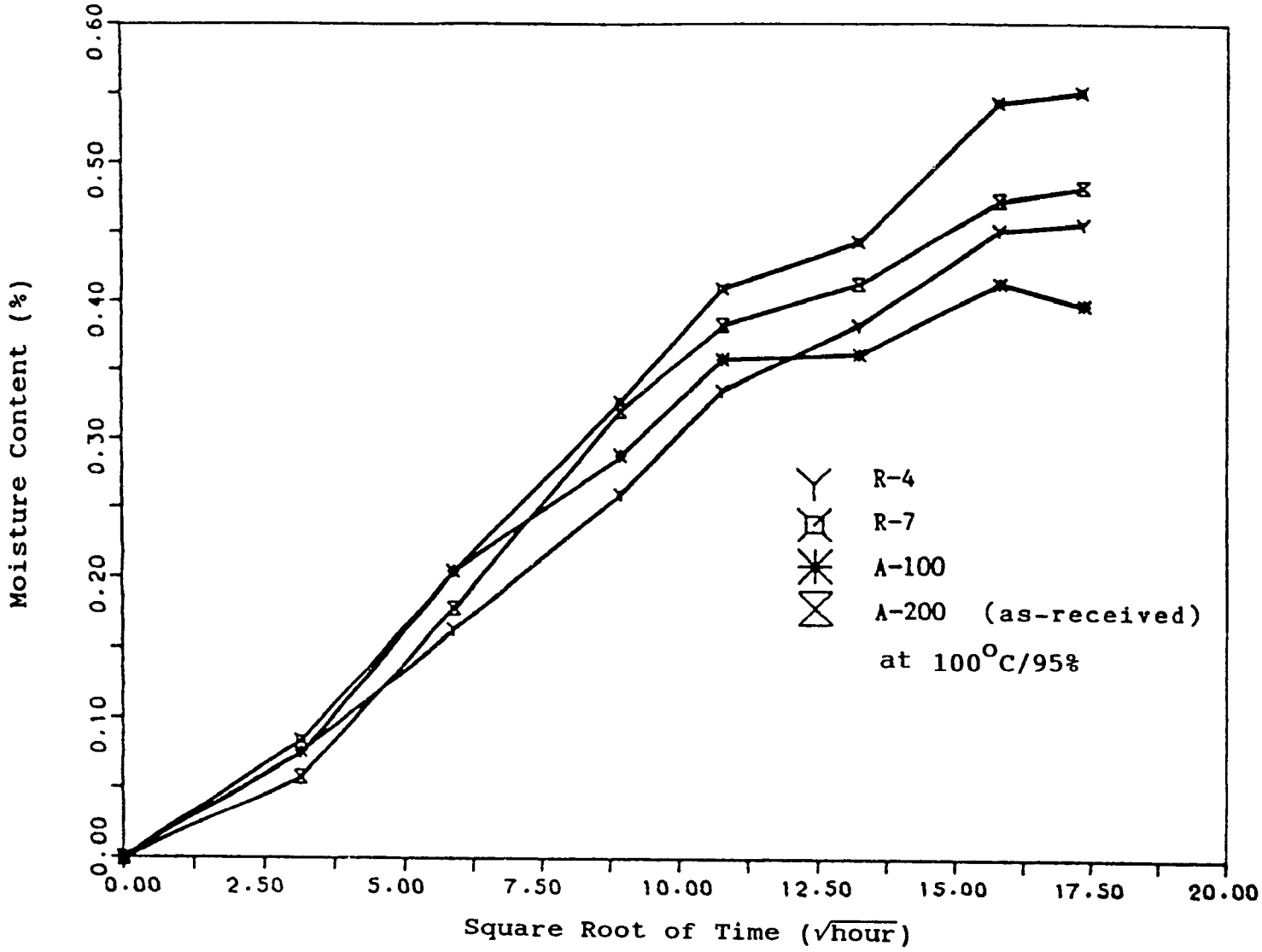

Figure 4.2. Moisture content versus square root of time for injection-molded glass/PPS composites.

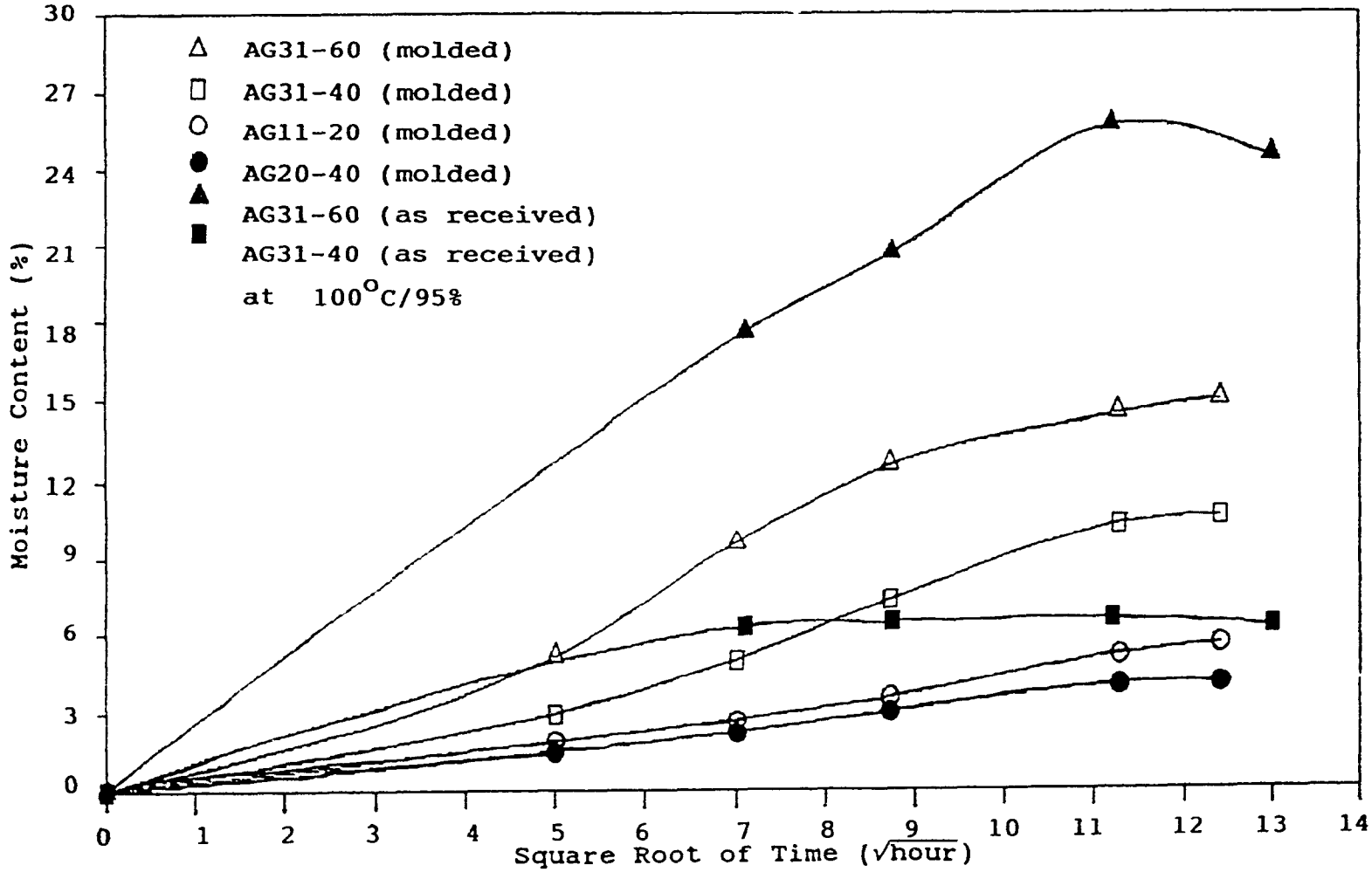

Figure 4.3. Moisture content versus square root of time for advanced glass/PPS composites.

4.2 Load-Displacement Response of the Carbon/PPS Laminate

The load-displacement curves, Figures 4.4 (a-p), were recorded to identify the various types of crack growth, where MC stands for moisture content. According to [11], there are three basic types of fracture behavior in the interlaminar fracture of thermoplastics. They are characterized as type I-ductile stable, Type II-brittle unstable and type III-brittle stable. All these three types of crack growth were observed in the present investigation.

For the virgin specimen test, shown in Figure 4.4(a), only brittle stable crack growth was observed. This gives the lowest G_{III} values among all the samples. Note that the crack length after crack initiation, a_1, was 51mm. The ratio, $a_1/L = (51-13)/85 = 0.45$.

For the 87°C/84% condition, shown in Figures 4.4(b-e), the crack growth exhibited brittle stable behavior, except one case of brittle unstable, the first loading of the sample at MC = 0.02% shown in Figure 4.4(c), where the ratio of a_1/L was only 0.30.

For the 127°C/84% condition, shown in Figures 4.4(f-i), the first loading caused the brittle unstable crack growth while the subsequent loadings caused the brittle stable crack growth for almost all the samples, except one case, shown in Figure 4.4(g), which showed brittle unstable,

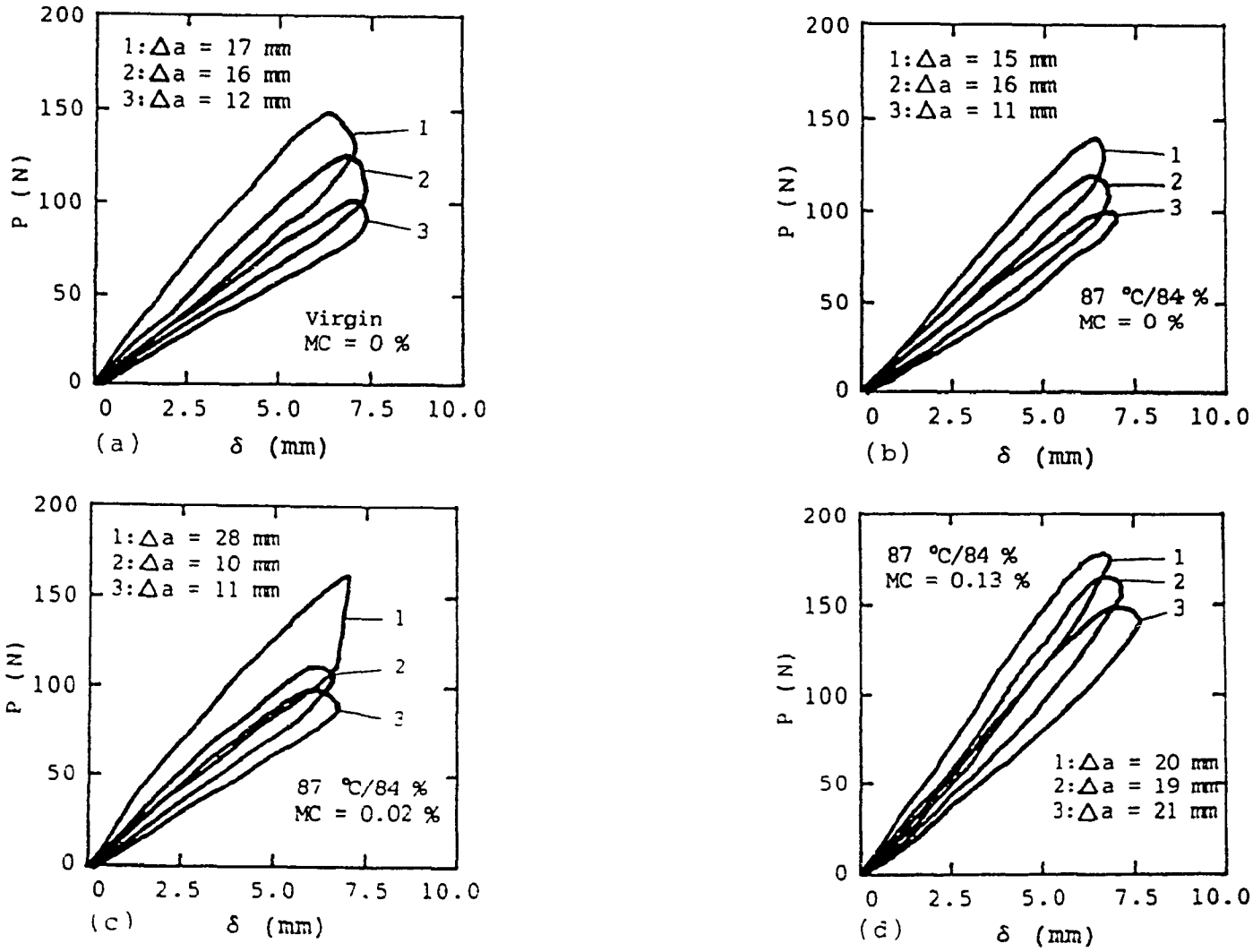

Figure 4.4. Load versus vertical displacement curves for AC40-66 laminate.

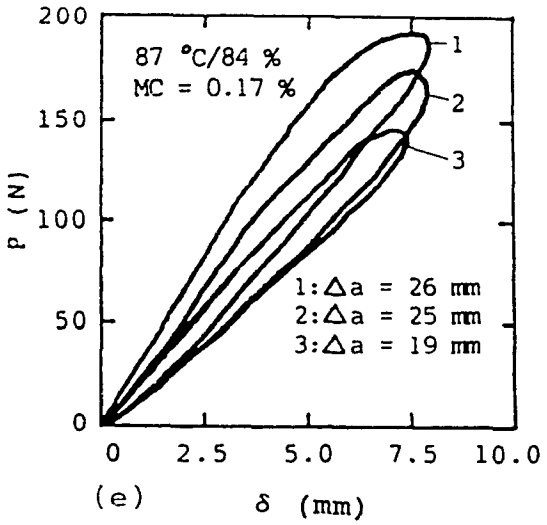

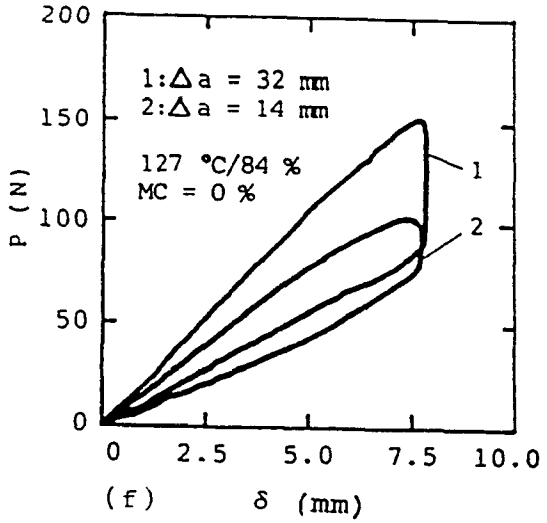

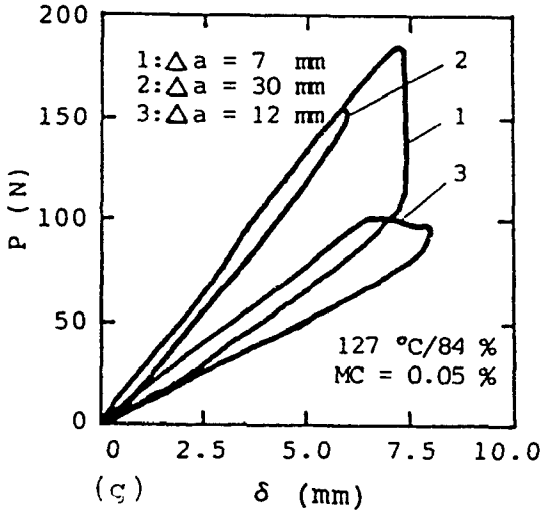

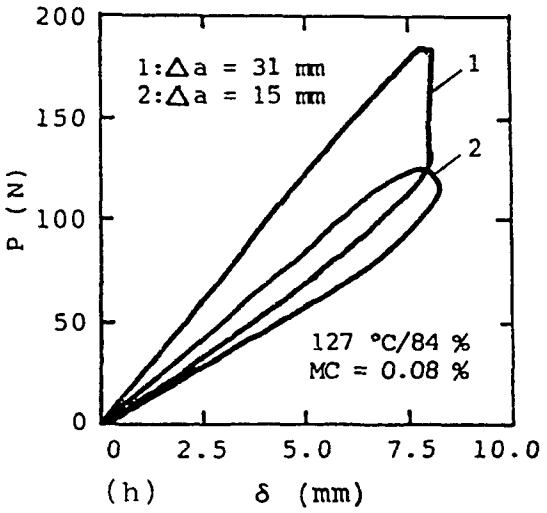

Figure 4.4. Load versus vertical displacement curves for AC40-66 laminate (continued).

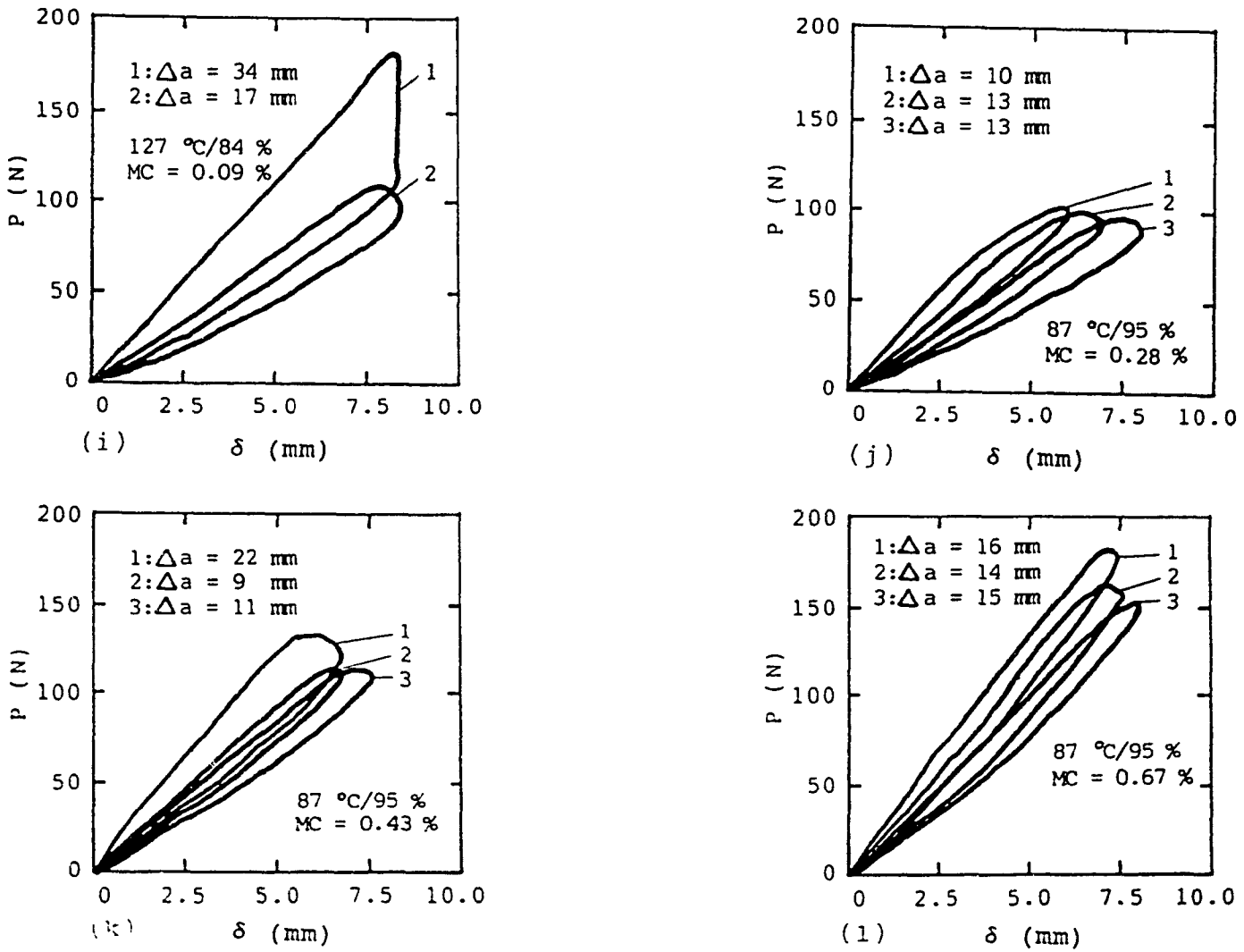

Figure 4.4. Load versus vertical displacement curves for AC40-66 laminate (continued).

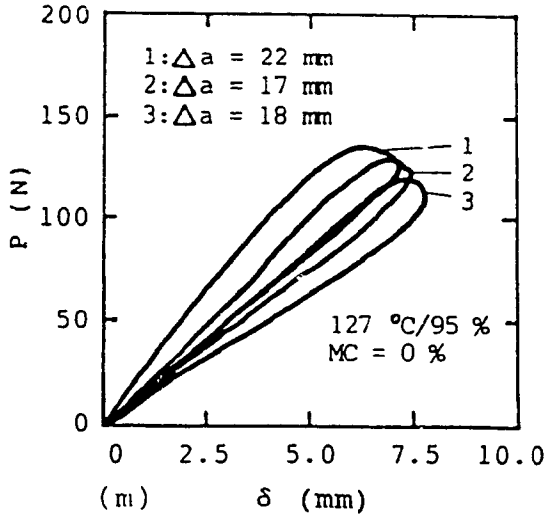

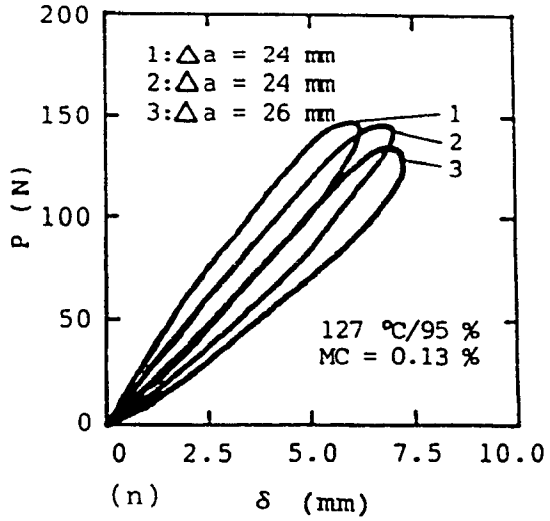

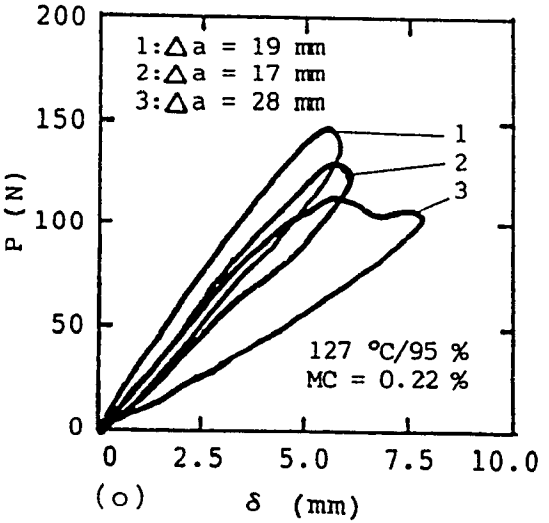

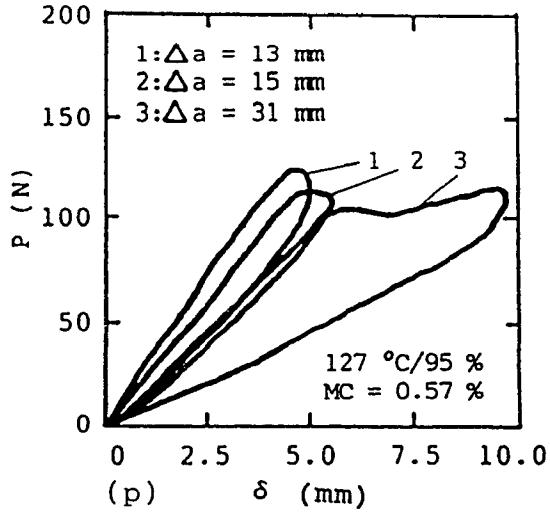

Figure 4.4. Load versus vertical displacement curves for AC40-66 laminate (continued).

brittle stable and ductile stable crack growths in sequence.

For the 87°C/95% condition, shown in Figures 4.4(j-l), the crack growth exhibited mixed type (more type I and some type III) crack growth.

For the 127°C/95% condition, shown in Figures 4.4(m-p), type I (ductile stable crack growth) became more obvious, especially at the third loading, shown in Figure 4.4(o-p), where the moisture contents were higher.

It was also indicated that the critical load and the displacement became larger with the increases of the moisture content and temperature. According to [9], both moisture and heat increase the ability of polymers to dilatate. Moisture may infuse into the polymers, separating the polymer molecules, thus reducing their secondary bond attraction, thereby making is easier for the molecules to move past the critical strain levels. This process is a form of plasticization. Heat creates a similar effect. Higher temperature, especially approaching the glass transition temperature (T_g), causes the materials to expand, thus creating more free volume.

It is concluded from the above observation that the crack growth is becoming stabler as the ratio of the crack length to the span is larger than 0.55 as predicted in Section 3.2, and that the PPS matrix is brittle at low

temperature and low moisture content. However, when the moisture content and temperature are high, the matrix exhibits plastic deformation. High moisture content and high temperature soften the PPS matrix and even cause fiber bridging. This will be shown in the fractography study section.

4.3 Stress-Strain Curves of the Glass/PPS Composites

Stress-strain curves for the injection-molded samples at typical moisture contents are shown in Figures 4.5 to 4.8. As expected, all samples showed a drop in both tensile modulus and strength as the moisture content increased. The R-4 and R-7 samples showed smaller fracture strains in comparison with the A-100 and A-200 samples. All injection-molded samples showed a tensile strength of about 50 to 60 MPa.

Stress-strain curves for the advanced composite samples at typical moisture content levels are shown in Figures 4.9 to 4.12. There are significant reductions in both modulus and strength in all the samples, the largest one being that of samples AG31-60 (as-received). The tensile strengths of the molded advanced glass/PPS composites at different moisture contents are listed in Table 4.1. The drops in moduli of all the glass/PPS composites exposed to the hot-moist condition at some typical moisture contents are shown in Table 4.2.

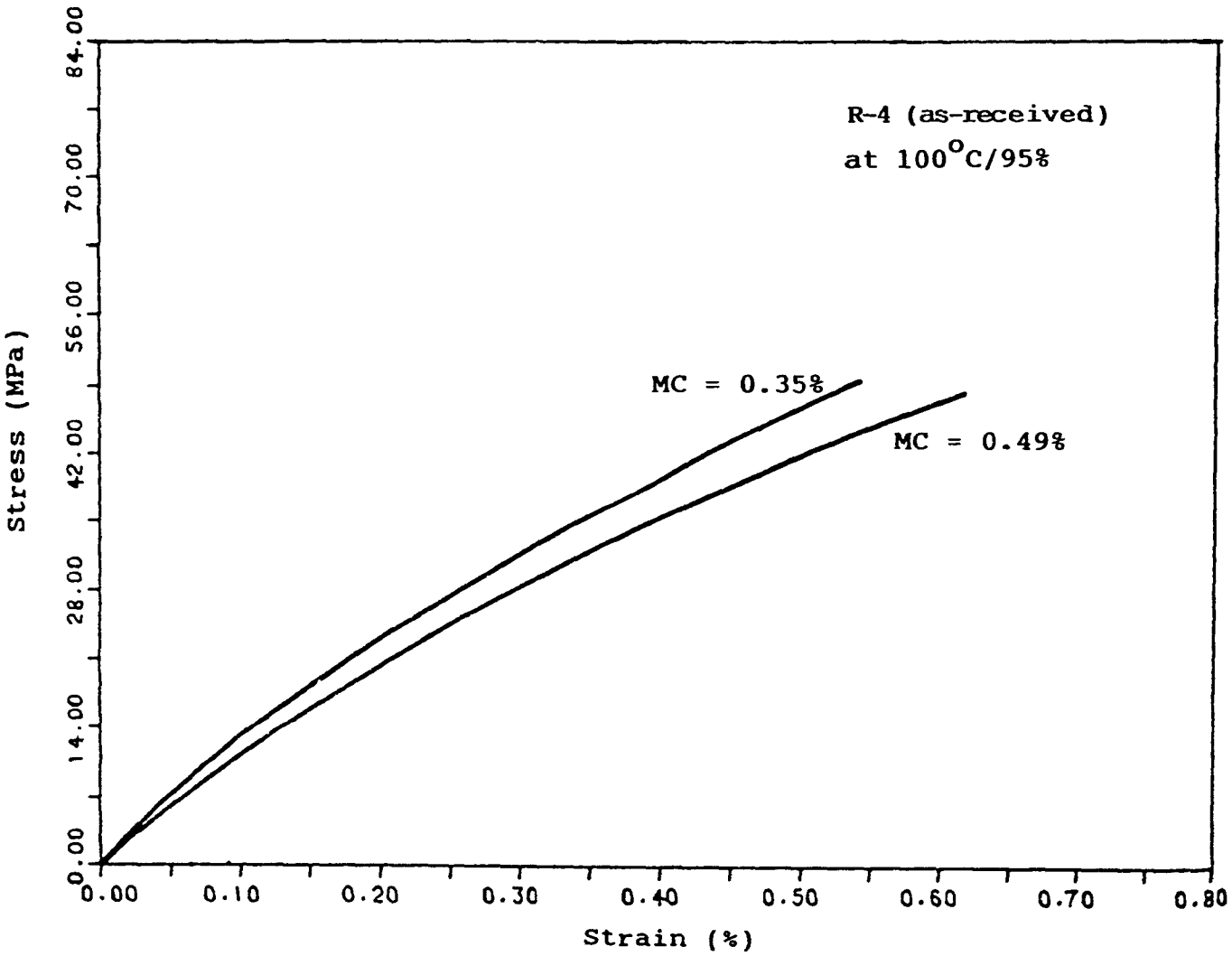

Figure 4.5. Stress-strain diagram with moisture content as a parameter for R-4 (as-received).

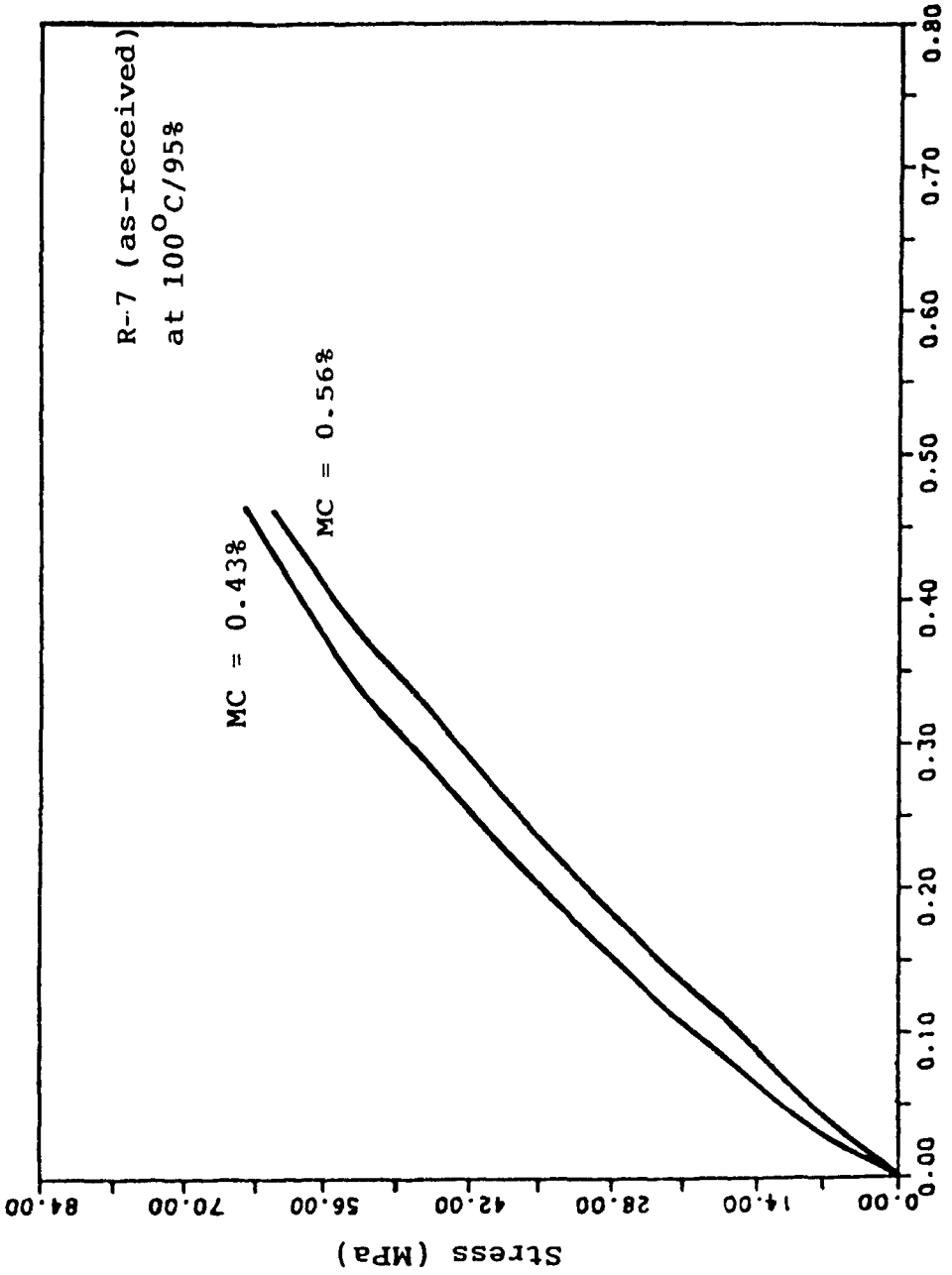

Figure 4.6. Stress-strain diagram with moisture content as a parameter for R-7 (as-received).

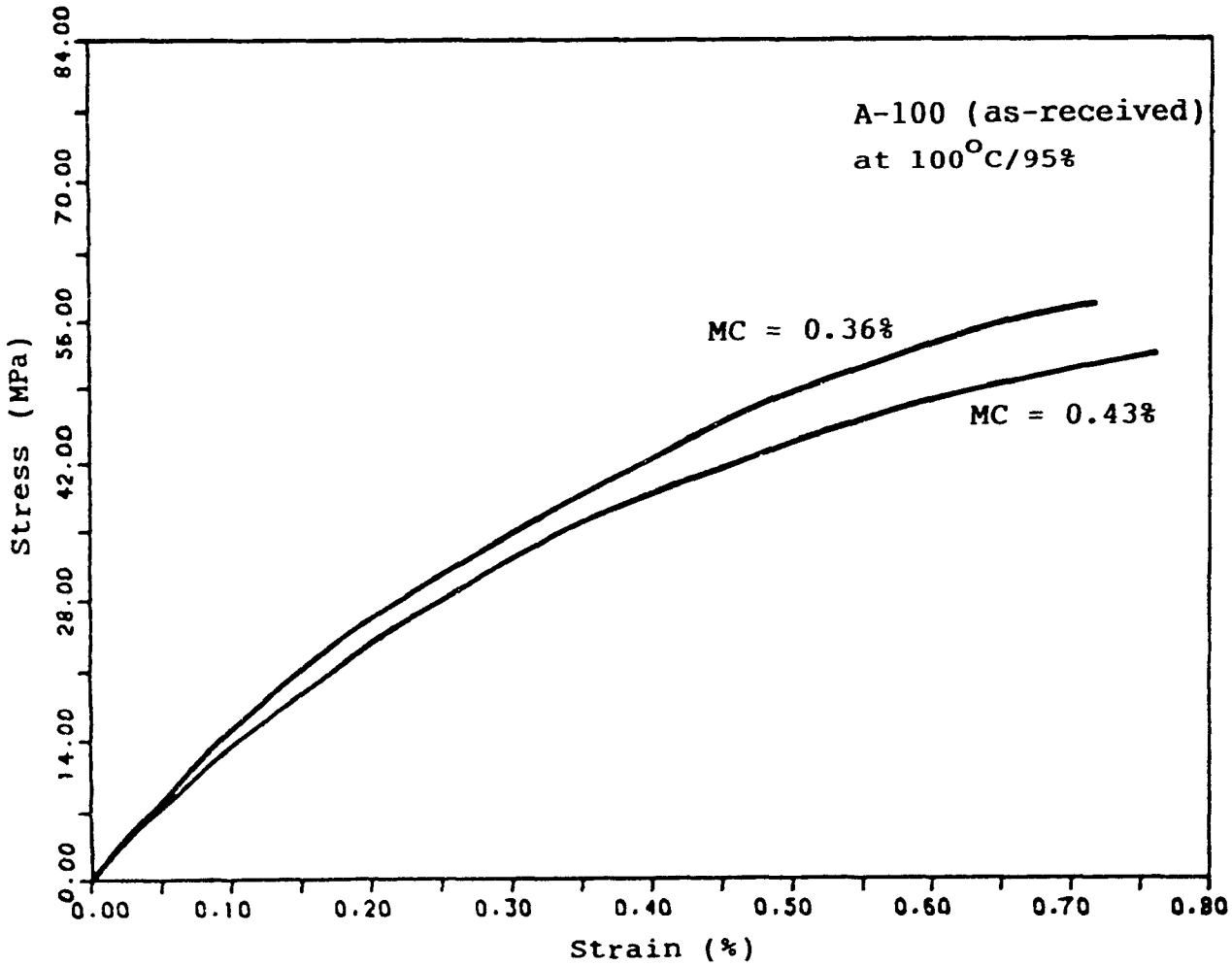

Figure 4.7. Stress-strain diagram with moisture content as a parameter for A-100 (as-received).

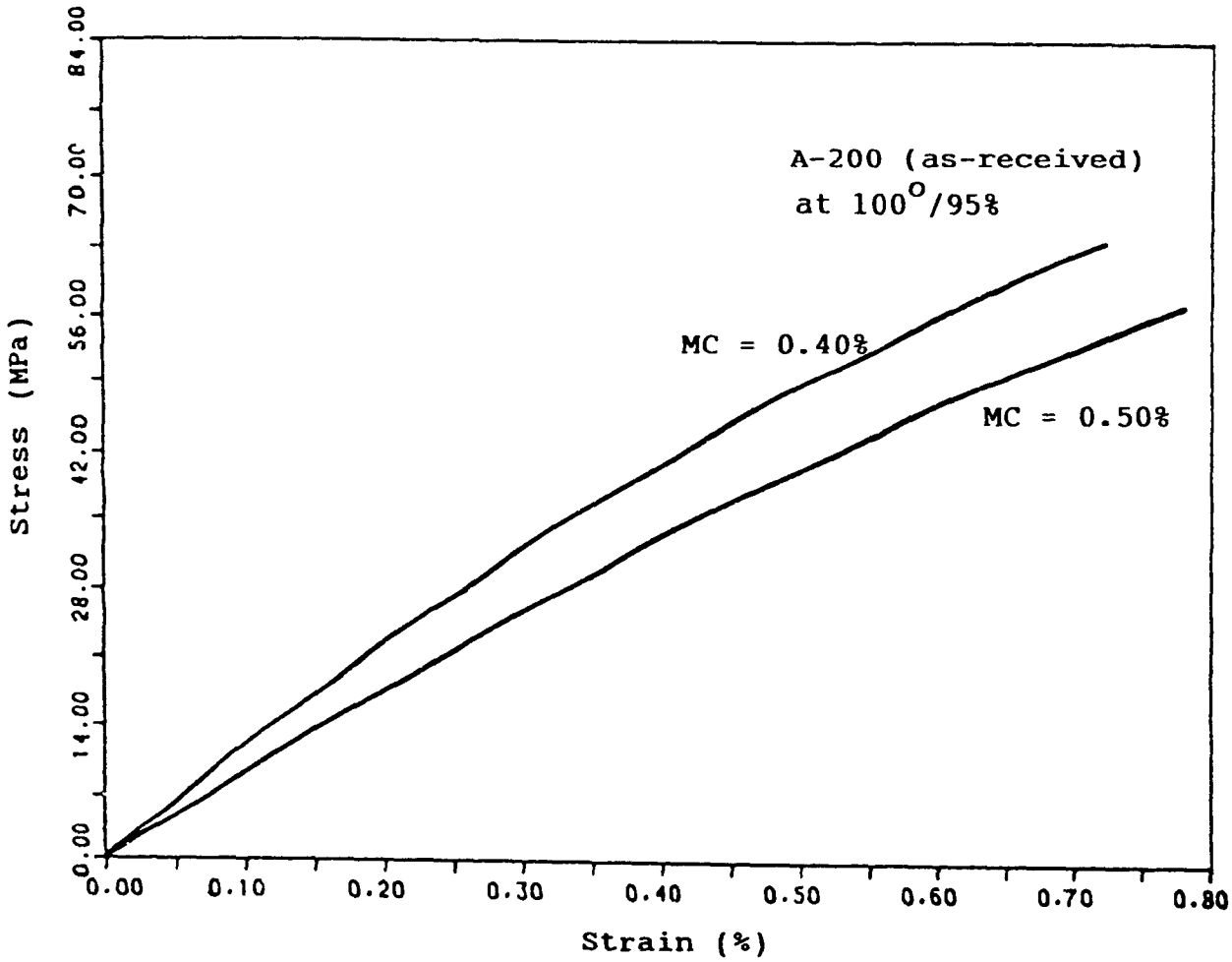

Figure 4.8. Stress-strain diagram with moisture content as a parameter for A-200 (as-received).

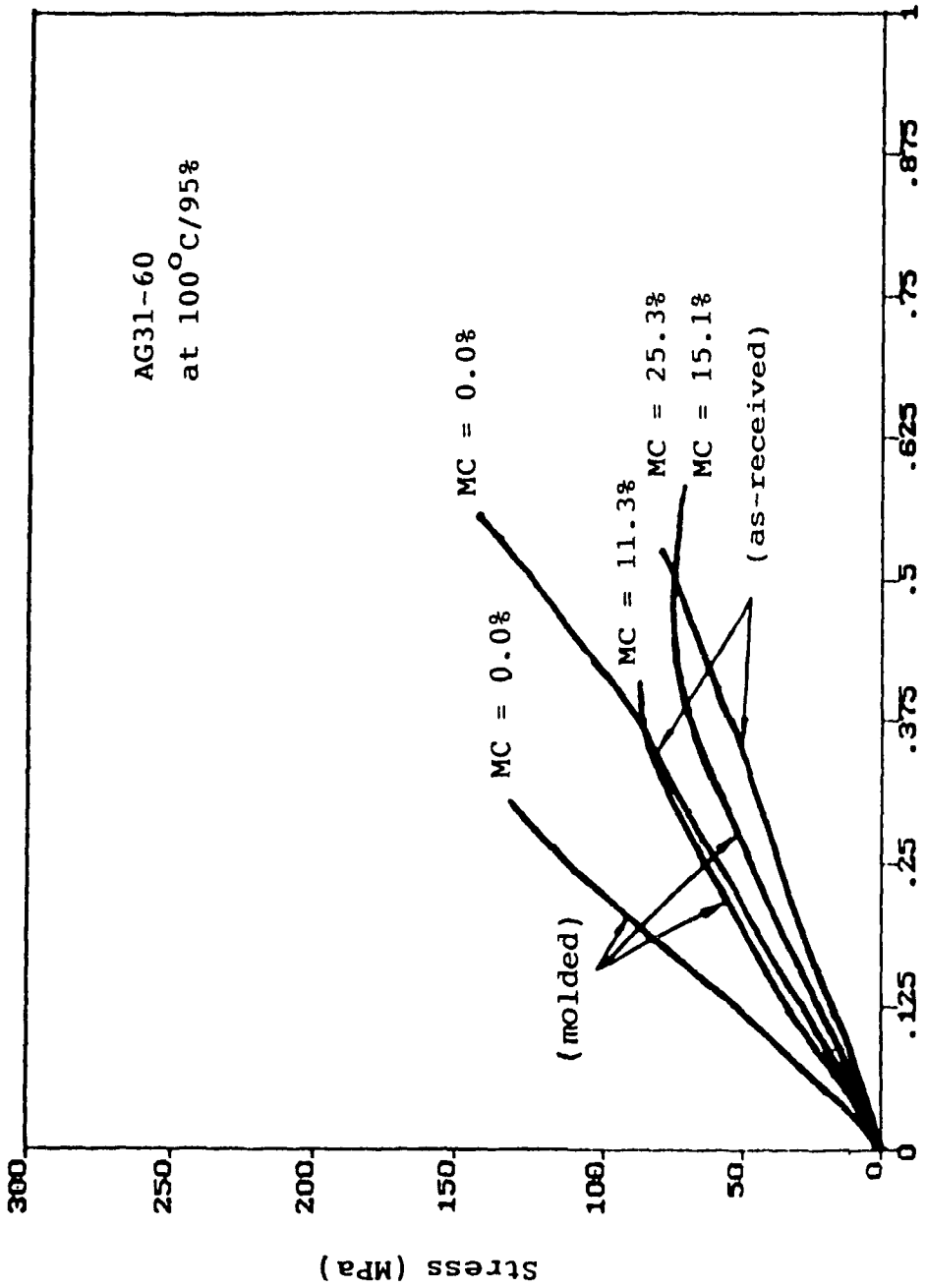

Figure 4.9. Stress-strain diagram with moisture content as a parameter for AG31-60.

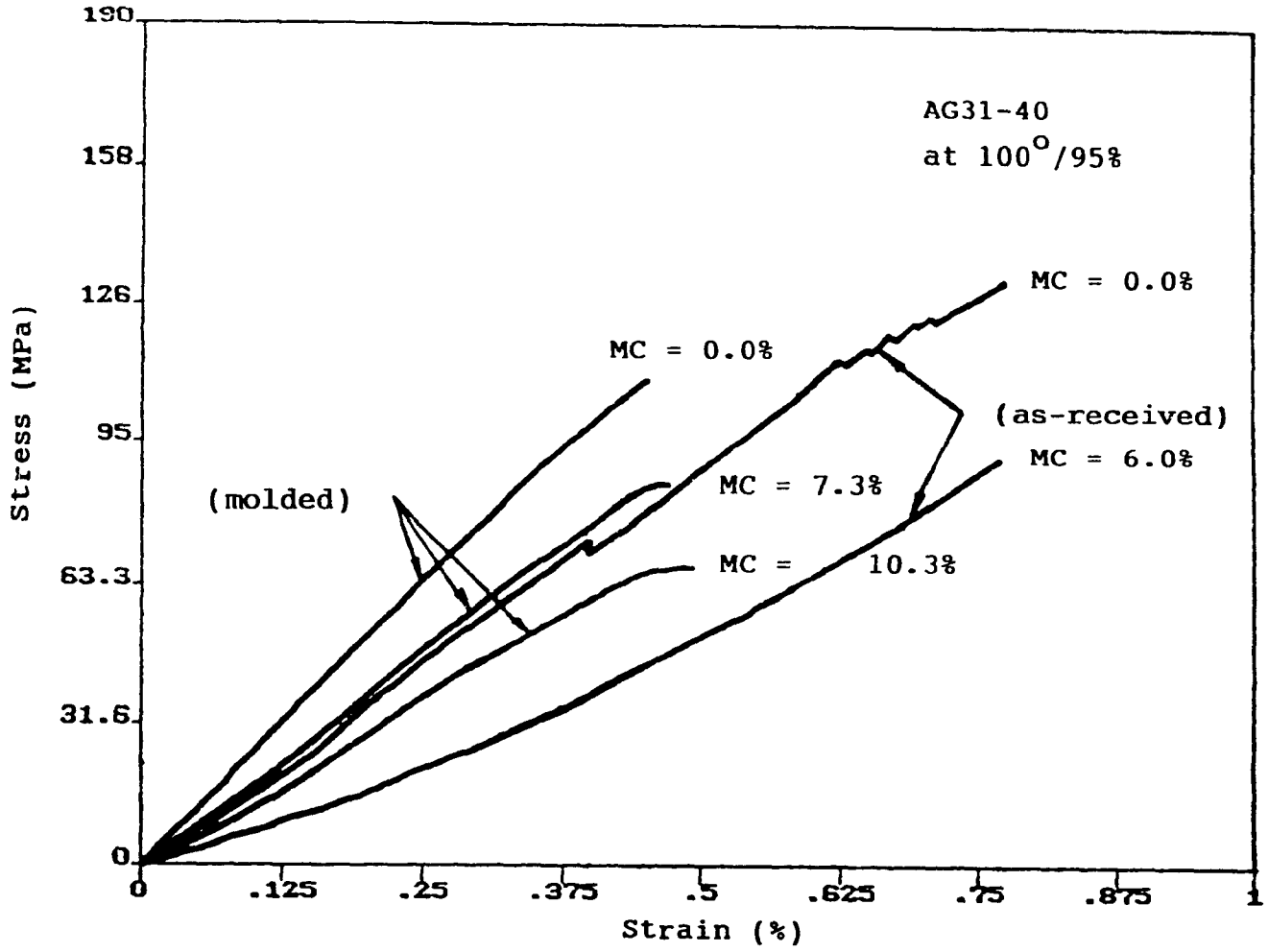

Figure 4.10. Stress-strain diagram with moisture content as a parameter for AG31-40.

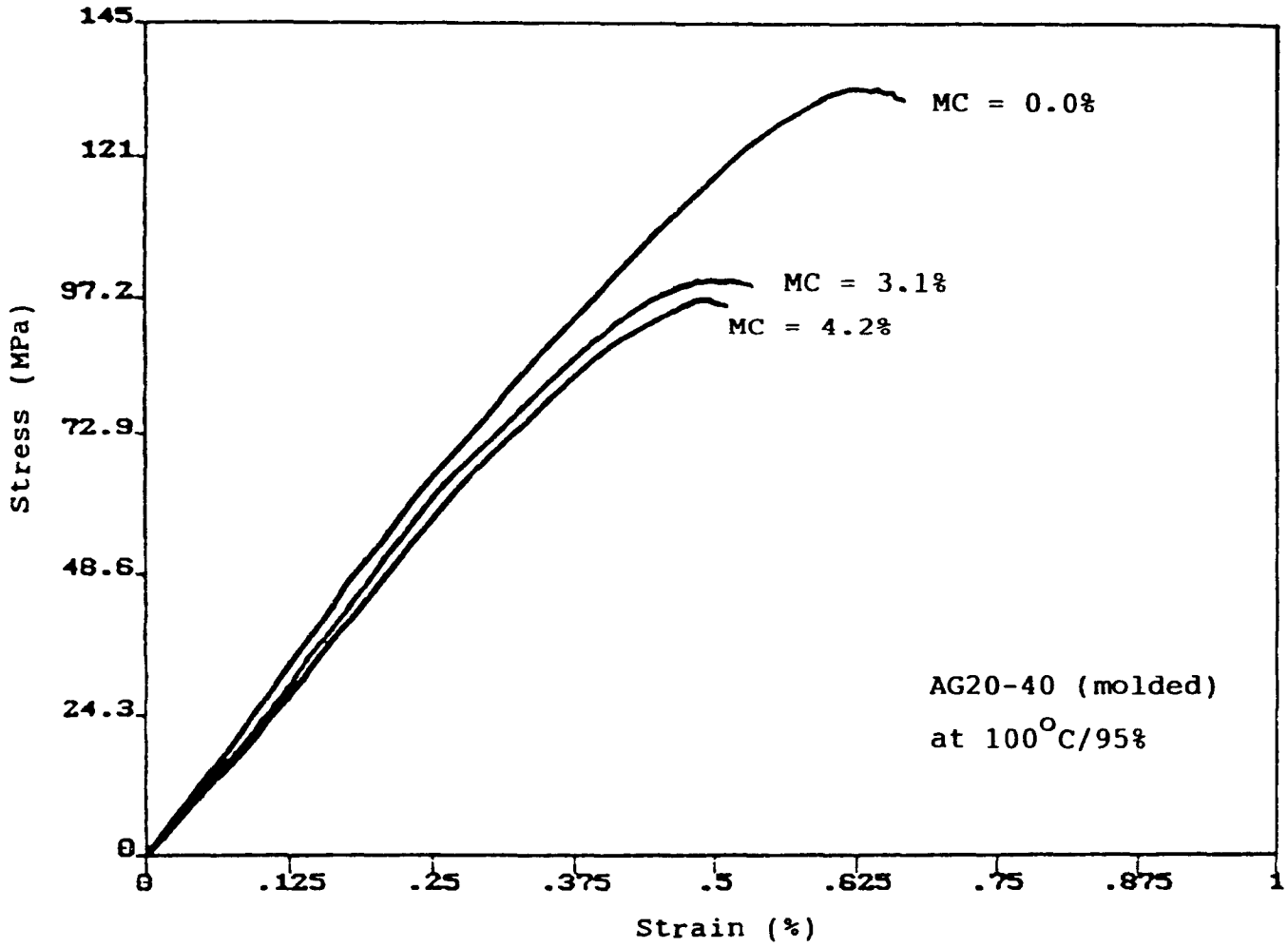

Figure 4.11. Stress-strain diagram with moisture content as a parameter for AG20-40 (molded).

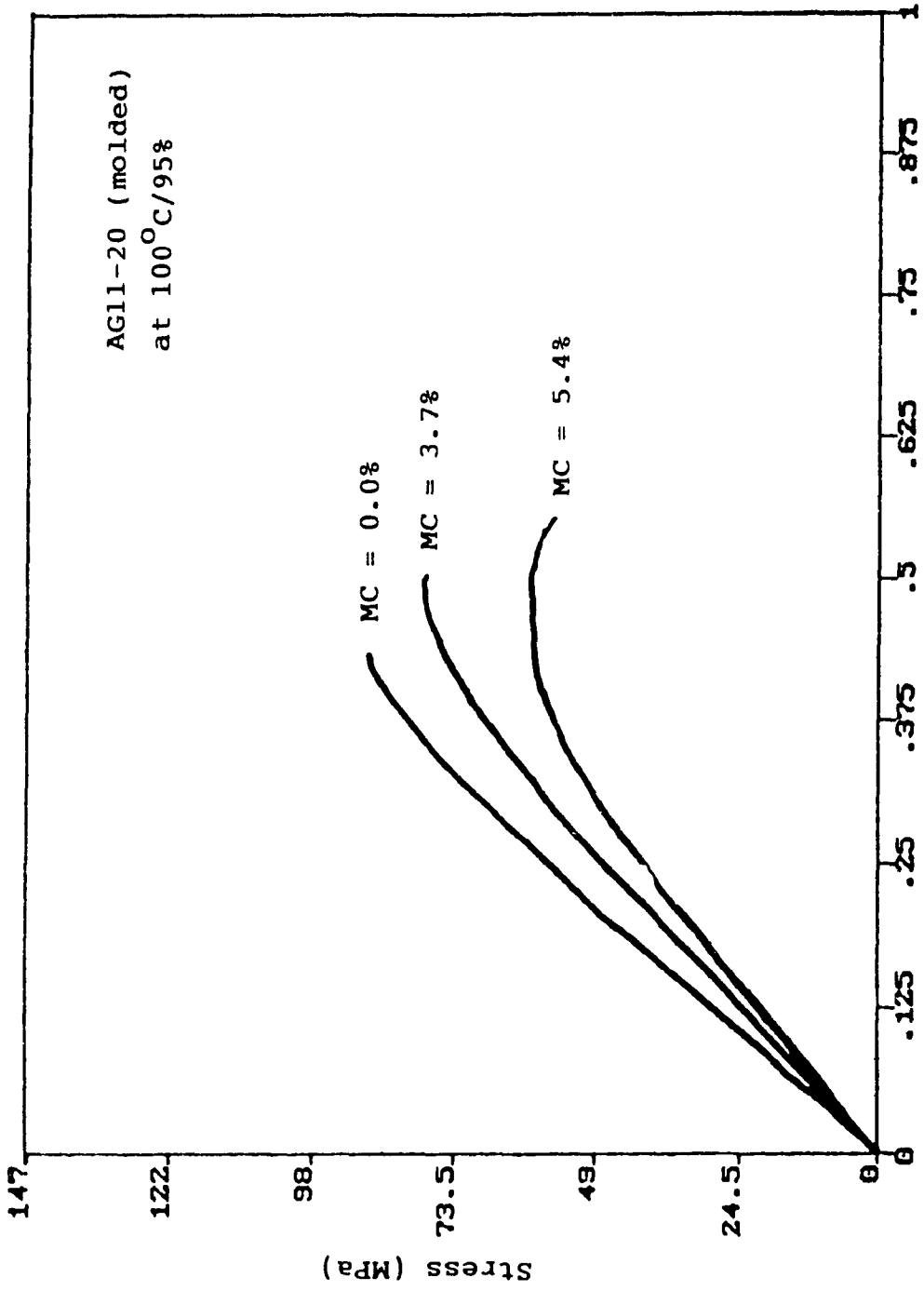

Figure 4.12. Stress-strain diagram with moisture content as a parameter for AG11-20 (molded).

Table 4.1. Tensile strengths of the advanced glass/PPS samples (molded).

Composites	Width (mm)	Thickness (mm)	Moisture Content(%)	Tensile (MPa)
AG31-60	13.56	1.47	0.00	133.44
(4 layers)	13.63	1.55	0.00	155.67
	13.63	1.45	0.00	154.33
	13.71	1.52	0.00	119.97
	13.67	1.37	11.27	90.77
	13.98	1.40	11.01	86.64
	13.82	1.50	10.92	87.54
	13.63	1.51	11.21	104.18
	13.60	1.52	15.23	74.98
	13.71	1.48	14.93	73.93
	13.64	1.40	14.62	78.55
	13.76	1.54	15.11	77.87
AG31-40	13.61	2.32	0.00	110.85
(4 layers)	13.69	2.18	0.00	122.30
	13.68	2.20	0.00	129.59
	13.63	2.12	0.00	115.94
	13.67	2.20	7.32	91.44
	13.64	2.23	7.07	103.56
	13.69	2.20	7.21	104.56
	13.68	2.31	7.78	88.61
	13.70	2.49	11.00	64.69
	13.65	2.22	10.66	77.55
	13.66	2.72	10.32	72.67
	13.65	2.42	10.03	63.57
AG11-20	13.52	3.66	0.00	97.80
(2 layers)	13.56	3.28	0.00	104.55
	13.59	3.37	0.00	89.70
	13.62	3.35	0.00	88.90
	13.97	3.23	3.72	74.24
	13.85	3.25	3.11	76.65
	14.00	3.24	3.63	71.65
	13.59	3.36	5.22	61.32
	13.69	3.28	5.36	55.68
	13.69	3.42	5.03	53.40
AG20-40	13.65	3.42	0.00	124.24
(2 layers)	13.65	3.02	0.00	135.85
	13.62	3.32	0.00	131.58
	13.60	3.30	0.00	122.52
	13.59	3.19	3.61	96.50
	13.59	3.17	3.06	96.33
	13.69	3.37	2.78	97.79
	13.68	3.13	4.15	93.42
	13.66	3.07	4.32	88.81
	13.65	3.05	3.73	91.87

Table 4.2. Elastic moduli of the glass/PPS composites calculated from the stress-strain curves with the change of moisture content.

Composites	Moisture Content (%)	Elastic Moduli (GPa)
	Injection Molded (as-received)	
R-4	0.35	15.4
	0.49	12.5
R-7	0.43	25.9
	0.56	16.8
A-100	0.36	16.5
	0.43	14.4
A-200	0.40	13.0
	0.50	9.5
	Advanced Composites (molded)	
AG31-60	0.00	42.1
	11.27	26.7
	15.11	19.0
AG31-40	0.00	26.6
	7.32	19.0
	10.32	14.9
AG11-20	0.00	24.5
	3.72	20.1
	5.36	17.3
AG20-40	0.00	27.1
	3.06	24.6
	4.15	23.1

4.4 Hygrothermal Effect on the Mode II Interlaminar Fracture Toughness of the Carbon/PPS Laminate

The critical strain energy release rate, G_{IIc}, of the virgin specimen was found to be 524 ± 8 J/m^2 (mean ± standard deviation) by DCB and 372 ± 5 J/m^2 by the area method. Compared to the graphite/epoxy system, where the mean value of G_{IIc} was about 160 J/m^2, and to the graphite/PEEK (polyetheretherketone) system, where the value of G_{IIc} was about 1765 ± 235 (mean ± standard deviation) [9], carbon/PPS laminate rates between these two thermoplastics.

The values of G_{IIC} both by DCB and by the area method at different moisture levels are listed in Table 4.3(a-b). The values of G_{IIC} by DCB and the average values of G_{IIC} by the area method at different moisture levels are plotted in Figures 4.13(a-b).

As can be seen from Figures 4.13(a-b), critical strain energy release rate of carbon/PPS laminates during crack propagation under Mode II loading increases with an increase of moisture content. At a lower relative humidity of 84% and a temperature of 87°C, the critical strain energy release rate, G_{IIC}, increases with an increase of moisture content, from about 551 J/m^2 to 594 J/m^2 (an increase of 8%). At 127°C/84%, G_{IIC} increases with an increase of moisture content, from about 571 J/m^2 to 603 J/m^2 (5.5%). At a higher relative humidity of 95% and a temperature of 87°C, G_{IIC} also increases with an increase of moisture content, from about 563 J/m^2 to 596 J/m^2 (5.9%). At 127°C/95%, G_{IIC} increases from about 577 J/m^2 to 615 J/m^2 (6.7%). It is also indicated that for a fixed moisture content, G_{IIC} increases with an increase of temperature, and that G_{IIC} increases more with temperature at higher moisture contents.

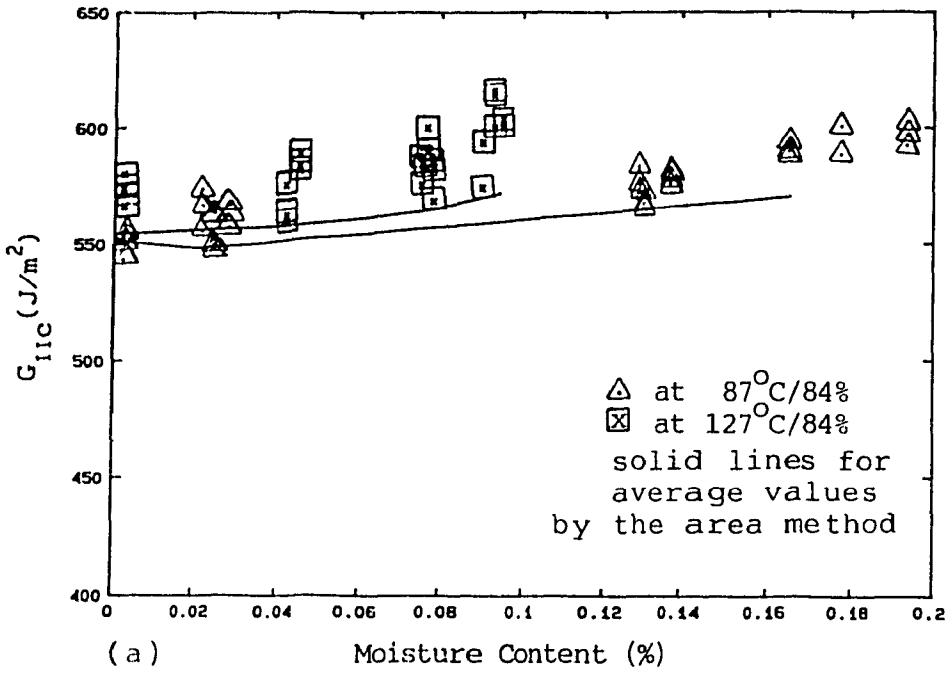

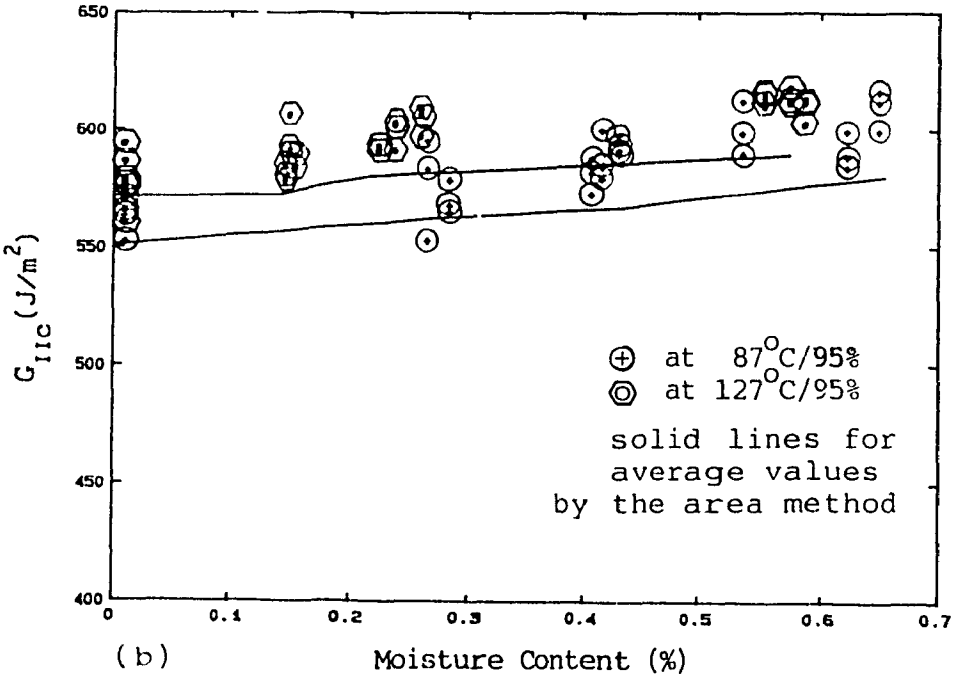

Figure 4.13. Critical strain energy release rate versus moisture content with temperature as a parameter for AC40-66 laminate.

Table 4.3a. Comparison of the critical strain energy release rate of the carbon/PPS laminate at low relative humidity by DCB and by the area method.

For 87°C/84%

Moisture Content(%)	G_{IIC}(J/m^2) DCB	G_{IIC}(J/m^2) A. Method	Mean ± Stand. Devi. DCB	Mean ± Stand. Devi. A. Method
0.0000	551.99 543.49*	381.34 385.54	550.98	383.53
	553.13 555.33*	389.56 377.66	± 5.19	± 5.15
0.0225	566.60 555.26	423.27 420.35	565.17	423.17
	573.65	425.89	± 9.28	± 2.77
0.0253	563.25 549.49	419.24 420.28	553.49	418.76
	547.74	416.76	± 8.49	± 1.81
0.0283	566.87 562.15	423.35 419.56	561.98	423.55
	556.91	427.74	± 4.98	± 4.09
0.1288	575.89 572.12	460.25 457.35	576.18	466.77
	573.36 583.36	475.59 473.90	± 5.04	± 9.31
0.1301	567.46 572.31	456.15 458.23	568.32	460.23
	565.18	466.31	± 3.64	± 5.37
0.1374	577.72 576.03	473.35 470.26	578.99	475.11
	580.60 581.60	475.27 481.54	± 2.57	± 4.76
0.1648	591.91 589.76	495.36 489.57	591.62	489.19
	593.18	482.65	± 1.73	± 6.36
0.1774	588.60 587.33	490.29 487.76	592.19	488.86
	600.64	488.54	± 7.35	± 1.30
0.1939	592.33 597.03	496.43 489.25	598.32	495.22
	605.59	499.98	± 6.72	± 5.47

For 127°C/84%

0.0000	565.83 571.32	402.46 397.57		
	566.39 566.34*	399.55 406.67	570.66	404.49
	580.21 573.88*	411.87 408.82	± 5.70	± 5.56
0.0426	575.27 559.23	418.25 415.35	565.43	414.34
	561.79	409.43	± 8.62	± 4.50
0.0458	588.80 581.58	431.12 445.13	584.52	435.04
	583.17	428.87	± 3.79	± 8.81
0.0756	586.29 586.90	464.45 458.32	582.78	461.29
	575.14	461.09	± 6.62	± 3.07
0.0768	582.95 599.76	470.50 472.04	590.73	472.76
	589.47	475.75	± 8.48	± 2.70
0.0783	568.08 582.25	435.56 446.64	578.53	443.85
	585.25	449.35	± 9.17	± 7.31
0.0895	593.23 593.49	490.25 507.36	586.87	505.05
	573.90	517.53	±11.24	±13.79
0.0923	616.07 615.66	511.34 520.45	610.57	516.96
	599.98	519.08	± 9.17	± 4.91
0.0945	612.51 613.53	509.87 511.36	608.68	506.60
	599.99	498.56	± 7.54	± 7.00

* The values of G_{IIC} at dry condition (MC = 0%) may be from different samples for different crack lengths.

Table 4.3b. Comparison of the critical strain energy release rate of the carbon/PPS laminate at high relative humidity by DCB and by the area method.

For 87°C/95%

Moisture Content(%)	$G_{IIC}(J/m^2)$ DCB	$G_{IIC}(J/m^2)$ A. Method	Mean ± Stand. Devi. DCB	Mean ± Stand. Devi. A. Method
0.0000	551.99 573.49* 563.13 565.33*	379.35 383.45 387.29 392.46	563.48 ± 8.87	385.64 ± 5.59
0.2663	582.89 594.89 552.24	425.35 430.32 429.80	576.67 ±21.99	428.49 ± 2.73
0.2850	578.11 564.63 567.24	412.89 419.46 420.08	569.99 ± 7.15	417.48 ± 3.98
0.4060	587.76 581.55 572.31	457.25 455.53 449.06	580.54 ± 7.77	453.95 ± 4.32
0.4145	584.30 579.08 599.71	450.87 455.37 458.85	587.70 ±10.73	455.03 ± 4.00
0.4275	591.15 594.62 597.44 589.44	465.25 467.53 468.46 461.05	593.16 ± 3.57	465.57 ± 3.30
0.5329	612.18 589.47 578.41	518.29 508.29 511.63	593.35 ±17.22	512.74 ± 5.09
0.6213	583.77 599.27 583.47	498.02 504.03 501.89	588.84 ± 9.04	501.31 ± 3.05
0.6488	611.58 599.31 609.14	508.80 512.23 515.65	606.68 ± 6.50	512.23 ± 3.43

For 127°C/95%

0.0000	586.34 570.21	384.06 387.35		
	593.88 570.87*	392.04 379.34	576.72	384.66
	560.29 578.72*	395.35 369.82	±12.15	± 9.22
0.1440	584.75 574.38 579.44	421.25 423.37 419.87	579.52 ± 5.19	421.50 ± 1.76
0.1484	579.33 591.08 606.26	430.38 428.59 438.08	592.22 ±13.50	432.35 ± 5.04
0.1534	583.99 594.75 572.90	429.28 436.89 441.36	583.88 ±10.93	435.84 ± 6.11
0.2227	592.81 590.87 587.31	452.87 453.58 461.58	590.33 ± 2.79	456.01 ± 4.84
0.2373	591.08 602.84 612.00	452.36 463.47 458.32	601.97 ±10.49	458.05 ± 5.56
0.2606	591.97 603.46 612.16	479.38 471.47 485.38	602.53 ±10.13	478.74 ± 6.98
0.5525	620.26 621.44 603.27	512.49 506.32 516.45	614.99 ±10.17	511.75 ± 5.11
0.5742	627.99 621.53 602.58	521.04 517.84 516.67	617.37 ±13.21	518.52 ± 2.26
0.5862	622.91 623.50 594.34	514.43 509.74 518.52	613.58 ±16.67	514.16 ± 4.30

* The values of G_{IIC} at dry condition (MC = 0%) may be from different samples for different crack lengths.

It is indicated from Tables 4.3(a-b) that the G_{IIc} values obtained by the area method have the same trend as those by DCB even though the values by the area method are about 68% to 85% of the values by DCB. The difference range is comparable to that of 60% to 70% by [14] for graphite/epoxy system. The higher toughness of PPS resin may have contributed to the better linear load-displacement response, which in turn contributed to the better results by DCB as compared to the results by the area method.

This increase of the critical strain energy release rate is mainly due to the matrix softening and fiber bridging exhibited in the fractured surfaces by the scanning electron microscope and by examining the side view of the specimen using a regular microscope. This will be discussed in section 4.6.

4.5 Moisture Content Effect on the Tensile Strengths of the Glass/PPS Composites

Tensile strengths of injection-molded samples (as-received) at different moisture contents are shown in Figure 4.14. In general, there is a reduction of about 25% in tensile strength of all samples due to exposure to 100°C/95% hot-moist condition for as short a time as two weeks. Figure 4.15 shows the changes in tensile strengths of advanced composites samples due to exposure to the hot-moist condition. From an average virgin strength of about 150 MPa, the strength of AG31-60 samples (as-received) dropped to

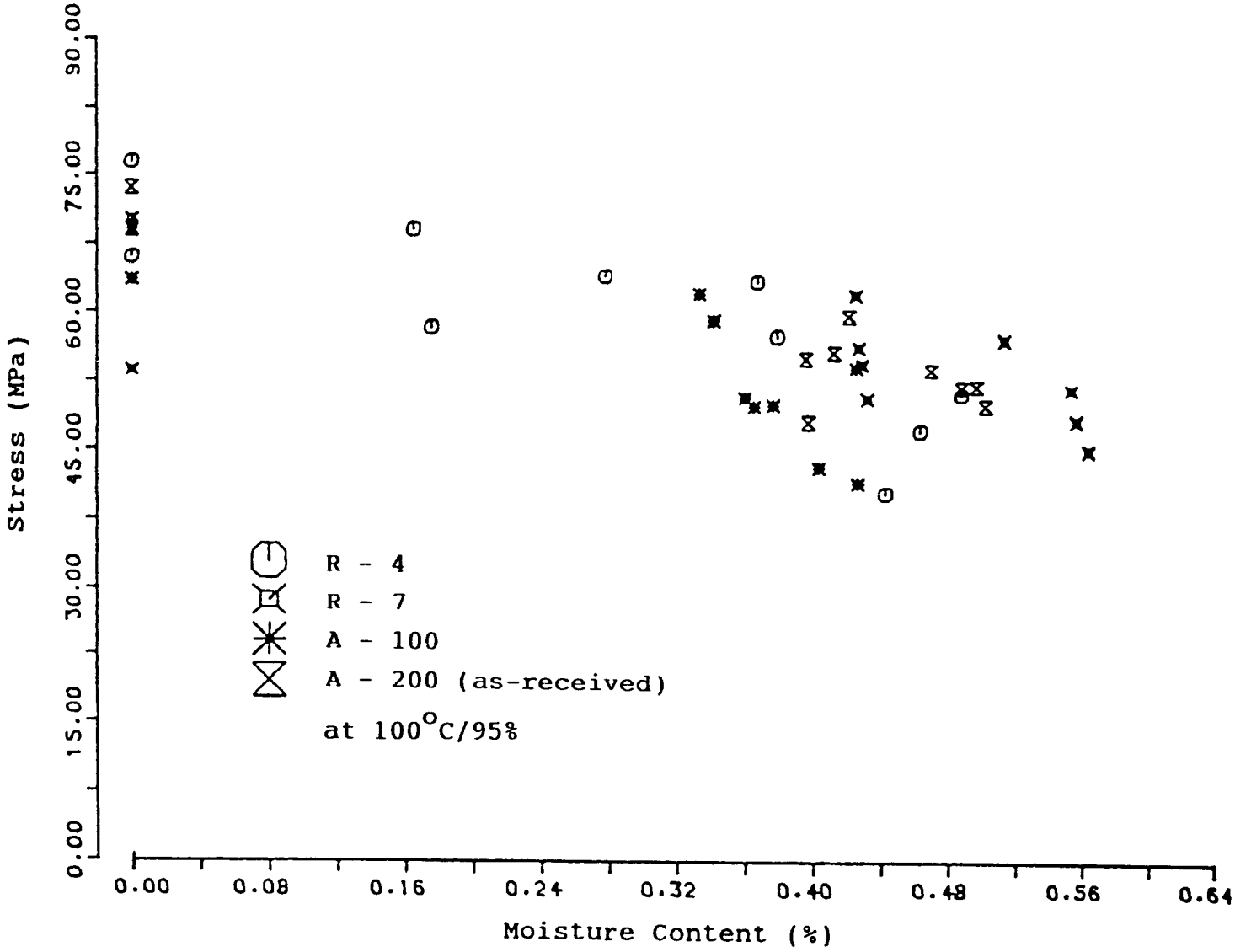

Figure 4.14. Change in tensile strength with moisture content for injection-molded glass/PPS composites.

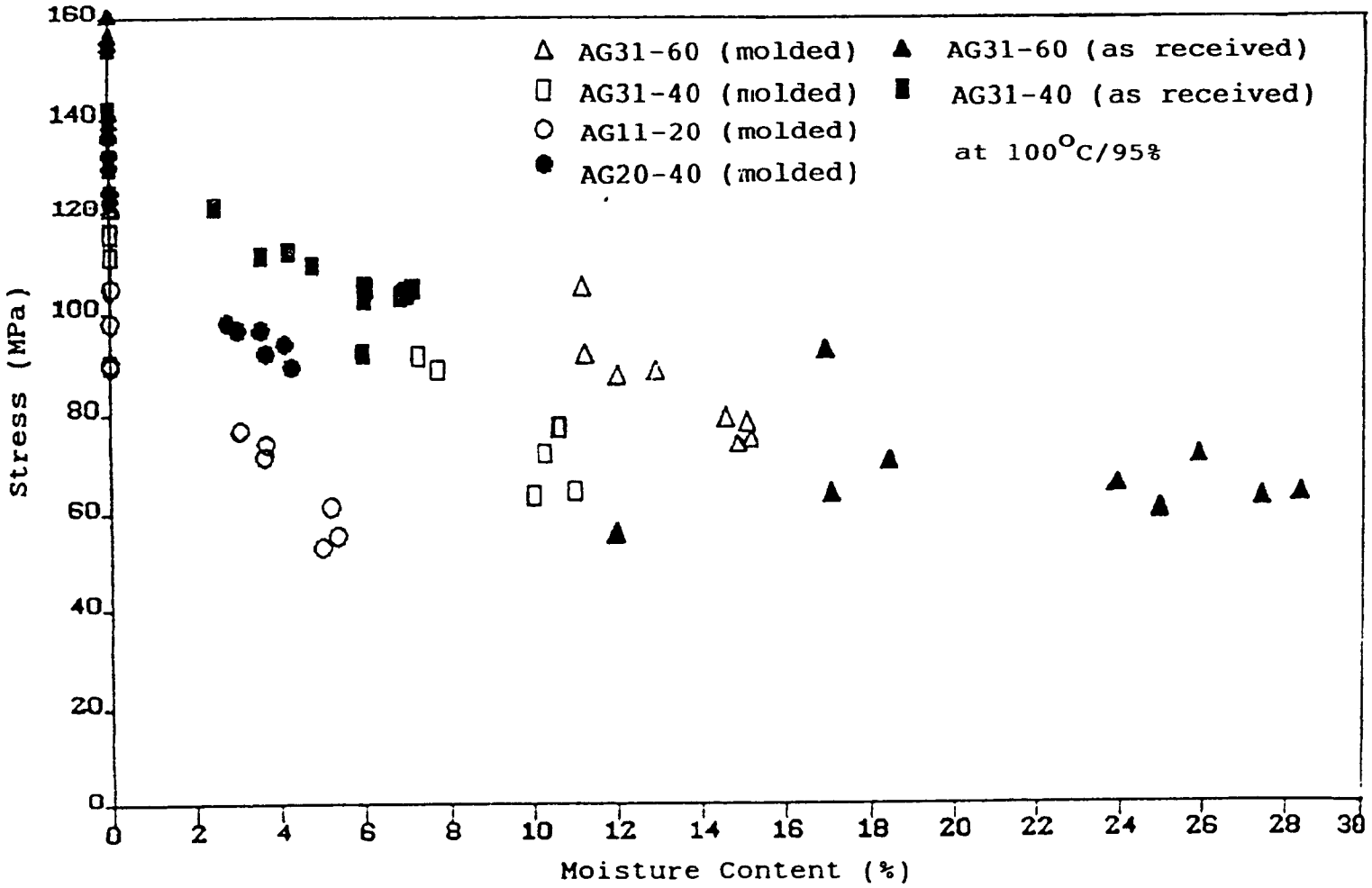

Figure 4.15. Change in tensile strength with moisture content for advanced glass/PPS composites.

about 60 MPa (60% reduction) with the absorption of about 25% of moisture. This is the largest reduction in strength among the samples. From an average virgin strength of about 150 MPa, the strength of AG31-40 samples (as-received) dropped to about 105 MPa (30% reduction) after about 7% moisture was absorbed. From an average virgin strength of 140 MPa, the strength of AG31-60 samples (molded) dropped to about 76 MPa (46% reduction) with the absorption of about 15% of moisture. From an average virgin strength of about 120 MPa, the strength of AG31-40 (molded) dropped to about 70 MPA (42% reduction) after about 10% moisture was absorbed. From an average virgin strength of about 95 MPa, the strength of AG11-20 samples (molded) dropped to about 57 MPa (40% reduction) after about 5% moisture absorption. From an average virgin strength of about 129 MPa, the strength of AG20-40 samples (molded) dropped to about 91 MPa (29% reduction) after 7 days of exposure (about 4% moisture absorption).

It is indicated from Figures 4.14 and 4.15 that the tensile strengths of the injection-molded sample (as-received) are usually lower than those of the advanced composites (either as-received or molded). It is noted that the larger the amount of glass fibers in the composites, the higher the virgin tensile strengths. It is shown that the larger the moisture content is, the more the reduction in tensile strength will be. The physical properties of glass-reinforced thermoplastics of all types generally

deteriorate upon exposure to moisture at elevated temperatures such as the present 100°C [23]. Even if the resin itself is hygrothermally stable, the moisture penetrates the materials by a wicking action and attacks the glass-resin interfaces, causing delamination or debonding; reinforced PPS is no exception as will be seen from the fractography study to be shown in the next section.

4.6 Fractography Study

4.6.1 Interlaminar Fracture of the Carbon/PPS Laminate

The microstructure of the cross-sectional view of the carbon/PPS laminate is shown in Figure 4.16. The laminate fabricated from the carbon/PPS prepreg tapes showed excellent fiber dispersion. The matrix-fiber bonding was seen to be good, and the distribution of the fibers was uniform.

Mode II interlaminar fractures of carbon/PPS laminates were dominated by different deformation and fracture mechanisms which will be shown by scanning electron microscopy (SEM) of typical samples at various temperatures and moisture contents.

The virgin specimens exhibit typical brittle fracture as indicated in Figure 4.17a. At 87°C, the fractured surface is more or less the same as the virgin specimen as indicated in Figure 4.17b. With a further increase of moisture

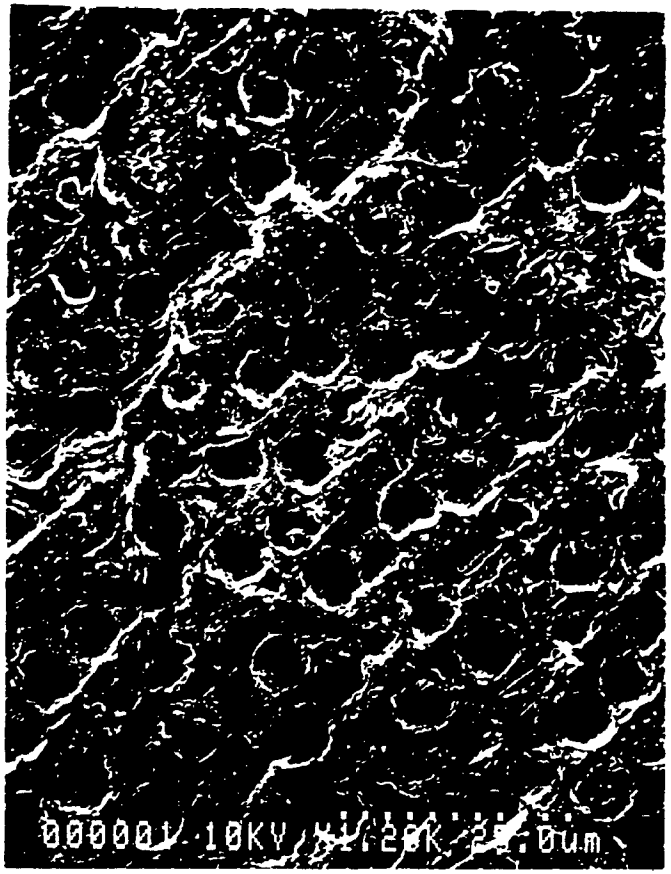

Figure 4.16. SEM of AC40-66 laminate at X1200 (cross-sectional view).

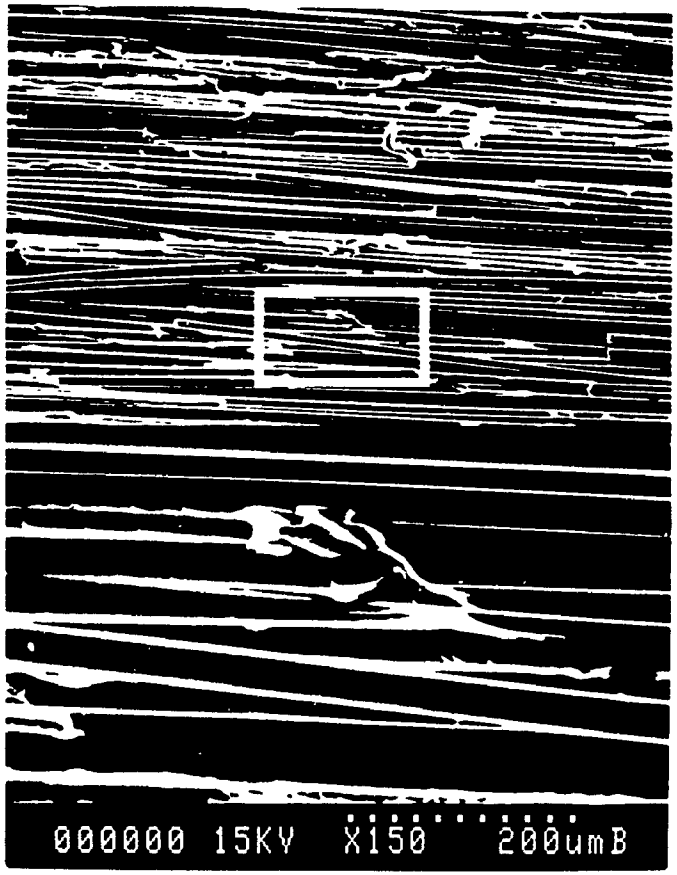

Figure 4.17a. SEM of the fracture surface of AC40-66 virgin laminate at X150 and X750.

Figure 4.17b. SEM of the fracture surface of AC40-66 laminate exposed to 87°C at X150 and X750.

Figure 4.17c. SEM of the fracture surface of AC40-66 laminate exposed to 87°C/84% (MC=0.18%) at X150 and X750.

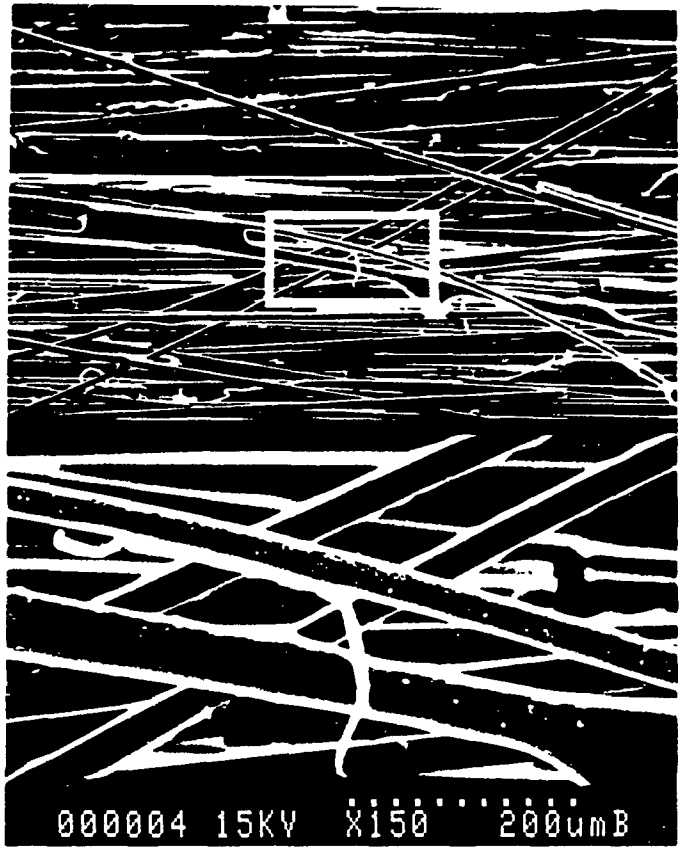

Figure 4.17d. SEM of the fracture surface of AC40-66 laminate exposed to 87°C/95% (MC=0.75%) at X150 and X750.

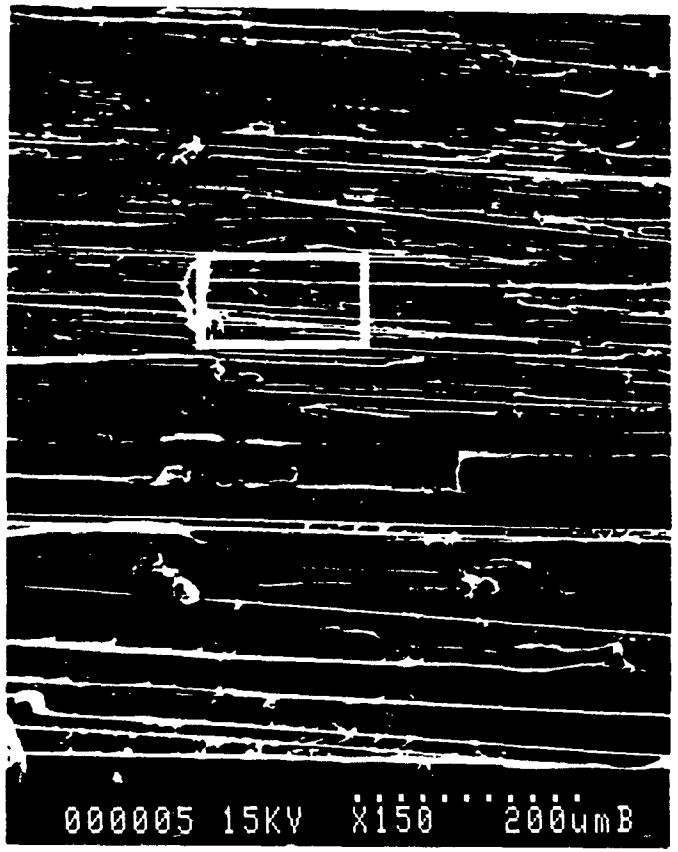

Figure 4.17e. SEM of the fracture surface of AC40-66 laminate exposed to 127°C at X150 and X750.

Figure 4.17f. SEM of the fracture surface of AC40-66 laminate exposed to 127°C/84% (MC=0.08%) at X150 and X750.

Figure 4.17g. SEM of the fracture surface of AC40-66 laminate exposed to 127°C/95% (MC=0.55%) at X150 and X750.

content, up to 0.75%, the softening of the resin was observed as shown in Figures 4.17c and 4.17d. At 127°C, such a softening of the matrix was found more evident and even resins surrounding the fibers experienced stretching to some degrees as seen in Figures 4.17e to 4.17g., which increased the effective fractured surfaces. All these factors account for the large amount of the critical strain energy dissipated during crack propagation as shown above.

Mode II crack extension in the unidirectional laminate remained essentially coplanar with the starter notch. However, the side-view pictures of the carbon/PPS specimens show some microcracking behavior. The microcracks are more evident at low temperature and low moisture content as shown in Figures 4.18a to 4.18c. At high temperature and moisture content, the fiber bridging and the plastic deformation of the matrix dominate the fracture process as indicated in Figures 4.18d to 4.18f. It is also clear that fiber bridging is from single fiber to bundle of fibers as the temperature and moisture content increase. Some fiber pullout was also observed due to the good bonding between the fibers and the resin. This process also increases the G_{IIC} of the carbon/PPS laminate.

4.6.2 Tensile Tests of the Glass/PPS Composites

Typical electron micrographs for the glass/PPS samples examined are shown in Figures 4.19 to 4.24. Figures 4.19 and

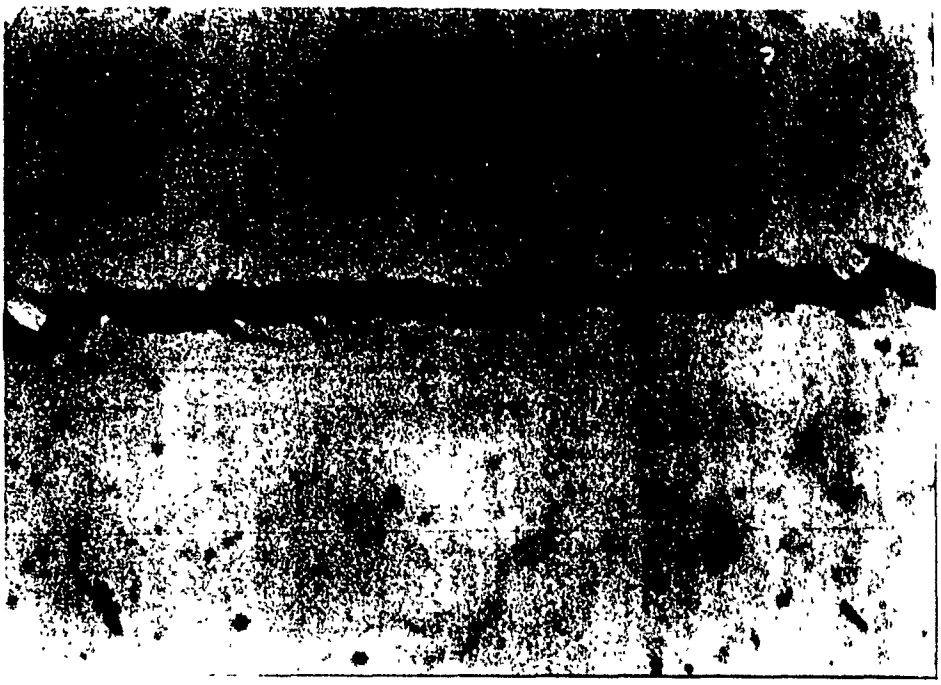

X5

X50

Figure 4.18a. Planar surface view of the fractured AC40-66 virgin laminate at X5 and X50.

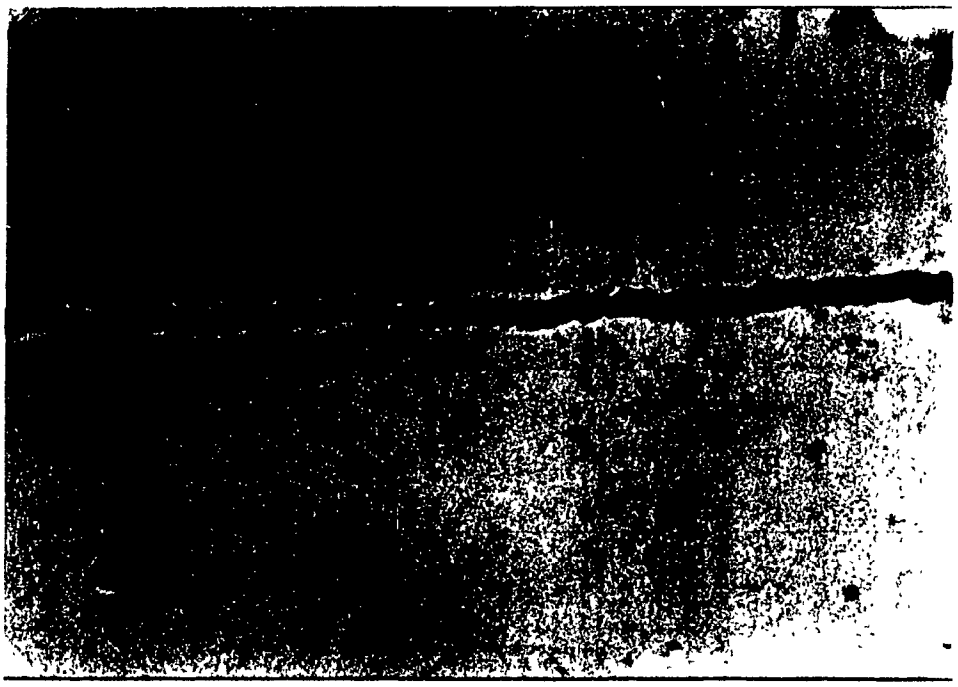

X5

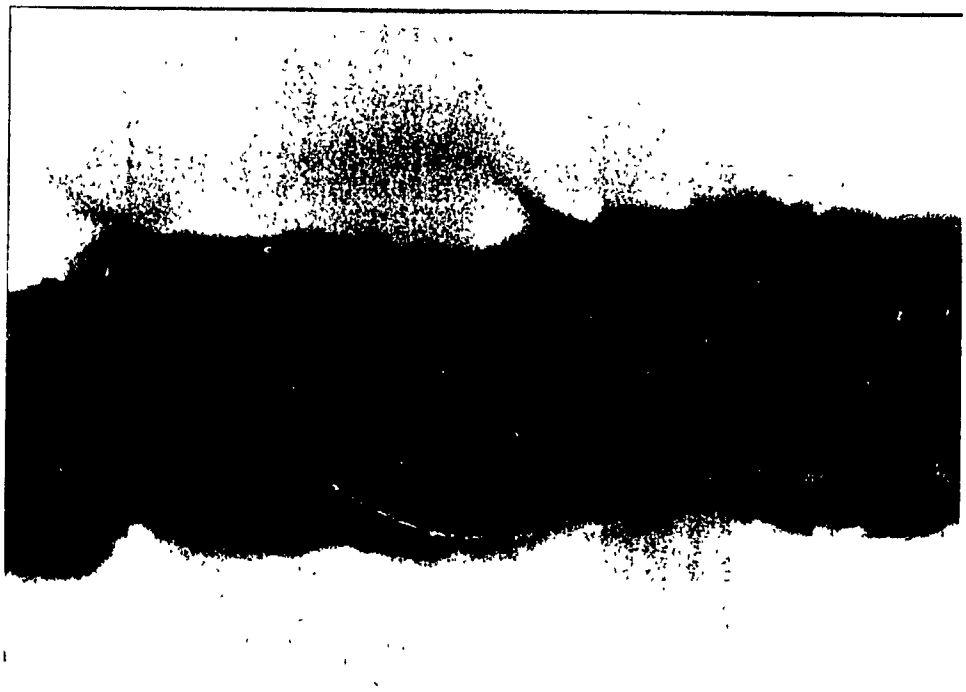

X50

Figure 4.18b. Planar surface view of the fractured AC40-66 laminate exposed to 87°C at X5 and X50.

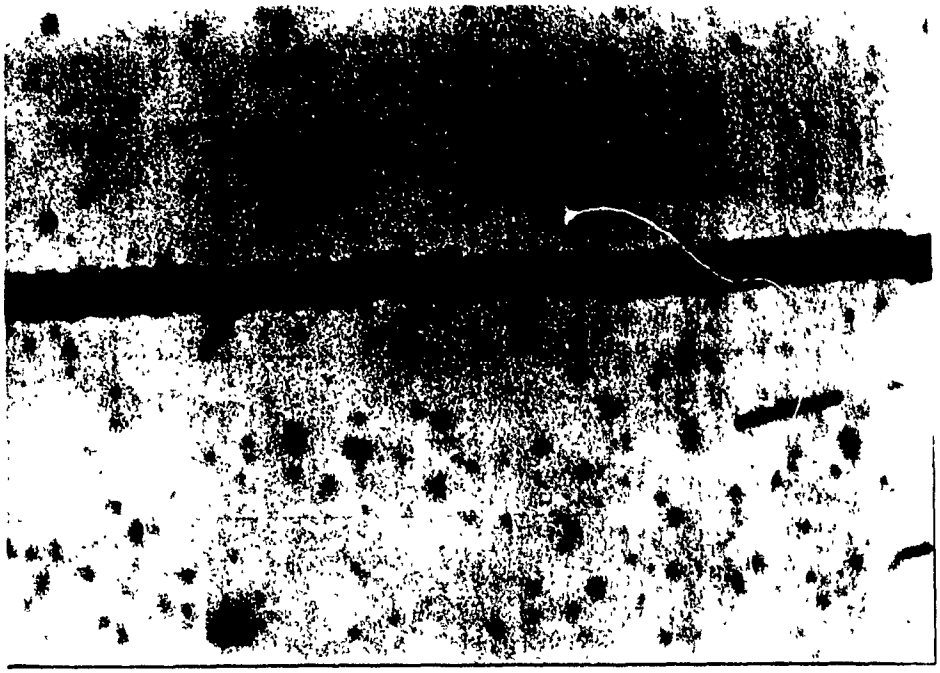

X5

X50

Figure 4.18c. Planar surface view of the fractured AC40-66 laminate exposed to 87°C/95% (MC=0.75%) at X5 and X50.

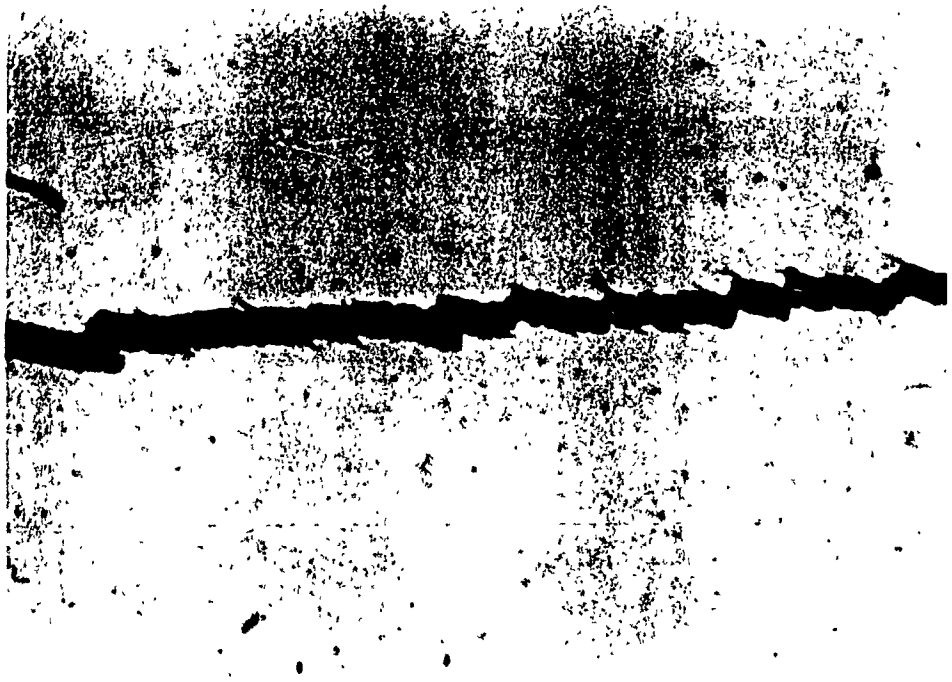

X5

X50

Figure 4.18d. Planar surface view of the fractured AC40-66 laminate exposed to 127°C at X5 and X50.

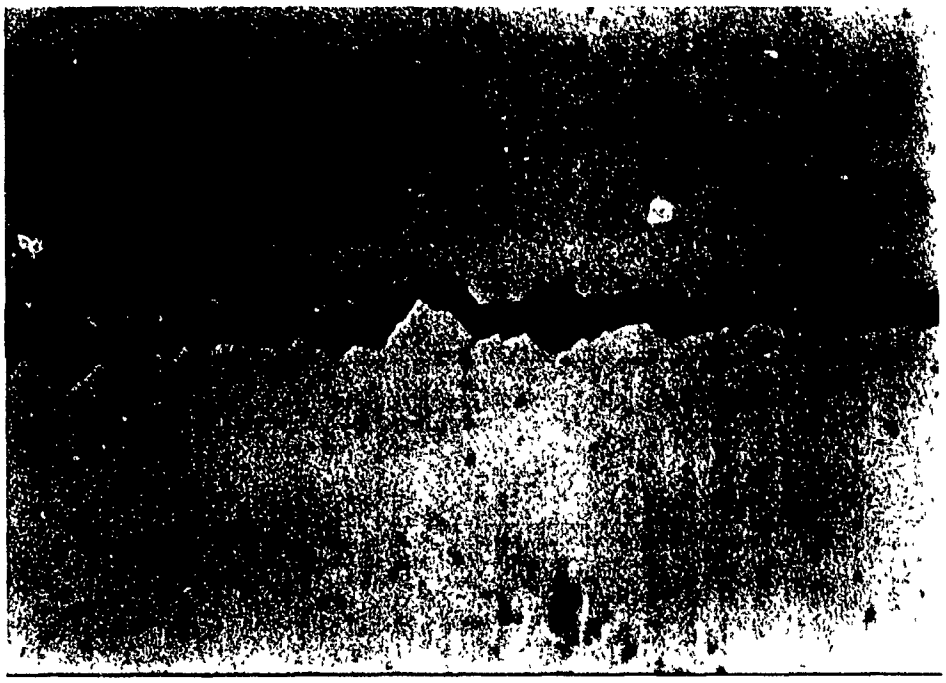

X5

X50

Figure 4.18e. Planar surface view of the fractured AC40-66 laminate exposed to 127°C/84% (MC=0.08%) at X5 and X50.

X5

X50

Figure 4.18f. Planar surface view of the fractured AC40-66 laminate exposed to 127°C/95% (MC=0.55%) at X5 and X50.

4.20 show the microstructures of samples R-7 and A-100, respectively. These micrographs show that the fibers are short (about 17 μm long) and are covered with the PPS matrix, with little exposure of the fiber-matrix interface. This is in contrast with the case of the advanced composites (Figures 4.21 to 4.24). Figures 4.21 and 4.22 show the microstructures of the stampable chopped-fiber samples AG11-20. There are many fiber-resin interfaces exposed and there are many capillaries which serve to suck in the moisture; fiber directions are also random. This lends the material to high transverse stresses and bending fracture of the fiber. Moisture tends to debond the glass fibers from the PPS resin as shown in Figure 4.22.

Figures 4.23 and 4.24 show the microstructures of the continuous-fiber satin weave fabric samples. The number of crevices and capillaries magnifies. The material appears very dry and many fibers are exposed. Capillary action is certainly dominant here. There appears to be little difference between the microstructures of AG31-60 and AG31-40 samples in terms of the number of crevices and capillaries. The marked difference in tensile strength reduction shown in Figure 4.15 can therefore be related to the lower degree of crystallinity in samples AG31-60 as discussed in Chapter II.

Figure 4.19. SEM of sample R-7 at X1500 (as-received).

Figure 4.20. SEM of sample A-100 at X1490 (as-received).

Figure 4.21. SEM of sample AG11-20 at X130 (as-received).

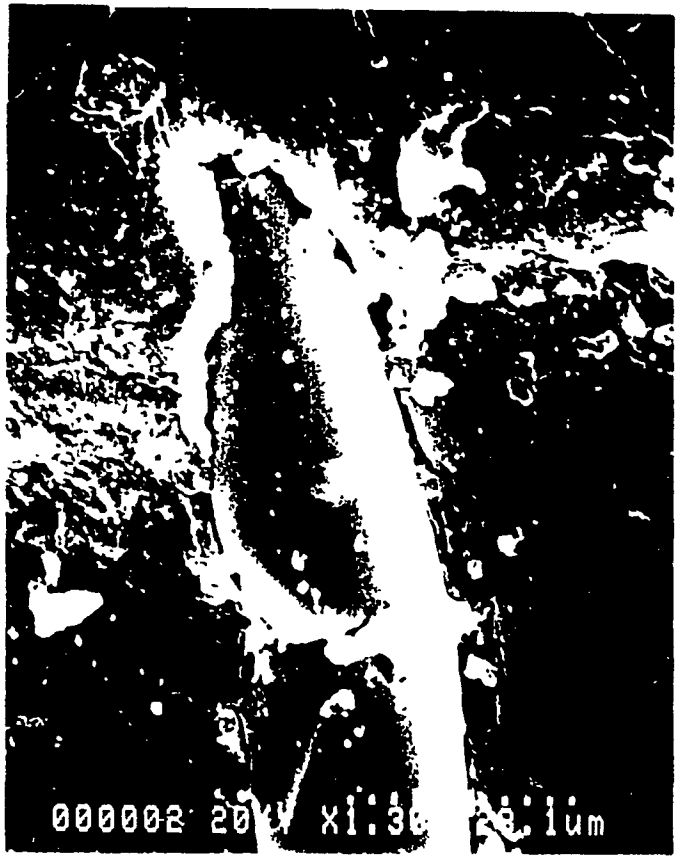

Figure 4.22. SEM of sample AG11-20 at X1300 (as-received).

Figure 4.23. SEM of sample AG31-60 at X120 (as-received).

Figure 4.24. SEM of sample AG31-40 at X300 (as-received).

CHAPTER V

CONCLUSIONS AND SUGGESTIONS FOR FUTURE WORK

5.1 Conclusions

The semicrystalline engineering thermoplastic, PPS, has been shown to be an excellent matrix for high performance fiber reinforced composites. Mode II interlaminar fracture toughness of the carbon/PPS laminate and tensile strengths of the glass/PPS composites for various hygrothermal conditions have been determined. From this investigation, the following conclusions can be drawn:

1. Compared to the critical strain energy release rate under Mode II loading of graphite/epoxy laminates, which is about 160 J/m^2 [9], the carbon/PPS laminate is tougher.
2. The crack propagates only through the resins by microcracking for virgin specimens and for those specimens exposed to low temperature and with low moisture content. The amount of resin deformation in these "smooth" fracture surfaces is small.
3. As the moisture content and temperature increase, an increase of the interlaminar fracture energy is found. This is due to the change in Mode II failure mechanism from the energy absorbing multiple matrix microcracking of the brittle matrix systems to the constrained plastic deformation of the toughened PPS

matrix system. The extensive deformation in the PPS resin accounts for the large amount of energy dissipated during crack propagation.

4. The injection-molded samples showed less degradation due to exposure to 100°C/95% hot-moist condition than advanced composite samples (with the understanding that the advanced composite samples were stronger initially). Debonding between the glass fibers and the PPS resin happened because of the large amount of moisture absorption.
5. The degree of crystallinity in the PPS resin has a significant effect upon the degradation due to hot-moist condition. The mechanical properties and the moisture absorption of the PPS composites can be improved by annealing the material between the glass transition temperature and the melting temperature.

5.2 Suggestions for Future Work

A failure criterion based on the strain energy release rate, G, has been expressed [9] in the form of

$$\frac{G_I}{G_{IC}} + \frac{G_{II}}{G_{IIC}} = 1 \qquad (5.1)$$

For the tougher resin materials where G_{II} is nearly equal to G_{IC}, we can assume

$$G_{IC} = G_{IIC} = G_C \qquad (5.2)$$

Substituting Equation (5.2) into Equation (5.1) results in

$$G_I + G_{II} = G_T = G_C \qquad (5.3)$$

The total strain energy release rate G_T is much simpler to calculate than individual components according to [24 & 25]. Simple strength of materials approaches often give adequate estimates of G_T whereas they do poorly predict G_I and G_{II} components. Equation (5.3) is a reasonable static failure criterion for many tough resin systems while Equation (5.1) may be appropriate for brittle materials where G_{IIC} is much larger than G_{IC}.

From the above discussion, the following work is felt necessary:

1. Mode I (opening mode) tests of this carbon/PPS under various temperature/wet conditions need to be investigated to provide information on the critical strain energy release rate for Mode I loading, G_{IC}, in order to establish a failure criterion for mixed mode fracture.
2. Considering the difference between the results by DCB and those by the area method, non-linear mathematical fracture mechanics models need to be developed to accommodate the anelastic behavior of the thermoplastic resins and the complex crack tip activities involved in the fracture process.

REFERENCES

1. Edmonds, J. T., Jr. and Hill, H. W., Jr., "Production of P-phenylene Sulfide Polymers from Aromatic Compounds," U.S. patent 3,354,129 (1967).
2. O'Connor J. E., Lou, A. Y., and Beever W. H., "Polyphenylene Sulfide - A Thermoplastic Polymer Matrix for High Performance Composites," Proceedings of the 5th International Conference on Composite Materials, San Diego, California, July-August (1985), pp. 963-970.
3. Ma, C. C. M., O'Connor, J. E., and Lou, A. Y., "Polyphenylene Sulfide: Resin, Prepreg and High Performance Composites," Proceedings of the 30th SPI Reinforced Plastics/Composites Conference (1984), paper 11E.
4. Brady, D. G., "Long Fiber Reinforced PPS - A New Dimension in Toughness," SPE Antec Proceedings 42, 690, (1984).
5. Brady, D. G. and Hill, H. W., Jr., "Polyphenylene Sulfide," Engineering Thermoplastics: Properties and Applications, Chapter 8, J. M. Margolis, Ed., Dekker, New York (1985).
6. Krone, J. R. and Walker, J. H., "Thermoforming Woven Fabric Reinforced Polyphenylene Sulfide Compounds," Proceedings of Composites in Manufacturing, vol. 5, Los Angeles, CA, January (1986).
7. Vanderkley, P. S., "Mode I - Mode II Delamination Fracture Toughness of a Unidirectional Graphite/Epoxy Composite," a thesis of Master of Science at Texas A&M

University (1981).

8. Russell, A. J. and Street, K. N., "The Effect of Matrix Toughness on Delamination: Static and Fatigue Fracture Under Mode II Shear Loading of Graphite Fiber Composite," Toughened Composites, ASTM STP 937, Norman J. J., ed., American Society for Testing and Materials, Philadelphia (1987), pp. 275-294.

9. Johnson, W. S. and Mangalgiri, P. D., "Influence of the Resin on Interlaminar Mixed-Mode Fracture," Toughened Composites, ASTM STP 937, Norman J. J., ed., American Society for Testing and Materials, Philadelphia (1987), pp. 295-315.

10. Mall, S., Law, G. E., and Katouzian, M., "Loading Rate Effect on Interlaminar Fracture Toughness of a Thermoplastic Composite," J. Composite Materials, vol. 21, June (1987), pp. 569-579.

11. Smiley, A. J. and Pipes, R. B., "Rate Effect on Mode I Interlaminar Fracture Toughness in Composite Materials," J. Composite Materials, vol. 21, July (1987), pp. 670-687.

12. Russell, A. J. and Street K. N., "Factors Affecting the Interlaminar Fracture Energy of Graphite/Epoxy Laminates," Progress in Science and Engineering of Composites, edited by T. Hayashi, K. Kawata & S. Umekawa, ICCM-IV, Tokyo (1982), pp. 279-286.

13. Su, K. B., "Mechanisms of Interlaminar Fracture in a Thermoplastic Matrix Composite Laminate," Proceedings of the Fifth International Conference on Composite

Materials, San Diego (1985), pp. 995-1006.

14. Hibbs, M. F., Tse, M. K. and Bradley W. L., "Interlaminar Fracture Toughness and Real-Time Fracture Measurement of Some Toughened Graphite/Epoxy Composites," Toughened Composites, ASTM STP 937, Norman J. J., ed., American Society for Testing and Materials, Philadelphia (1987), pp. 115-130.

15. Jordan, W. M. and Bradley W. L., "Micromechanisms of Fracture in Toughened Graphite-Epoxy Laminates," Toughened Composites, ASTM STP 937, Norman J. J., ed., American Society for Testing and Materials, Philadelphia (1987), pp. 95-114.

16. Hirschbuehler, K. R., "A Comparison of Several Mechanical Tests Used to Evaluate the Toughness of Composites," Toughened Composites, ASTM STP 937, Norman J. J., ed., American Society for Testing and Materials, Philadelphia (1987), pp. 61-73.

17. Wilkins, D. J., J. R. Eisenmann, R. A. Camin, and R. A. Benson, "Characterizing Delamination Growth in Graphite /Epoxy," Damage in Composite Materials, ASTM STP 775, (1980), PP. 168.

18. Vives, V. C., Dix, J. S. and Brady, D. G., "Polyphenylene Sulfide (PPS) in Harsh Environments," Effects of Hostile Environments on Coatings and Plastics, D. P. Garner and G. A. Stahl, Eds., American Chemical Society, Washington, DC (1983).

19. Kays, A. O. and Hunter, J. D., "Characterization of Some Solvent-Resistant Thermoplastic Matrix Compo-

sites," Composite Materials: Quality Assurance and Processing, ASTM STP 797, edited by C. E. Browning, American Society of Testing and Materials (1983), pp. 119-132.

20. Mascia, L., Thermoplastics: Materials Engineering, Applied Science Publishers Ltd., New York (1982).

21. Beever, W. H., Ryan, C. L. O'Connor, J. E. and Lou, A. Y., "Ryton® - PPS Carbon Fiber Reinforced Composites: The How, When, and Why of Molding," Toughened Composites, ASTM STP 937, Norman J. J., ed., American Society for Testing and Materials, Philadelphia (1987), pp. 319-327.

22. Williams, J. G., "Large Displacement and End Block Effect in the DCB Interlaminar Test in Mode I & II," J. Composite Materials, vol. 21, April (1987), pp. 330-347.

23. Wake, W. C., Fillers for Plastics, Chapter 1, Butterworth, London (1971).

24. Mall, S. and Johnson, W. S., "Characterization of Mode I and Mixed-Mode Failure of Adhesive Bonds Between Composite Adherents," Composite Materials: Testing and Design (Seventh Conference), ASTM STP 893, J. M. Whitney, Ed., American Society for Testing and Materials, Philadelphia (1986), PP. 322-336.

25. Mall, S., Johnson, W. S. and Everett, R. A., Jr., "Cyclic Debonding of Adhesively Bonded Composites," in Adhesive Joints, K. L. Mittle, Ed., Plenum Press, New York (1984), PP. 639-658.

26. Carlsson, L. A., Gillspie, J. W., Jr., and Pipes, R. B., "On the Design and Analysis of the End Notched Flexure (ENF) Specimen for Mode II Testing," J. Composite Materials, vol. 20 (1986), pp. 594-604.

APPENDIX A

Compliance of the End Notched Cantilever Beam Specimen

With reference to Figure A1 and using beam theory, the moment at an arbitrary location x is

$$M_x = P(L - x) = EI \frac{d^2\Delta}{dx^2} \qquad (A1)$$

where I is the moment of inertia and Δ is the flexural deflection at location x.

Integrating Equation (A1) gives

$$\Delta(x) = \frac{P}{EI} \left(\frac{L}{2}x^2 - \frac{1}{6}x^3 + C_1 x + C_2\right) \qquad (A2)$$

where C_1 and C_2 are constants which can be determined from these two boundary conditions:

$$\Delta(x) = 0 \qquad \text{at } x = 0$$

and

$$\frac{d\Delta}{dx} = 0 \qquad \text{at } x = 0$$

as

$$C_1 = 0 \quad \text{and} \quad C_2 = 0$$

Therefore, the flexural deflection at x is

$$\Delta(x) = \frac{Px^2}{6EI} (3L - x) \qquad (A3)$$

Then the maximum flexural deflection of a cantilever beam is

$$\Delta_{max} = \Delta(C) = \frac{PL^2}{6EI} (3L - L) = \frac{PL^3}{3EI} \qquad (A4)$$

Along the undelaminated segment of the specimen, the

moment of inertia

$$I_{undel} = B(2D)^3/12 = 2BD^3/3 \qquad (A5)$$

Substituting Equation (A5) into Equation (A3) yields

$$\Delta(x) = x^2(3L - x)P/4EBD^3 \qquad (A6)$$

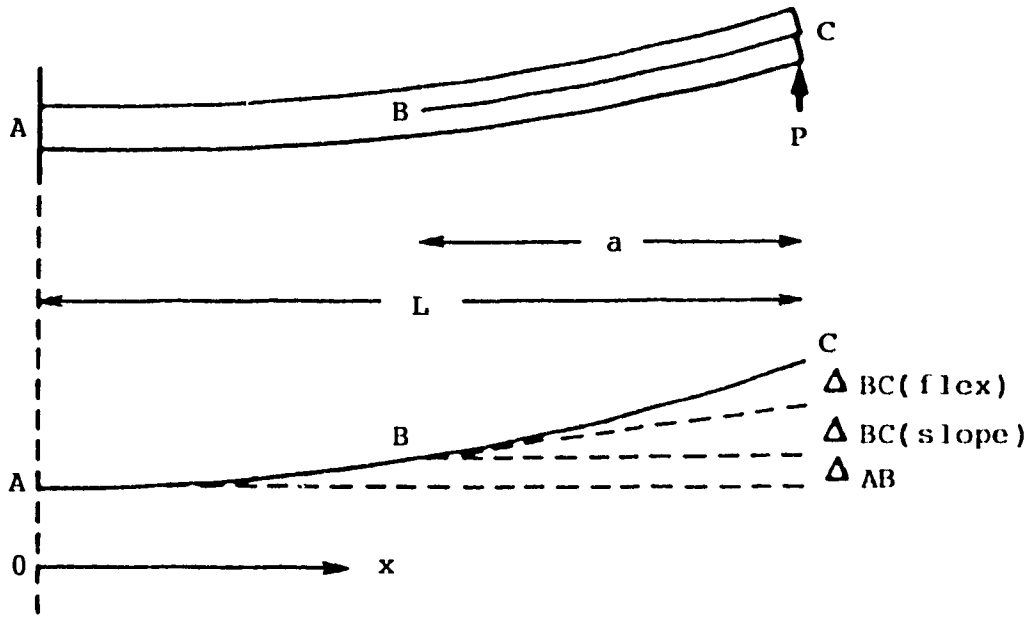

Figure A1. Specimen deflections.

at $x = L - a$

$$\Delta AB = (2L^3 - 3aL^2 + a^3)P/4EBD^3 \qquad (A7)$$

A portion of the deflection of the delaminated region of the specimen results from the slope at B which is obtained by differentiating Equation (A6)

$$d\Delta/dx = (6Lx - 3x^2)P/4EBD^3 \qquad (A8)$$

which at $x = L - a$,

$$= 3(L^2 - a^2)P/4EBD^3 \qquad (A9)$$

resulting in a deflection as a result of the slope at B of

$$\Delta BC(slope) = a \frac{d\Delta}{dx} = 3a(L^2 - a^2)P/4EBD^3 \qquad (A10)$$

The flexural deflection of the delaminated part of the specimen, assuming both halves carry equal loads and making use of Equation (A4), is given simply by

$$\begin{aligned} \Delta BC(flex) &= (\frac{P}{2})a^3/3EI \\ &= Pa^3/(6EBD^3/12) \\ &= 2a^3P/EBD^3 \end{aligned} \qquad (A11)$$

Provided that the total deflection is small, these three terms can be summed arithmetically to obtain the total deflection

$$\begin{aligned} \delta = \Delta AC &= \Delta AB + \Delta BC(slope) + \Delta BC(flex) \\ &= P(L^3 + 3a^3)/2EBD^3 \end{aligned} \qquad (A12)$$

and hence, the flexural compliance of the specimen is given by

$$C = \delta/P = (L^3 + 3a^3)/2EBD^3 \qquad (A13)$$

APPENDIX B

Expression of the Critical Strain Energy Release Rate

The energy approach, which stems from the original Griffith treatment, is based on a thermodynamic criterion for fracture by considering the energy, available for crack growth, of the system on one hand and the surface energy required to extend an existing crack on the other hand. A potential H may be defined for a cracked body as

$$H = W - U \tag{B1}$$

where W is the work supplied by the movement of the external forces, and U is the elastic strain energy stored in the body. If G_c is the work required to create a unit crack area, it is possible to formulate a criterion for crack growth,

$$\delta H \geq G_c \delta A \tag{B2}$$

where δA is the increase in crack area.

Critical conditions occur when the net energy supplied just balances the energy required; i.e.,

$$\delta H = G_c \delta A \tag{B3}$$

The equilibrium becomes unstable when the net energy supplied exceeds the required crack tip energy,

$$\delta H > G_c \delta A \tag{B4}$$

The strain energy release rate, G, is defined as

$$G = \frac{\partial H}{\partial A} \tag{B5}$$

In terms of G, the fracture criterion may thus be formulated as

$$G \geq G_c \tag{B6}$$

This concept will be illustrated for a linear elastic body containing a crack of length a and a + δa, respectively. Figure B1 shows the load, P, versus displacement, u, behavior for the cracked body where crack growth is assumed to occur either at constant load (fixed load) or at constant displacement (fix grip).

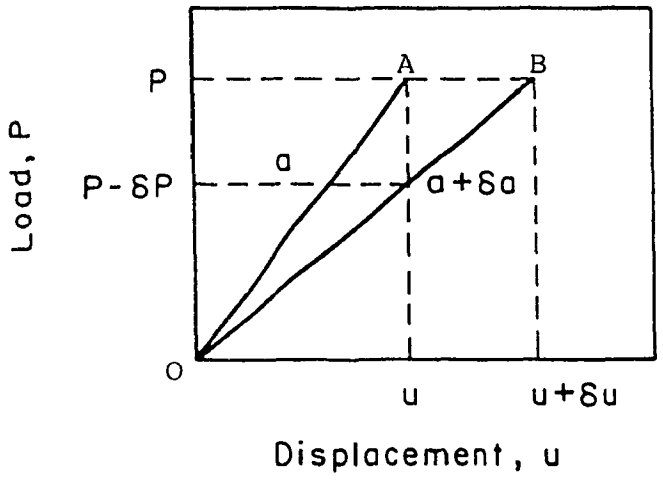

Figure B1. Load-displacement behavior for a cracked body.

For the fixed load case,

$$\delta U = P\delta u/2$$

$$\delta W = P\delta u \tag{B7}$$

Equation (B1) gives

$$\delta H = P\delta u - P\delta u/2 = P\delta u/2, \tag{B8}$$

and Equation (B5) gives

$$G = \frac{P}{2} \frac{\partial u}{\partial A} \tag{B9}$$

For the fixed grip case, the work term vanishes and

$$\delta U = u\delta P/2 \tag{B10}$$

Note that δP is negative because of the loss in stiffness followed by crack extension, and G is

$$G = -\frac{u}{2} \frac{\partial P}{\partial A} \tag{B11}$$

For a linear elastic body, the relation between load and displacement may be expressed as

$$u = CP \tag{B12}$$

where C is the compliance of the specimen. Substituting Equation (B12) into Equation (B9) (fixed load) gives

$$G = \frac{P^2}{2} \frac{\partial C}{\partial A} \tag{B13}$$

and substitution of P = u/C into Equation (B11) (fixed grip) gives

$$G = \frac{u^2}{2C^2} \frac{\partial C}{\partial A} = \frac{P^2}{2} \frac{\partial C}{\partial A} \tag{B14}$$

Consequently, both Equation (B9) and Equation (B11) reduce to the same expression.